School of Electrical Engineering, Computing and Mathematical Sciences
Department of Electrical and Computer Engineering

Channel Modelling and Impulsive Noise Mitigation for Relay-assisted PLC Systems

Angie Ann Gie Liong
0000-0002-3272-1430

This thesis is presented for the Degree of
Doctor of Philosophy
of
Curtin University

July 2021

Declaration

To the best of my knowledge and belief this thesis contains no material previously published by any other person except where due acknowledgement has been made.

This thesis contains no material which has been accepted for the award of any other degree or diploma in any university.

Signature:

Date: 24 July, 2021

To

my beloved family

Acknowledgements

First and foremost, I would like to express my sincere gratitude to my supervisors, Associate Prof. Lenin Gopal, Dr. Filbert Juwono, Dr. Raymond Chiong and Prof. Yue Rong for their inspiration, motivation, knowledge, constant support and encouragement during the entire period of my PhD study. Their invaluable guidance and timely correspondence directed me to the goal. They were constantly patient and caring in their support which made all this achievable.

Beside my supervisors, I would like to extend my gratitude to my chairperson of my thesis committee, Associate Prof. Zhuquan Zang, for his necessary administrative guidance and help this research work.

I am grateful to the Fundamental Research Grant Scheme (FRGS) from Ministry of Higher Education Malaysia and Faculty of Engineering and Science, Curtin University Malaysia for their financial and administrative support provided during the course of my PhD study.

I would like to thank my family and my relatives for their continuous understanding, support, guidance and love during this study. Many sincere thanks goes to all my friends and colleagues, especially rotaractors and rotarians from Rotaract club of Curtin Malaysia and Rotary Club of Bandar Seri Begawan for their lovely, caring and emotional support to cheer me up during my hard time.

Last and not least, I would like to dedicate this PhD thesis to my late grandfather. We walked together through the hard time in the beginning of my studies before he got badly sick. I would like to finish off by saying I am blessed, grateful and appreciated. Many many thanks.

Abstract

Power Line Communication (PLC) is one of the most attractive technologies for communication as a power-line can be used as the medium to deliver electricity and support the local area network (LAN) without any installation of new cables. Since the power-line is not designed for high-frequency signal transmission, it suffers from frequency-selective fading and noise. However, Orthogonal Frequency Division Multiplexing (OFDM) is not appropriate to handle the multipath fading due to impulsive noise. Therefore, a blanking preprocessor bank is proposed to mitigate the effect of the impulsive noise in PLC systems without knowing the noise parameter. The proposed blanking outperforms in bit-error-rate (BER) and outage probability. Due to the harsh environment of the power-line, relays are suggested to improve reliability of the PLC systems. However, many PLC applications need two-way communication links. The rest of thesis focuses on two-way amplify-and-forward (AF) relay-assisted PLC systems. A general method of modelling the two-way relay-assisted PLC channel is proposed. Different signalling paths existing in the relay-assisted PLC channels are transformed into a group of an equivalent point-to-point (P2P) PLC channels. The simulation results show that the two-way channels are highly correlated than the one-way relay-assisted PLC channels. The two-way single-relay PLC systems are extended to two-relay PLC systems for enhancing the performance of PLC systems. The two-way two-relay PLC channel model is proposed. The composite channel transfer function (CTF) for a certain link is the summation of their respective CTFs of the signalling path. The simulation results show that the two-relay PLC systems take

advantage of the relays by giving a deeper attenuation at certain frequency for non-direct link, whereas the single-relay PLC system has better performance than the two-relay PLC system for direct links. Since the bottom-up approach is preferred for relay-assisted PLC system, the bottom-up multipath channel model is proposed for a two-way single-relay PLC system based on the modification of parameters of the top-down Zimmermann-Dostert model. The simulation results show that the proposed model does not have many fluctuate especially in the high frequency, which makes a similar profile with other bottom-up channel models. With the two-way single-relay PLC systems, the power allocation with quality-of-service (QoS) considerations are examined to optimise the total power consumption. Since the QoS constrained power allocation problem is highly non-convex, the proposed power optimisation algorithm is used. The simulation results show that the proposed algorithm outperforms with shorter processing delays and reduces the total power required by the system by about 40% compared to the conventional system under the same QoS requirement.

Publications arising from the Thesis

Parts of the contents in this thesis and concepts have been previously published in the following conference papers or submitted in the following journals.

Journal Publications

[1] A. A. G. Liong, L. Gopal, F. H. Juwono, C. W. R. Chiong, Y. Rong, and Z. Zang "Power Optimization of a Three-Node Two-Way Relay-assisted Power Line Communications Systems," IEEE Trans. Smart Grid, submitted, Jul. 2021.

[2] A. A. G. Liong, F. H. Juwono, L. Gopal, C. W. R. Chiong and Y. Rong, "Multiple Blanking Preprocessors for Impulsive Noise Mitigation in OFDM-based Power-line Communication Systems," Int. J. Electrical Power Energy Systems, vol. 130, Sept. 2021.

Conference Publications

[1] A. A. G. Liong, L. Gopal, F. H. Juwono, C. W. R. Chiong and Y. Rong, "A Comparison of Three-node Two-way PLC Channel Models," IEEE Int. Conf. Adv. Technol. Commun. (ATC), Nha Trang, Vietnam, Oct. 8-10, 2020.

[2] A. A. G. Liong, L. Gopal, F. H. Juwono, C. W. R. Chiong and Y. Rong, "Channel Characteristics Comparison of Single-Relay and Two-Relay Two-Way PLC Systems," IEEE Int. Conf. Comp. Commun. Netw. Technol. (ICCCNT), West Bengal, India, Jul. 1-3, 2020.

[3] A. A. G. Liong, L. Gopal, F. H. Juwono, C. W. R. Chiong and Y. Rong, "A Channel Model for Three-node Two-way Relay-aided PLC Systems," IEEE Int. Conf. Signal Image Process. Appl. (ICSIPA), Kuala Lumpur, Malaysia, Sept. 17-19, 2019, pp. 52-57.

Contents

List of Figures

List of Tables

Acronyms

AC	alternating current
AF	amplify-and-forward
AMR	Automatic meter reading
AN	access network
AO	alternating optimization
ASC	averaged subchannel capacity
AWGN	additive white Gaussian noise
BB-PLC	broadband PLC system
BDT	bidirectional direct transmission
BER	bit-error-rate
BG	Bernoulli-Gaussian
BICM	bit-interleaved coded modulation
BMA	broadcast-and-multiaccess
CCDF	cumulative distribution function
CFR	channel frequency response
CIR	channel impulse response
CP	cyclic prefix
CSI	channel state information
CTF	channel transfer function
DF	decode-and-forward
DFT	discrete fourier transform

EMI	electromagnetic interference
ETSI	European Telecommunications Standards Institute
GBN	general background noise
HDTV	high definition television
HPPA	HomePlug Powerline Alliance
HV	high voltage
i.i.d	independent and identically distributed
ICI	inter-carrier interference
IDFT	inverse discrete Fourier transform
IEEE	Institute of Electrical and Electronics Engineers
ISI	inter-symbol interference
ITU	International Telecommunication Union
KKT	Karush-Kuhn-Tucker
LAN	local area network
LPTV	linear periodical time-varying
LV	lower voltage
MAC	medium access control
MCA	Middleton Class A
MIMO	multiple-input-multiple-output
ML	maximum likelihood
MTL	multiconductor transmission line
MUSIC	multiple signal classification
MV	medium voltage
NB-PLC	narrowband PLC system
OFDM	Orthogonal Frequency Division Multiplexing
OPERA	Open PLC European Research Alliance
P2P	point-to-point
PAPR	peak-to-average power ratio
PDF	Power density function

PHY	physical
PLC	Power Line Communication
PSD	power spectral density
QAM	quadrature amplitude modulation
QoS	quality-of-service
QPSK	quadrature phase shift keying
R2WX	relay-assisted two-way information exchange
rms	root mean square
SαS	Symmetric α-stable
S/P	serial to parallel
SINR	signal-to-impulse-noise ratio
SL0	smoothed-ℓ_0
SNR	signal to noise ratio
TDD	time-division duplexing
TL	transmission line
UPA	Universal Powerline Association
VRA	voltage ratio approach
WGN	white Gaussian noise
WT	wavelet transform

List of Symbols

α_i	attenuation factor for i-th path
α_q	real-valued constant chosen
β	amplitude gain
ΔT	threshold steps
ϵ_r	Dielectric coefficient
Γ	reflection coefficient
γ	propagation constant
γ_q	output SNR of each blanking preprocessor (dB)
Γ_{bin}	background-to-impulse noise ratio
$\bar{\mathbf{c}}$	codeword
$\hat{\bar{\mathbf{c}}}$	optimal maximum likelihood bit metric
$\mathbf{b}$	Bernoulli sequence vector
$\mathbf{c}$	interleave codeword
$\mathbf{F}$	DFT unitary matrix
$\mathbf{g}$	AWGN vector
$\mathbf{H}$	circulant matrix

$\mathbf{i}$	impulsive noise vector
$\mathbf{n}$	Gaussian vector
$\mathbf{r}$	received signal
$\mathbf{s}$	channel output
$\mathbf{u}$	information sequence
$\mathbf{X}$	modulated signal vector
$\mathbf{x}$	OFDM signal
$\mathbf{Y}$	OFDM demodulator
$\mathbf{z}$	total PLC noise
$\mathcal{C}$	coding scheme
$\mathcal{N}$	set of indices of null subcarriers
$\mathcal{O}$	complexity
$\mathcal{X}$	constellation set
$\mathcal{X}_q^p$	subset of the information symbols
ω_0	resonance angular frequency
$\overline{C}$	average sub-channel capacities (bits/s/Hz/subcarrier)
$\overline{q}$	minimal ASC requirement (bits/s/Hz/subcarrier)
σ_b^2	variance of background noise
σ_g^2	variance of random Gaussian distribution
τ_i	delay at the branch i
$\tilde{c}_n$	time-domain filtered clipping noise

$\tilde{H}_{ab}$ CTF of the signalling path from a to b after the relay node is introduced

ε_{eq} relative permittivity of the material

ζ delay at the branch i

A impulsive index

$A^{(k)}$ amplitude of the Gaussian function (dBm/Hz)

a_0/a_1 attenuation parameters

A_c peak amplitude clipping threshold

A_F amplification factor

$B^{(k)}$ bandwidth of the Gaussian function (MHz)

b_n occurrence of impulsive noise having a Bernoulli sequence of 0 and 1

C capacitance per-unit-length (F/m)

c_0 speed of light (3×10^8 m/s)

C_k frequency domain of clipping noise

$c_{k,u}$ coded bit at u-th label of the k-th subcarrier

d length (m)

d_c degree of correlation

d_i length at branch i (m)

d_n blanking noise

f frequency (Hz)

$f(\cdot)$ blanking nonlinear preprocesor bank

$f_0^{(k)}$ center frequency of the Gaussian function (Hz)

f_1 parameter of shifted exponential (MHz)

G conductance per-unit-length (S/m)

g_i gain factor of path i

g_n amplitude of a random Gaussian distribution

H_{ab} CTF of the signalling path from a to b before the relay node is introduced

h_{ab} CFR of the signalling path from a to b

I mutual information

i_n Bernoulli-Gaussian impulse noise

L inductance per-unit-length (H/m)

n discrete-time index

N/K number of subcarriers

N_0 constant noise power density (dBm/Hz)

N_1 parameter of exponential function (dBm/Hz)

N_B^q number of blanked samples in q-th preprocessor

n_d type of cable

N_t number of channel taps

P power (W)

p probability

Q blanking preprocessor

Q_f quality factor

R resistance per-unit-length (Ω/m)

R' resistance at resonance

R_b information rate

S_{BN} PSD of background noise

S_{GBN} PSD of general background noise

S_{NN} PSD of narrow-band noise

T transmission coefficient

T_b Blanking threshold

T_d symbol duration

V voltage (V)

W noise power (W)

w_q weight for q-th preprocessor

w_n discrete-time index of general background noise

$x(n)$ time-domain signal

$X[k]$ frequency-domain signal

y_n output of blanking preprocessor bank

Z load impedance (Ω)

Z_0 characteristic impedance (Ω)

Z_b load impedance at the branch

Z_{eq} equivalent input impedance

z_n discrete-time index of total noise

Φ ABCD matrix of the backbone transmission line segment

Chapter 1

Introduction

Recent researches have developed several communication technologies to increase communication and data sharing information [1]. Communications are divided into two categories, which are wired communication and wireless communication. Wireless communication becomes the most commonly used as the wireless network has many advantages, such as mobility, rapid installation, as well as its technology. However, the biggest problem for wireless communication is the limited spectrum resources. The research on wired power-lines started in the late 1990s. Since then, power line communication (PLC) technology has been popular in data transmission for indoor and outdoor data communication as PLC system can be implemented in a power grid to maximise the efficiency of electricity generation, transmission, and distribution [2]. In this introductory chapter, the overview of PLC, PLC standards and the relay-assisted PLC systems are presented briefly. An overview of the thesis and thesis contributions are described in the last section.

1.1 Research Motivation

Although wireless communications are popular, the use of PLC is preferred since the power networks have been well-established, thereby reducing the installation and operational costs. More specifically, the advantages of the PLC systems include (1) cost-effectiveness, (2) minimum the cost of building new infrastructure, (3) extensive coverage, (4) high capacity, and (5) security [3]. The advantages of PLC eventually give fundamental benefit and cost-effectiveness in the area such as Sarawak, where the infrastructure network does not cover the whole region.

The PLC technology delivers information via electrical power lines. A power plant generates electric power, then transports it through high voltage (HV) power grid (voltage range from 110 to 500kV) to medium voltage (MV) substations [4]. Since the information can only be transmited up to this point, special devices are installed on the power-lines to act as a repeater. The coupler is used to allow information on the line to bypass transformers so that data can move easily without any degradation. The CT bridge used is capable to carry the signal and electricity on the power line as well as putting wireless links on the poles, and send the information wirelessly into homes. The substations change the MV (voltage range from 10 to 30kV) to lower voltage (LV) (voltage range from 110 to 400V) and distribute it to LV household appliances [4], [5]. One of the appliances is the broadband over power-line modem, which is plugged into the wall socket and connected to the computer via ethernet cable. The investigation of electricity distribution of LV grids on PLC system has been the most current research trend because of the various structures available. Since it uses the power cables that are easily found in each house, it can have speedy indoor information services such as local area network (LAN) while delivering power at the same time. Hence, it provides a communication path that can be directly controlled.

1.1.1 PLC Applications

Based on the bandwidth consideration, PLC applications can be classified into broadband PLC system (BB-PLC) and narrowband PLC system (NB-PLC). NB-PLC can be used in home automation and remote measure and control as it is capable of operating at a maximum data rate of 500 kbps and 500kHz of frequency [6]–[8]. Meanwhile BB-PLC is applied to indoor high speed LAN and internet access network (AN) which runs in a data rate of over 1Mbps and over 2MHz of frequency [6], [7]. This entire thesis focuses on BB-PLC on an indoor PLC system. It is applicable to connect all devices within 1.5km from the devices inside a building, giving a wide area of communication for home appliances through the power lines [7], [9]. There are some PLC applications that are used currently.

- **Home automation.** The user can remote control the appliances in the house with and without being in the house [10].
- **Broadcasting over NB-PLC.** Broadcasting over NB-PLC is usually used in European countries where the radio program signals are injected into LV power lines by a special transformer [11].
- **Home networking and internet access.** More computers can connect to share data among computers and other devices as well as obtain internet access using LAN cable without installing a new wire or cable. The devices obtain power from alternating current (AC) main outlets and, at the same time, enable communication connection. [12]
- **Automatic meter reading (AMR).** The meter data is automatically collected and transferred to the database for bill and data analysis. This saves the workload to purposely visit house by house to get the data every month. [13]

- **In-vehicle networking.** Wires are reduced for transmitting signals in aircraft and automotive. The use of battery supplied power cable is able to transmit all signals, and thus, it can reduce the use of total networking cables.
- **Smart Grid.** PLC has gained much attention since the rapid development of smart grid systems. This is because a two-way data exchange is required between the distribution system operator and the users/prosumers to enable the smart grid applications [14]–[17]. The power cables are used as a medium to deliver electricity and support information exchange between the power meters and transformers [18].

1.1.2 Issues with PLC

Since power cables are not designed for data transmission, there will be several issues with PLC. [19]–[21]

- **Varying channel model and time.** The transfer function of the line network is found from the channel model between two outlets in a house. Each segment of the power-line network uses different types of cables. Each cable has its load impedance varies with frequency. Thus, the amplitude and phase signal may vary widely with frequency. Therefore, the signal at the receiver may have lost over some frequency. Hence, the channel is described as random and time-varying with frequency-dependent signal to noise ratio (SNR) over transmission bandwidth. The termination of connected cables length by different impedance can eventually give a different transfer function.
- **High dependence of transceivers location.** The location of the transceivers can significantly affect the transmission quality. A receiver nearby to the noise source, i.e., devices plugged into the network, will experience a poor SNR compared to the far one.

Table 1.1: Current PLC standards available in the market

IEEE P1901	medium access control (MAC) and physical (PHY) specification for broadband PLC
ITU-T G.hn	standards for communication over phone lines and coaxial cables in home networking
UPA Digital Home	standard for inter-operable and coexisting PLC products
HomePlug 1.0	specification for connecting devices via indoor power lines
HomePlug AV	gives sufficient bandwidth for application, e.g. HDTV and VoIP
HomePlug AV2	using IEEE 1901 standard for MIMO transmission, efficient notching and power back-off
HomePlug green PHY	a low power consumption and low cost for home-area network
HomePlug BPL	broadband access network specification for "to-the-home"

- **Signal reflection, multipath fading and attenuation.** The reflection of a signal occurs when there is an impedance mismatch in the electric network. When an electric appliance is plugged in or unplugged out, the equivalent impedance of the signalling path changes significantly. The signal arriving at the receiver consists of several multipath components. All parameters should be assumed to be less than one and not more than five multipath because as the transmissions and reflections increase, the weighting factor decreases. Channel attenuation increases with increasing frequencies.
- **Noise.** The last most significant problem for PLC channel is the presence of noise. Some examples of noise sources are brush motor, fluorescent lamps, and switching power supplies. The noise in the power-line can be either impulse or frequency selective or both.

1.2 PLC Standards

It is important to place a standard to any modern communication technology. Some organisations, such as European Telecommunications Standards Institute (ETSI), HomePlug Powerline Alliance (HPPA), Institute of Electrical and Electronics Engineers (IEEE), International Telecommunication Union (ITU), PowerNet, Open PLC European Research Alliance (OPERA) and Universal Powerline Association (UPA), are trying to uplift their standards as time goes. Some of the current PLC standards available in the market are given in Table 1.1 [22].

This thesis focuses on the physical layer using HomePlug AV specification for an indoor broadband PLC system. The standard of HomePlug AV is specially designed for transmitting high definition television (HDTV) and VoIP around the home. Here is a summary of PHY specification of HomePlug AV used in this thesis simulation. [23], [24]

- HomePlug AV provides up to 200Mbps data rate and operates in the frequency range of 2-28 MHz.
- Turbo codes with varying code rates are employed to gain additional resilience to noisy environments and increase coding gain.
- Coherent modulation is supported. Modulation types are BPSK, QPSK, 8-QAM, 16-QAM, 64-QAM, 256-QAM, and 1024-QAM.
- HomePlug AV PHY can send and receive the frame control signals and utilises a similar synchronisation scheme.
- Several robust modes of operation are provided for communicatation of network synchronisation information, session setup, multi-cast, and broadcast mode.
- The critical element of the HomePlug AV system is channel estimation. HomePlug AV employs higher-order modulation up to 1024-QAM to support variable bit-loading, to monitor carrier SNR without channel estimation, and to track changes in the channel with high efficiency.

1.3 Relay-assisted PLC System

There are similar characteristics between the PLC and wireless communication. For example, both channels have frequency selective propagation properties and characteristics. Hence, many wireless-based signal processing techniques, such as compressing and sensing [25], cognitive radio [26] and multiple-input-multiple-output (MIMO) [27] can be implemented into the PLC systems. Furthermore, the wireless communication systems and PLC systems have a common broadcasting nature, making the possibility of introducing relay-assisted communication schemes into PLC systems. By plugging relay devices into the outlet, cooperative communication can happen in the indoor PLC environment. Thus, the research in relay-assisted PLC systems has become an attractive research topic.

In cooperative PLC, the use of relay has been mentioned and studied in some cases. A single frequency networking based relay-assisted PLC has been introduced and discussed in [28], [29]. The distributed space-time coding for multi-hop transmission using decode-and-forward (DF) relaying has been studied in [30], [31]. The introduction of cooperative multi-hop communication into PLC system has been discussed in [32]–[34]. Authors of [35] have proved that cooperative communication can improve reliability by allocating more source energy to the necessary path and efficiently manage the limited transmit power. The coverage increases with the use of repeaters which can reduce the length of the PLC network and lower the signal power. The robustness over the power-line also improves because of the diversity of the cooperative increases at the destination node.

However, it is important to note the difference between the relay-assisted PLC and wireless relay. In a relay-assisted PLC system, the signalling path of source-to-destination, source-to-relay, and relay-to-destination are highly correlated as they use the same power cable grid. Compared with wireless relaying channels, source, relay, and destination are independent of each other. Furthermore, under

relay-assisted PLC systems, the implementation of the relay node and distance between the transceiver will eventually affect the characteristics of the path and the whole network structure. In contrast, there is no effect on the path and network structure in the wireless system.

1.4 Research Gaps

Based on the findings collected, there are few research gaps identified as below:

- Blanking preprocessors use a threshold to detect the impulsive noise. In order to obtain optimal performance, an optimal threshold needs to be obtained. An incorrect threshold may lead to significant performance degradation. However, it is not an easy task to obtain the optimal threshold of blanking preprocessors. The optimal threshold depends on the impulsive noise parameter. It is common to assume the noise parameter is available to the receiver, which is not practical as the noise parameters at the receiver is actually based on estimation. The mitigate of impulsive noise without knowing the noise parameters is not discussed in the existing research works.
- In PLC scenario, the signalling paths are highly correlated to each other as they use the same power cables. The consideration of a relay device in a PLC system will influence the channel paths. Thus, the existing P2P PLC channel models cannot be directly used to the relay-assisted PLC system. In literature, a single-relay one-way channel model has been proposed. However, many PLC applications need two-way communication links. The channel model of the two-way relay-assisted PLC systems with the direct link between the source and destination terminal nodes have not been discussed in the existing research works.

- The performance of the system, such as the average capacity, coverage, and throughput, can be further improved by adding more relays. In literature, a bottom-up channel model for two-relay one-way PLC network has been shown that the use of two-relay degrades the CTF when compared to the use of one-relay only. Yet, many PLC applications need two-way communication links. Therefore, the channel characteristics of both systems need to be observed when opting for using a single-relay or two-relay two-way PLC system. The comparison of the single-relay and two-relay two-way PLC system is not available in the existing research works.
- A well-known top-down PLC model was proposed by Zimmermann and Dostert, where the PLC channel model is represented by the sum of multipath components. Since the bottom-up approach is preferred for relay-assisted PLC system as it represents the topology of the power-line network, a new bottom-up channel model can be developed. The bottom-up multipath channel model has not been discussed in the existing research works.
- As relays can be considered as transceiver nodes, relay-assisted PLC systems need more power consumption than the conventional PLC systems. Thus, it is necessary to optimise power usage to meet the system requirement and establish a green communication infrastructure. The two-way AF relay system for indoor PLC network was optimised with QoS consideration. However, the direct link in the relay-assisted PLC system was not available in this system. In contrast, a direct link in a general broadcast-and-multiaccess (BMA) multicarrier relay-assisted PLC system was optimised to minimise the total power consumption. But this system works in time-division duplexing (TDD) mode and did not include the reverse channels. However, many PLC applications need two-way communication links. The two-way power-optimised relay-assisted PLC systems with a direct link between the source and destination nodes have not been discussed in the existing research works.

1.5 Research Problems

Based on the research gaps, the research problems occur are listed as follows:

- The thresholds should be carefully predetermined. Any samples exceeding the threshold are considered as being contaminated by impulsive noise, and they are nulled according to blanking nonlinear function. The selection of threshold values affects the instantaneous output SNR of the blanking preprocessor bank, which will be analysed using outage probability.
- The existing PLC channel models are still based on P2P links. The limitation of P2P PLC systems occurs due to the harsh nature of the power line channels. This creates difficulties in modelling the PLC channel. The half-duplex mode of the PLC system has limited the function of the node to transmit or receive a signal at one particular time.
- By applying QoS criteria as the lower-bound of the system capacity, an optimisation problem is developed to make the most efficient utilisation of the system power. As the optimisation problem is non-convex, the exact solution to the optimisation problem is hard to obtain.

1.6 Thesis Objectives

The objective of this research is to develop a new and innovative channel model and impulsive noise mitigation for PLC systems. Distinctively, the objectives are:

- To develop a new and innovative channel model and impulsive noise mitigation for PLC systems.
- To develop a new and optimum scheme for relay-assisted PLC systems with theoretical justifications using a computationally efficient convex optimisation algorithm.
- To verify and validate the effectiveness of all the proposed design schemes using numerical analysis and computer simulations.

1.7 Contributions and Thesis outline

1.7.1 Contributions

The contribution of this thesis is as follows. This thesis focuses on the channel modelling and the impulsive noise mitigation of PLC systems. Chapter 3 focuses on mitigating the effect of the impulsive noise of a OFDM-based PLC system. Orthogonal Frequency Division Multiplexing (OFDM) has been widely used to overcome the multipath fading, and yet, it is still not powerful enough to handle the impulse noise in PLC systems, thereby causing the performance of the PLC system to degrade. Chapter 3 proposes a blanking preprocessor bank to mitigate the impulse noise blindly into PLC systems, which outperforms the optimal blanking for bit-error-rate (BER) and outage probability. With the help of the relay, the performances of the PLC systems can improve as the relay has a short delaying process and easily implemented into the system. However, many PLC applications need two-way communication links. The highlight of Chapter 4-7 focuses on the two-way relay-assisted PLC system. Chapter 4 proposes a new channel modelling of the two-way relay-assisted PLC system with consideration of the direct link between the source and destination terminal nodes and analyse the performance of the proposed channel model in terms of the degree of correlation. Chapter 5 improves the performance of the two-way relay-assisted PLC system by adding another relay. Chapter 6 recommends a bottom-up multipath channel model that has a similar profile as the other bottom-up two-way relay-assisted PLC channel models. Chapter 7 presents the power allocation of the two-way single-relay PLC system with QoS considerations to optimise the total power consumption.

1.7.2 Thesis Outline

Chapter 2 discusses the fundamental knowledge on the OFDM in PLC system. Few types of relay modes for a relay-assisted PLC system are reviewed. Chapter 3 illustrates the proposed blanking preprocessor bank consisting of multiple blanking preprocessors with different thresholds to mitigate the impulse noise blindly without knowing the noise parameters in PLC systems. Chapter 4 explains the channel modelling of a two-way relay-assisted PLC system. The degree of correlation on the one-way and two-way channels are calculated and compared. In Chapter 5, the channel modelling is designed for two-way two-relay PLC systems. The channel characteristics of the two-way single-relay and two-way two-relay PLC systems are compared. Chapter 6 illustrates the proposed bottom-up multipath channel model for single-relay two-way PLC systems. Channel transfer function (CTF) of the bottom-up multipath model is compared with ABCD and voltage ratio approach (VRA) models. Chapter 7 analyses the optimal power of the proposed two-way relay-assisted PLC systems with the consideration of QoS constraints. Chapter 8 summarises this thesis and highlights some potential future works. The organisation of this thesis is as follows:

In Chapter 2, the fundamental knowledge about the OFDM-based PLC system is discussed. The OFDM model used in PLC system is reviewed. Two types of PLC channel modelling approaches are explained, i.e., the top-down approach, which is suitable to use when there is no relay in PLC system, and the bottom-up approach, which is preferred for relay-assisted PLC system. The existing Canate's point-to-point (P2P) channel model is used to get the transfer function. Different types of noises in PLC are discussed. In a relay-assisted PLC system, the relay nodes work in amplify-and-forward (AF) and decode-and-forward (DF) relaying modes. It is assumed that AF relay is used in this thesis.

In Chapter 3, a blanking preprocessor bank consisting of multiple blanking preprocessors with different thresholds is proposed. The proposed method does not need to know the noise parameter to mitigate the impulse noise in PLC systems. The threshold values are considered carefully where the lower and higher thresholds are set to be not too large and small, respectively. The results show that the proposed method outperforms the optimal blanking for BER and outage probability, even 50% of the best values is considered. Chapter 3 is based on the following journal publication:

- A. A. G. Liong, F. H. Juwono, L. Gopal, C. W. R. Chiong and Y. Rong, "Multiple Blanking Preprocessors for Impulsive Noise Mitigation in OFDM-based Power-line Communication Systems," Int. J. Electrical Power Energy Systems, vol. 130, Sept. 2021.

In Chapter 4, the modelling of the circuit and relay-assisted channels are discussed. With the channel characteristics and circuit model, the CTF of a two-way relay-assisted PLC channel is derived. Simulation results indicate that the proposed two-way relay-assisted PLC channel has a high correlation among the path compared to one-way. Chapter 4 is based on the following conference publication:

- A. A. G. Liong, L. Gopal, F. H. Juwono, C. W. R. Chiong and Y. Rong, "A Channel Model for Three-node Two-way Relay-aided PLC Systems," IEEE Int. Conf. Signal Image Process. Appl. (ICSIPA), Kuala Lumpur, Malaysia, Sept. 17-19, 2019, pp. 52-57.

In Chapter 5, the single-relay PLC system is extended to two-relay PLC system. The technique of modelling the channel is presented, and the CTFs are derived. Based on the proposed design scheme, the composite CTF for a certain link can be found by summing the respective CTFs of the constructive segments. The results show that two-way two-relay systems are better in taking advantage of the number of relays for non-direct links while two-way single-relay PLC systems work well for direct channel transmission only.

Chapter 5 is based on the following conference publication:

- A. A. G. Liong, L. Gopal, F. H. Juwono, C. W. R. Chiong and Y. Rong, "Channel Characteristics Comparison of Single-Relay and Two-Relay Two-Way PLC Systems," IEEE Int. Conf. Comp. Commun. Netw. Technol. (ICCCNT), West Bengal, India, Jul. 1-3, 2020.

In Chapter 6, the model of a bottom-up multipath channel for single-relay two-way PLC systems is proposed. This model is derived based on the parameter modification of the top-down Zimmermann-Dostert model. The modelling and formulation of the proposed bottom-up multipath, ABCD, and VRA models are discussed. The simulations of the models are compared, which showed that the proposed model does not have much fluctuation compared with the ABCD and VRA models. In the direct path, the three models give similar CTFs. In the SRD path, the proposed model has similar attenuation as the ABCD model at high frequencies. Whereas, for the DRS path, the proposed model has better attenuation than ABCD at high frequencies. Chapter 6 is based on the following conference publication:

- A. A. G. Liong, L. Gopal, F. H. Juwono, C. W. R. Chiong and Y. Rong, "A Comparison of Three-node Two-way PLC Channel Models," IEEE Int. Conf. Adv. Technol. Commun. (ATC), Nha Trang, Vietnam, Oct. 8-10, 2020.

In Chapter 7, the system model of a two-way relay-assisted multi-carrier scheme is proposed for an indoor PLC system. The optimal powers are derived with the consideration of QoS constraint. Since QoS constraint power allocation is highly non-convex, the alternating optimization (AO) algorithm is used to decompose the problem to sub-problems. Using Karush-Kuhn-Tucker (KKT) condition, the problems are solved. The numerical examples show that AO algorithm has a short processing delay, and more transmission power is needed to increase the minimal averaged subchannel capacity (ASC) requirement in order to meet the QoS constraint in a relay-assisted PLC system. The proposed system

is able to make the system attain the same QoS requirement with less total power compared with the conventional bidirectional direct transmission (BDT) system and with insignificant additional power compared with the relay-assisted two-way information exchange (R2WX) system. Chapter 7 is based on the following article that has been submitted to:

- A. A. G. Liong, L. Gopal, F. H. Juwono, C. W. R. Chiong, Y. Rong and Z. Zang, "Power Optimization of a Three-Node Two-Way Relay-assisted Power Line Communications Systems," IEEE Trans. Smart Grid, submitted, Jul. 2021.

In Chapter 8, this thesis concludes with the main highlight of this research in each chapter. There are some interesting topics given out for future research.

Chapter 2

OFDM-based PLC System

This chapter discusses the OFDM-based PLC system. Section 2.1 analyses and discusses the OFDM model used in PLC system. Section 2.2 reviews the channel modelling approaches and the existing P2P PLC channel model. Different types of noise modelling are discussed in Section 2.3. In Section 2.4, two relay processing methods available in relay-assisted PLC system are illustrated. Finally the chapter is briefly summarised in Section 2.5.

2.1 Orthogonal Frequency Division Multiplexing

OFDM is among one of the best methods of digital data transmission over a limited bandwidth using the well-known digital multicarrier communication technique. The limited bandwidth causes an increase in the symbol duration, which reduces the effect of multipath delay spreading on the signal. The basic OFDM model used in PLC system is shown in Figure 2.1 [36]–[40].

The input data is applied to the channel coding for achieving higher reliability. The coding scheme is designed to detect and correct independent errors. The interleaving technologies are used for eliminating the development of bulk

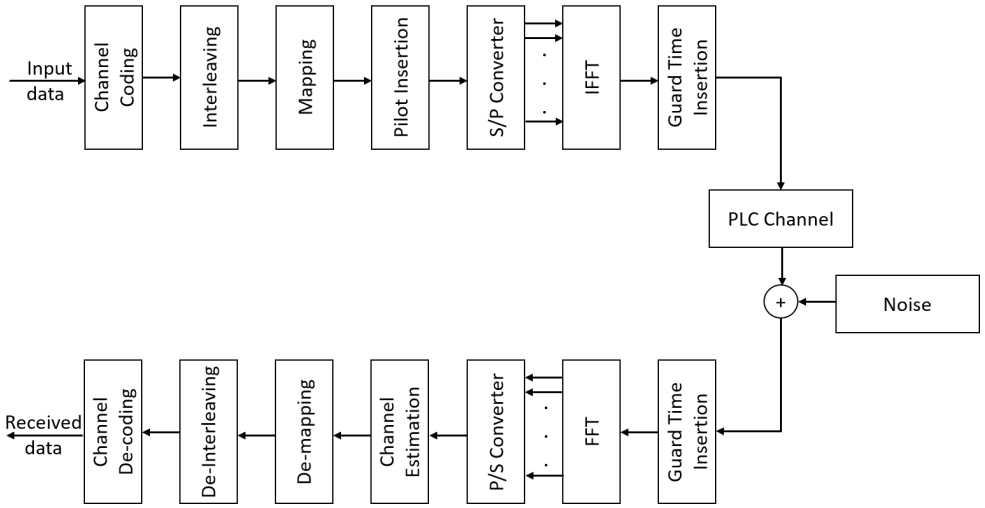

Figure 2.1: OFDM-based PLC system

errors during the transfer by altering the order of symbols within the stream of coding between two encoders. The data bits mentioned are transferred to become symbols through the mapping block. Pilot insertion synchronises time and frequency using particular pilot symbols. Both coherent modulation and pilot insertion are needed for channel estimation in OFDM system. The data for the subcarriers is arranged using a serial to parallel (S/P) converter. Time-domain signals are created by using the inverse discrete Fourier transform (IDFT). The analog OFDM time-domain signal is given by

$$x(t) = \frac{1}{N} \sum_{k=0}^{N-1} X\,[k]\, e^{j2\pi kt/T_d} \quad \text{for} \quad 0 \leq t \leq T_d, \tag{2.1}$$

where $X[k]$ is the frequency domain signal, N is the number of subcarriers and T_d is the symbol duration. The n-th sample of the digital OFDM signal at $T_s = T_d/N$ is given by

$$x_n = IDFT\{X[k]\} = \sum_{k=0}^{N-1} X[k] e^{j2\pi kn/N}, \tag{2.2}$$

In every OFDM symbol, the guard interval and cyclic prefix (CP) are introduced to solve and eliminate both inter-symbol interference (ISI) and inter-carrier interference (ICI). The main cause of ISI and ICI is the loss of orthogonality of

the time-variance of the power-line channel between subcarriers. Next, the user's data is sent to PLC channel and the noise.

On the other hand, the receiver removes the CP, applies the discrete fourier transform (DFT), and converts from parallel to serial to obtain the required frequency domain signal. Channel estimation is applied to the serial data and then transfers the symbols into data bits de-mapping. Lastly, the decoding is used to achieve the initially transmitted data bits.

2.2 Channel Modelling

Designing a PLC system requires the channel characteristics and the knowledge model. In fact, there are research works on the power-line channel modelling to assist PLC research. In general, PLC channel models are grouped into top-down (parametric) approach and bottom-up (physical) approach. In each group, it can be distinguished into a deterministic and statistical model. The deterministic model focuses on the description of one or a small set of PLC channel realisations. In contrast, the statistical model focuses at reflecting a wide range of channel realisations according to their probability of occurrence. The statistical model is considered in this thesis.

The top-down approach uses parameters to describe the channel and behaviour characteristics of PLC networks. The parameter values are derived from statistical analysis based on measurement. This approach can work in either the time domain or frequency domain. However, it is hard to connect with the physical topology due to the difficulties in setting up large test loops with physical characteristics and configurations. Thus, this approach is considered when there is no relay in PLC system.

The bottom-up approach represents the topology of the power-line network. It implements the transmission line (TL) theory to obtain the CTF using the network information [41]–[43]. This approach is convenient to characterise power line channels with relay as relaying makes data transmission more reliable in long-

distance communication [44]. However, a fixed structural model with various physical network behaviour is difficult to get for indoor PLC channels due to the different topology of the power network and its harsh nature. Yet, many researchers are able to model the PLC channel. In [31], [43], [45], a random channel simulator based on a bottom-up approach has been found using the topology generator.

Of all channel modelling approaches, the bottom-up approach is preferred for this thesis as the approach deals with relay-assisted PLC systems which represents the topology of the power-line network. Authors in [46] show that the indoor PLC has a time-varying nature or so-called as the linear periodical time-varying (LPTV) system. In LPTV, the frequency response gain varies over the main period [47]. Therefore, the channel parameters do not change within one signalling phase in order to have a quasi-stationary P2P PLC channel. However, relay-assisted PLC channel will change over different signalling phases. This thesis uses Canate's P2P channel model from [46] as a basic tool to solve the relay-assisted PLC channel modelling problem, and the details of this model are discussed below.

2.2.1 Network Structure

The simplified network layout of Canate's hybrid P2P channel model is given in Fig. 2.2. It consists of four segments between transceivers and three branches terminated with load impedances $Z_{b,1}$, $Z_{b,2}$ and $Z_{b,3}$.

2.2.2 Cables

A power cable pair is included in each segment, where it is characterised based on the types, parameters, and lengths. The five commonly used cables with their characteristics are shown in Table 2.1 [48]. ε_{eq} and Z_0 are the relative permittivity of the material and characteristic impedance, respectively. R, L, C and G are the per-unit-length resistance (Ω/m), inductance (H/m), capacitance (F/m), and

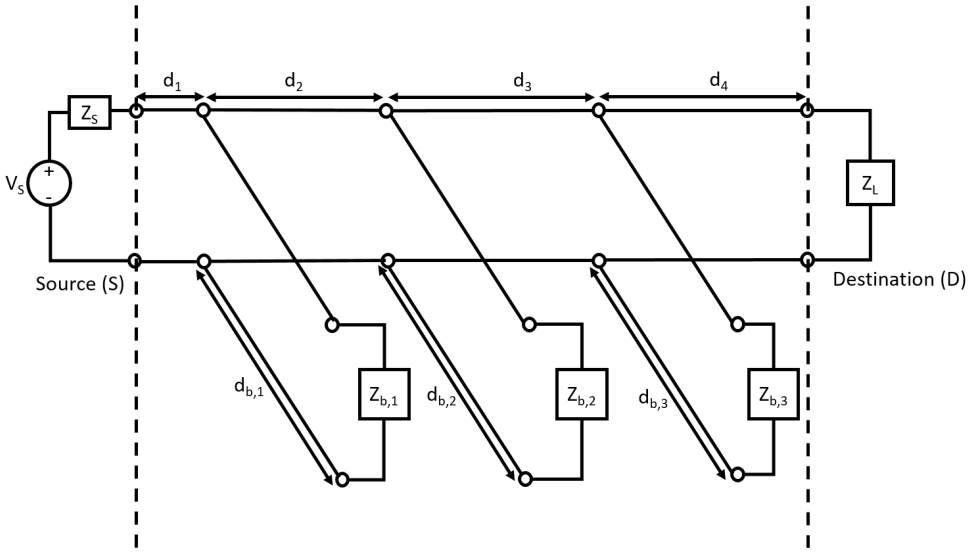

Figure 2.2: Network layout of segment

Table 2.1: Characteristics of indoor power cables

Cable type index	1	2	3	4	5
$section(mm^2)$	1.5	2.5	4.0	6.0	10.0
ε_{eq}	1.45	1.52	1.56	1.73	2.00
$Z_0(\Omega)$	270	234	209	178	143
$C(pF/m)$	15	17.5	20	25	33
$L(\mu H/m)$	1.08	0.96	0.87	0.78	0.68
R_0	12	9.34	7.55	6.25	4.98
G_0	30.9	34.7	38.4	42.5	49.3
$R = R_0 10^{-5}\sqrt{f}(\Omega/m)$					
$G = 5G_0 10^{-14} 2\pi f(S/m)$					

Table 2.2: Parameters for Canate's PLC channel model

Line section	Length	Cable type	Terminated load
Backbone 1	d_1	n_{d_1}	N/A
Branch-tap 1	$d_{b,1}$	$n_{d_{b,1}}$	$Z_{b,1}$
Backbone 2	d_2	n_{d_2}	N/A
Branch-tap 2	$d_{b,2}$	$n_{d_{b,2}}$	$Z_{b,2}$
Backbone 3	d_3	n_{d_3}	N/A
Branch-tap 3	$d_{d,3}$	$n_{d_{b,3}}$	$Z_{b,3}$
Backbone 4	d_4	n_{d_4}	N/A
Transmitting inner impedance: Z_S			
Receiving load impedance: Z_L			

conductance (S/m), respectively. Thus, the characteristic impedance, $Z_0(f)$ and the propagation constant, $\gamma(f)$ of TL theory can be calculated as below [49].

$$Z_0(f) = \sqrt{\frac{R + j2\pi fL}{G + j2\pi fC}} \tag{2.3}$$

$$\gamma(f) = \sqrt{(R + j2\pi fL)(G + j2\pi fC)} \tag{2.4}$$

2.2.3 Loads

In P2P PLC model, the three loads ($Z_{b,1}$, $Z_{b,2}$ and $Z_{b,3}$) can behave in three states, which are (1) constant impedance, (2) time-invariant frequency-selective impedance and (3) time-varying frequency-selective impedance. It is assumed that only the first two states, constant impedance and time-invariant frequency-selective impedance are considered for simplicity. With the information shown in Table 2.2, the frequency response of a P2P PLC channel is calculated using TL theory which will be discussed in Chapter 4.

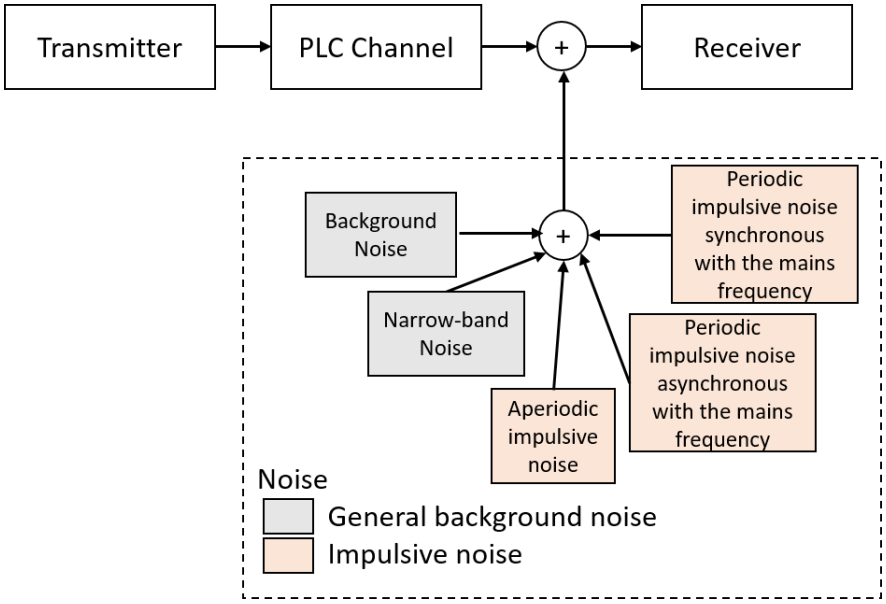

Figure 2.3: Network layout of noise

2.3 Noise Modelling

The power line is not designed to be used at high-frequency signal transmission because it will be interfered by various noises in high-frequency [50], [51]. The noise in PLC systems mentioned in Section 2.1 consists of five types of noise, which are classified into two classes, namely general background noise and impulsive noise as illustrated in Fig. 2.3.

2.3.1 General Background Noise

Background noise is caused by the sum effect of several low power noise sources. For example, power spectral density (PSD) the electronic equipment decreases as frequency increases [52]. Meanwhile, narrow-band noise is a sinusoidal signal with a modulated amplitude caused by medium and short wave broadcasts. The consideration of combining both background and narrow-band noises gives general background noise (GBN).

Table 2.3: PDF of N_0, N_1 and f_1 for the background noise

Parameter	N_0	N_1	f_1
Unit	dBm/Hz	dBm/Hz	MHz
Distribution	Normal	Uniform	Shifted Exponential
	$\sigma_{N_0} = 1.29$	$a_{N_1} = 23.06$	$\lambda_{f_1} = 1.3$
	$\mu_{N_0} = -135$	$b_{N_1} = 74.97$	$f_{shift} = 0.096$

Normally, GBN has a stable PSD. The noise in PLC cannot be modelled as simple additive white Gaussian noise (AWGN) due to the presence of power converters and electrical components. Since there is not an acceptable impulse noise available, the impact of GBN is considered where the PSD of the GBN noise is assumed to be stationary over a long period.

Based on extensive measurements, Benyousef proposed a synthesis power process where a white Gaussian noise (WGN) is passed through a coloured filter to give an approximate stationary GBN [53]. Since Benyousef's noise model is used to generate noise samples to test the relay schemes, some details of this model are mentioned. Modelling GBN can be done by superposition the background noise and the narrow-band noise [54]. There is a need to add a colouring filter to each component to give a stationery PSD function independently.

(a) Background noise. The PSD of the background noise can be expressed using first-order exponential function [55].

$$S_{BN}(f) = N_0 + N_1 exp(-\frac{f}{f_1}), \tag{2.5}$$

where f, N_0, N_1 and f_1 are frequency and the parameters of the exponential function. Table 2.3 give the power density function (PDF) of the N_0, N_1 and f_1 under the scenario of office building.

Table 2.4: PDF of N, $B^{(k)}$ and $A^{(k)}$ for the narrow-band noise

Parameter	N	$B^{(k)}$	$A^{(k)}$
Unit		MHz	dBm/Hz
Distribution	Normal	Shifted Exponential	Normal
$f \in (0-30\text{MHz})$	$\sigma_N = 12$ $\mu_N = 1.4$	$\lambda_{B^{(k)}} = 0.33$ $B_{shift} = 0.19$	$\sigma_{A^{(k)}} = 16.6$ $\mu_A = 4.8$

(b) Narrow-band noise. The PSD of Gaussian function of k-th (out of N) narrow-band noise is [55]

$$S_{NN}^{(k)}(f) = A^{(k)} exp\left[-\frac{\left(f - f_0^{(k)}\right)^2}{2\left(B^{(k)}\right)^2}\right], \tag{2.6}$$

where $A^{(k)}$, $B^{(k)}$ and $f_0^{(k)}$ are amplitude, bandwidth and center frequency of the Gaussian function, respectively. Meanwhile, N is the total number of interference. Table 2.4 give the PDF of N, $B^{(k)}$ and $A^{(k)}$ for the scenario of office building.

The GBN samples can be found by the total sum of PSD used for background and narrow-band noises from (2.5) and (2.6).

The PSD can be illustrated as

$$\begin{aligned} S_{GBN}(f) &= S_{BN}(f) + \sum_{k=1}^{N} S_{NN}^{(k)}(f) \\ &= N_0 + N_1 e^{-\frac{f}{f_1}} + \sum_{k=1}^{N} A^{(k)} exp\left[-\frac{\left(f - f_0^{(k)}\right)^2}{2\left(B^{(k)}\right)^2}\right]. \end{aligned} \tag{2.7}$$

2.3.2 Impulsive Noise

Due to its high amplitudes that can surpass 50dBs, impulsive noise in PLC system has become the biggest cause of communication problems when compared to other type of noise [56]. In the literature, the three most common impulse noise models are Bernoulli-Gaussian (BG), Middleton Class A (MCA) and Symmetric α-stable (SαS) [57]. These three impulse noise models are discussed and compared as follows.

(a) The BG is a statistical model for impulsive noise, which has a two-component Gaussian mixture model as well as a special case of MCA PDF [58]. The BG impulse noise is formulated as [59]

$$i_n = b_n \cdot g_n, \tag{2.8}$$

where n is the discrete-time index, b_n is the occurrence of the impulse noise having a Bernoulli sequence of 0 and 1, with the probabilities of $1-p$ and p, respectively, and g_n is its amplitude having a random Gaussian distribution with zero mean and $2\sigma_g^2$ variance. Therefore, the total noise $n_{n,BG}$ is the sum of general background noise, w_n and the BG impulse noise, i_n.

$$n_{n,BG} = w_n + i_n. \tag{2.9}$$

The PDF of a BG noise, $n_{n,BG}$ is given by [60]

$$f_{n_n}(n_{n,BG}) \quad = \quad (1-\psi)G(n_n, 0, \sigma_w^2) + \psi G(n_n, 0, \sigma_w^2 + \sigma_g^2), \tag{2.10}$$

where ψ is the probability of occurrence of impulsive noise and $G(x, 0, \sigma^2) = \frac{1}{\sqrt{2\pi\sigma^2}} \exp(-(\frac{x^2}{2\sigma^2}))$. The BG model has a wide range of applications such as multicarrier quadrature amplitude modulation (QAM) [59], OFDM [61] and PLC systems [62].

(b) Another significant statistical model for PLC impulsive noise modeling is the MCA distribution, which comprises of large number of Gaussian random variables with varying variances [63]. Because of the simplicity of its PDF, MCA distribution is often used as impulsive noise model in PLC systems. The PDF of a complex-valued MCA noise, $n_{n,MCA}$ is given by [64]

$$f_{n_n}(n_{n,MCA}) = \sum_{m=0}^{\infty} \frac{e^{-A_i} A_i^m}{m!} \frac{1}{\sqrt{2\pi\sigma_m^2}} exp\left(-\frac{|n_{n,MCA}|^2}{2\sigma_m^2}\right), \quad (2.11)$$

where $\sigma_m^2 = \left(1 + \frac{1}{\Gamma}\right)\left(\frac{m/A_i+\Gamma}{1+\Gamma}\right)\sigma_b^2$, σ_b^2 is the background noise variance, Γ_n is the background-to-impulse noise ratio, and A_i is the impulsive index . MCA noise has a narrower bandwidth than receiver and is normally used in electromagnetic and communication problem.

(c) In recent years, SαS model has developed as an essential alternative to model impulsive noise given the fact that MCA and BG models cannot accurately characterize tail characteristics [65]. Unlike the two models, SαS model could not obtain the output SNR of the nonlinear preprocessor due to the absence of closed-form PDF expression and does not follow Gaussian distribution [66]. SαS model is commonly used with a variety of applications, including diversity combining techniques for single-user communication [67] and near optimal receiver design [68].

2.4 Relay Processing at Relay Nodes

There are few types of relaying modes: amplify-and-forward (AF) and decode-and-forward (DF), for a relay-assisted PLC system to work.

For the regenerative scheme or so-called DF relaying, the received signal is first decoded at the relay node before being re-encoded and forwarded to the destination node. In the DF relaying, the relay works in two ways, which are (1)

the relay node keeps working without carrying its received signal, which results in a low SNR and causes no improvement to the system performance and (2) the relay will forward signal only when the received signal is fully decoded [69], [70].

For a non-regenerative scheme, or so-called AF relaying, the received signal is amplified and then forwarded to the destination. This makes the AF relay scheme having shorter processing delays and easy to implement as it is less complicated [71]–[73]. In this thesis, it is assumed that AF relay is used in relay nodes as it have lower computation load and can be easily implemented in PLC system.

Since all signalling paths used the same power cables, the signalling paths are highly correlated in PLC system. Adding a relay device in a PLC systems is not straight forward and will affect the channel modelling as the existing P2P PLC channel models cannot be directly used to the relay-assisted PLC systems. Further details on channel modelling of a relay-assisted PLC systems are discussed in Chapter 4.

2.5 Chapter Summary

In this chapter, the basic OFDM-based PLC system is discussed. OFDM has been widely used to overcome the impairments from high-frequency signal transmission. The PLC channel and noise model play an important role in the OFDM-based PLC system. The two types of channel modelling are mentioned. Considering the two-channel approaches, the top-down approach is used when there is no relay in the PLC systems. On the other hand, the bottom-up approach is preferred for relay-assisted PLC systems where Canate's P2P channel model is used to get the CTF. Moreover, the different types of noises in PLC are discussed and analysed too. An approximate stationary GBN can be obtained using the proposed method by Benyousef. Meanwhile, these three impulsive noise model are discussed and compared too. In a relay-assisted PLC system, the relay nodes work in two modes, i.e. AF and DF. It is assumed that AF relay is used in this thesis as AF relay can be easily implemented into PLC system.

Chapter 3

Blanking Preprocessor Bank

Since the power-line is not designed for high frequency signal transmission, it suffers from frequency-selective fading and noise. OFDM has been widely used to overcome the multipath fading, and yet, it still not appropriate to handle the impulsive noise in PLC system, thereby causing the performance of the PLC system to degrade. In this chapter, a blanking preprocessor bank, which consists of multiple blanking preprocessors with different thresholds, is proposed to mitigate the impulsive noise blindly without knowing the noise parameters in PLC systems. Its performance is compared with the optimal blanking preprocessor. An introduction of blanking is described in Section 3.1. Section 3.2 represents the system model of the proposed blanking preprocessor bank. The numerical examples will be shown in Section 3.3 through simulations. Finally, the chapter summary is highlighted in Section 3.4.

3.1 Introduction

As a power-line was not designed to transmit data with high frequency, it suffers from frequency-selective fading and noise [50], [51]. Frequency-selective fading is caused by multiple branches of the power-lines and impedance mismatches. On the other hand, noise in a power-line cannot be modelled as a simple AWGN due

to the presence of power converters and electrical components. In PLC systems, the noise consists of background, narrowband, and impulsive noise [56]. Both background noise and narrowband noise have a slowly changing root mean square (rms) amplitude so that they are usually combined and modelled as AWGN [74], [75]. In contrast, the RMS amplitude of impulsive noise changes rapidly in a short duration, and its occurrence is random. It is common to model impulsive noise as a Bernoulli-Gaussian random process [59] in BB-PLC and cyclostationary random process in NB-PLC [76], [77].

Multicarrier modulation techniques have been proposed for PLC. DFT- and wavelet transform (WT)- orthogonal OFDM have been widely used to overcome these impairments in PLC systems [78]–[81]. OFDM has been widely used to overcome these impairments. Although OFDM is well known to work well in multipath fading, it is not powerful enough to handle the impulsive noise in PLC systems, thereby leading to performance degradation. This chapter is focused on DFT-OFDM-based (or simply 'OFDM-based') BB-PLC.

There have been many techniques proposed by researchers to mitigate the effect of impulsive noise. In the literature, they can be grouped into threshold-based, compressive sensing-based, and hybrid techniques [82]. The threshold-based techniques include nonlinear preprocessing and iterative methods. In threshold-based techniques, any samples exceeding the threshold are considered contaminated by impulsive noise, and they are treated according to blanking nonlinear function. The nonlinear preprocessing methods include clipping, blanking, joint blanking/clipping, deep clipping [79], and adaptive joint blanking/clipping methods [83]. The iterative methods, such as in [84], [85], can be further employed to improve the nonlinear preprocessing. In addition to the nonlinear preprocessor, the iterative method can be combined with an artificial neural network, as proposed in [86]. On the other hand, the compressive sensing technique uses null-subcarriers of the OFDM symbol to reconstruct the sparse impulsive noise. Algorithms for impulsive noise reconstruction available in the literature include,

among others, smoothed-ℓ_0 (SL0) [87], sparse Bayesian learning [76], and multiple signal classification (MUSIC) [51]. Finally, the hybrid method combines the threshold-based and compressive sensing techniques, such as proposed in [88].

In this chapter, blanking nonlinear preprocessors are used since they have the simplest characteristic and have been used in many works [16], [89]–[91]. In order to obtain optimal performance, an optimal threshold needs to be obtained. It is worth mentioning that an incorrect threshold may lead to significant performance degradation [92]. Getting the optimal threshold of a blanking preprocessor is not an easy task as the optimal threshold depends on the impulsive noise parameters [16], [79]. Therefore, it is common to assume that the noise parameters are available to the receiver, which is not practical. Alternatively, it can estimate the noise parameters at the receiver [77]. An approach of getting the good performance of blanking nonlinear preprocessor without estimating the noise parameters is to use the information from the received signal as proposed in [84]. However, the scheme in [84] needs a complex structure that employs feedback loops and requires additional computation for getting the received signal properties.

This chapter proposes a simple blanking preprocessor bank consisting of multiple blanking preprocessors with different thresholds which can handle the impulsive noise without prior information. The individual output from each preprocessor is then weighted and combined with other weighted outputs. The thresholds should be carefully predetermined to make the system perform satisfactorily.

Furthermore, as OFDM signals have a large peak-to-average power ratio (PAPR), the blanking nonlinear preprocessor may falsely detect the impulsive noise. Some works have proposed using PAPR reduction technique to reduce the false alarm [93]–[95]. In this chapter, the effect of the PAPR reduction technique will also be evaluated based on the system performance. Here, the clipping method used in [78] is adopted, which will not deteriorate the BER performance as the PAPR reduction technique.

The selection of threshold values affects the instantaneous output SNR of the blanking preprocessor bank, which will be analyzed using outage probability. On the other hand, the BER performance of the blanking preprocessor bank is better compared with the one using the optimal blanking preprocessor. The contributions are summarized as follows:

- Propose a blind blanking nonlinearity scheme where the optimal threshold is not required to be predetermined.
- Evaluate the effect of PAPR reduction on the performance of the proposed scheme.
- Compare the proposed system with the one using the SL0 technique.

3.2 System Model

A bit-interleaved coded modulation (BICM) scheme for OFDM-based PLC system is adapted as shown in Fig. 3.1 [96]. Note that in this chapter, all variables used are in vector notation. Information sequence $\mathbf{u} = \{0, 1\}$ is generated and passed to a convolutional encoder to obtain a codeword $\bar{\mathbf{c}}$, where $\bar{\mathbf{c}} \in \mathcal{C}$ and $\mathcal{C}$ is the coding scheme defined over $\{0, 1\}$. A constellation set, $\mathcal{X}$, of size 2^m is used. A random ideal interleaver is applied to interleave the codeword over N OFDM subcarriers. Among N subcarriers, only K subcarriers are used to carry data and $N-K$ subcarriers are nulled. Note that the pratical PLC also employs some null subcarrier. The interleaved codeword is given by

$$\mathbf{c} = [c_{0,1}, c_{0,2}, \cdots, c_{k,u}, \cdots, c_{N-1,m}], \tag{3.1}$$

where $c_{k,u}$ is the coded bit at the u-th label ($u = 1, \cdots, m$) of the k-th subcarrier. The coded bits are then mapped by the M-QAM or M-PSK modulator, where $M = 2^m$ as mentioned previously. The modulated signal vector, $\mathbf{X} = [X_0, \cdots, X_k, \cdots, X_{N-1}]^T$, where $(\cdot)^T$ denotes the transpose operation, is then formed the OFDM signal, $\mathbf{x} = [x_0, \cdots, x_n, \cdots, x_{N-1}]^T = \mathbf{F}^H\mathbf{X}$, where $\mathbf{F}$ is

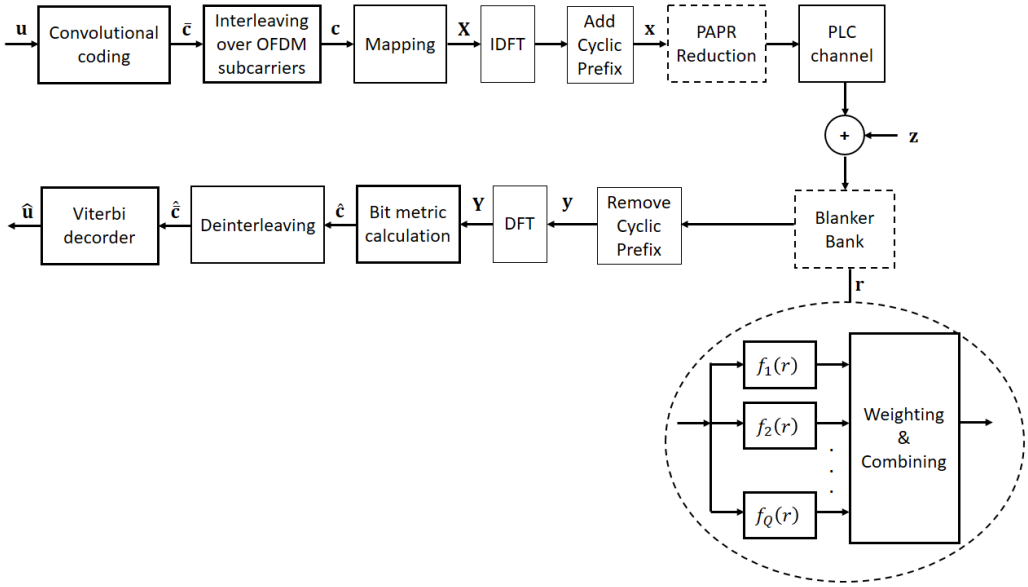

Figure 3.1: System Model of BICM scheme.

the DFT unitary matrix and $(\cdot)^H$ denotes the Hermitian operator. As a result, the OFDM signal can be expressed as

$$x_n = \frac{1}{\sqrt{N}} \sum_{k=0}^{N-1} X_k e^{j2\pi nk/N}. \tag{3.2}$$

A PAPR reduction technique may be applied to the OFDM signal after appended by a cyclic prefix. Cyclic prefix is used to overcome ISI. Without loss of generality, the transmit power is assumed to be unity. The received signal, $\mathbf{r} = [r_0, \cdots, r_n, \cdots, r_{N-1}]^T$ is given by

$$\mathbf{r} = \mathbf{s} + \mathbf{z}, \tag{3.3}$$

where $\mathbf{s} = [s_0, \cdots, s_n, \cdots, s_{N-1}]^T = \mathbf{Hx}$ is the channel output, $\mathbf{H}$ is the $N \times N$ circulant matrix of the PLC channel impulse response (CIR), $\mathbf{h} = [h_0, \cdots, h_n, \cdots, h_{N_t-1}]^T$, where N_t is the number of channel taps, and $\mathbf{z} = [z_0, \cdots, z_n, \cdots, z_{N-1}]^T$ is the total PLC noise which consists of AWGN and impulsive noise.

At the receiver, the blanking nonlinear preprocessor bank, $f(\cdot)$, is applied to $\mathbf{r}$, resulting in $\mathbf{y} = [y_0, \cdots, y_n, \cdots, y_{N-1}]^T$ after removing the cyclic prefix. The

output of the blanking preprocessor bank is then input to the OFDM demodulator, $\mathbf{Y} = [Y_0, \cdots, Y_k, \cdots, Y_{N-1}]^T = \mathbf{F}f(\mathbf{r})$. The optimal maximum likelihood (ML) bit metric is given by [97]

$$\hat{\mathbf{c}} = \arg\min_{\mathbf{c}\in\mathcal{C}} \sum_{k=0}^{N-1} \sum_{u=1}^{m} \lambda(Y_k, c_{k,u}), \tag{3.4}$$

where $\lambda(Y_k, c_{k,u})$ is the bit metric for the u-th bit at the k-th subcarrier given by

$$\lambda(Y_k, c_{k,u}) = \min_{X_k \in \mathcal{X}^u_{c_{k,u}}} |Y_k - G(k,k)X_k|^2, \tag{3.5}$$

$\mathcal{X}^p_q$ denotes the subset of all the information symbols whose p-th bit has the value of $q \in \{0, 1\}$, and $G(k, k)$ is the k-th diagonal component of $\mathbf{G} = \mathbf{FHF}^H$. The bit metric is then used by the Viterbi decoder to extract the information.

3.2.1 PAPR Reduction Technique

In this chapter, the peak amplitude clipping is used as discussed in [78]. The peak amplitude clipping block diagram is shown in Fig. 3.2. Without loss of generality, the oversampling factor is set to be unity. Oversampling is used to obtain denser discrete-time samples from a continuous-time signal. It is useful to analyze the performance of PAPR reduction. Many researchers suggested that the oversampling factor is set at least four to get a more accurate PAPR distribution. As the focus of this chapter is not PAPR reduction, i.e., the effect of PAPR reduction on the system performance is shown, where the unity oversampling factor is used for the sake of simplicity.

The OFDM signal is transmitted to the clipping block which is formulated as

$$\hat{x}_n = \begin{cases} x_n, & |x_n| \leq A_c, \\ 0, & \text{otherwise}, \end{cases} \tag{3.6}$$

where A_c is the peak amplitude clipping threshold; the clipping noise is then

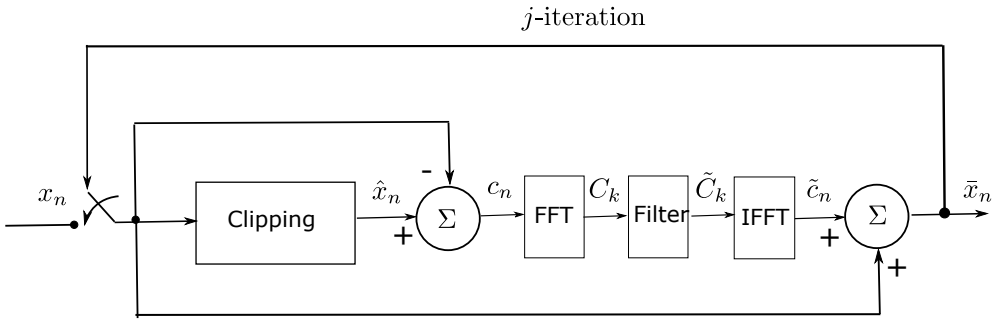

Figure 3.2: Peak amplitude clipping.

calculated by subtracting x_n from $\hat{x}_n$. The clipping noise is transformed into the frequency domain, C_k through FFT. Let $\mathcal{N}$ be the set of indices of null subcarriers, and $\mathcal{N}^c$ be the complement. The following filtering process is then performed as

$$\tilde{C}_k = \begin{cases} C_k, & k \in \mathcal{N}, \\ 0, & k \in \mathcal{N}^c. \end{cases} \tag{3.7}$$

The time-domain filtered clipping noise signal, $\tilde{c}_n$, is obtained through IFFT. Finally, $\tilde{c}_n$ is summed with x_n to get $\bar{x}_n$. The process can be iterated to suppress the peak regrowth.

3.2.2 PLC Channel Model and Noise Model

The PLC channel can be modelled using the existing L-path channel model given by [98]

$$H(f) = \sum_{i=1}^{L} g_i e^{-(a_0 + a_1 f^{\zeta})d_i} e^{-j2\pi f \tau_i}, \tag{3.8}$$

where the variables are defined in Table 3.1. Also, the CIR is normalised such that $\sum |h_n|^2 = 1$.

As mentioned previously, the total PLC noise consists of AWGN and impulsive noise, i.e. $\mathbf{z} = \mathbf{n} + \mathbf{i}$. The AWGN is a Gaussian vector with mean 0 and variance $2\sigma_n^2$.

Table 3.1: PLC channel parameters

Notation	Description	Remark
g_i	gain factor for path i	
a_0 and a_1	attenuation parameters	
ζ	exponent of the attenuation factor	between 0.5 and 1
d_i	length of branch i	
τ_i	delay at branch i	$\tau_i = d_i\sqrt{\epsilon_r}/c_0$
ϵ_r	Dielectric coefficient	
c_0	speed of light	$c_0 = 3 \times 10^8$ m/s

On the other hand, the impulsive noise is modelled as the Bernoulli-Gaussian process, which mathematically can be expressed as

$$\mathbf{i} = \mathbf{b} \circ \mathbf{g}, \tag{3.9}$$

where $\mathbf{b}$ is a sequence vector of 1 and 0 with probability of p and $1-p$, respectively, $\mathbf{g}$ is a vector of AWGN with mean 0 and variance of $2\sigma_g^2$, and '$\circ$' denotes the Hadamard product. The impulsive noise is characterized by a signal-to-impulsive noise ratio given by $SINR = 1/2\sigma_g^2$.

3.2.3 Proposed Blanking Preprocessor Bank

The blanking preprocessor bank consists of Q blanking preprocessors with different thresholds. Each blanking preprocessor is denoted by $y_n^q = f_q(\cdot)$, where $q = 1, \cdots, Q$, and given by

$$y_n^q = \begin{cases} r_n, & |r_n| \leq T_q, \\ 0, & \text{otherwise}, \end{cases} \tag{3.10}$$

To better analyse the nonlinear preprocessing characteristic, a linearised form is commonly used as follows

$$y_n^q = \alpha_q s_n + d_n, \tag{3.11}$$

where α_q is a real-valued constant chosen such that $E[d_n s_n^*] = 0$, '$*$' is the complex conjugate operator and $E[\cdot]$ denotes expectation, and d_n can be considered as the blanking noise. Note that it is preferred to carefully choose the threshold such that $\alpha_q \approx 1$ [79].

The constant α_q is defined by $\alpha_q = E[y_n^{q*} s_n]$. As a nonlinear preprocessor processes the blanking operation on an OFDM symbol level, in practice, α_q is approximated for each blanking block with $\alpha_q = 1 - N_B^q/N$, where N_B^q is the number of blanked samples in the q-th preprocessor [99]. This way, the preprocessor does not need the knowledge of the noise or transmit signal statistics.

It is obvious that (3.11) is similar to received signal in multiple fading paths. Furthermore, the output SNR of each blanking preprocessor can be calculated by

$$\begin{aligned} \gamma_q &= \frac{E[|\alpha_q s_n|^2]}{E[|y_n^q - \alpha_q s_n|^2]} \\ &= \left(\frac{E[|y_n^q|^2]}{\alpha_q^2} - 1 \right)^{-1}. \end{aligned} \tag{3.12}$$

Note that $E[|s_n|^2] = 1$ as assumed previously.

The output of the blanking preprocessor bank is given by

$$y_n = \sum_{q=1}^{Q} w_q y_n^q, \tag{3.13}$$

where w_q is the weight for q-th preprocessor. Following maximal ratio combining (MRC) scheme, an optimal performance can be obtained using $w_q = \alpha_q$.

Table 3.2: PLC channel parameters for real-world networks

Path No	1	2	3	4
d_i (meters)	150	188	264	397
g_i	0.4	-0.4	-0.8	-1.5
$\zeta = 0.5$, $a_0 = 0$, $a_1 = 8 \times 10^{-6}$, $\epsilon_r = 4$				

3.3 Numerical Examples

This chapter used a BICM OFDM PLC system with quadrature phase shift keying (QPSK) modulation, the number of subcarriers is $N = 512$, and only $K = 480$ subcarriers carry data. The null subcarriers are selected to be positioned at low frequencies. The convolutional codes are used with code rate 1/2 and generator polynomial $[171, 133]_8$. The number of iterations of the peak amplitude clipping is chosen to be $j = 1$, and the corresponding threshold is $A = 1.2$, as suggested in [78]. The PLC channel parameters are given in Table 3.2 [98].

The PLC system is analysed using the proposed blanking preprocessor bank in two scenarios. In the first scenario, the impulsive noise parameters are fixed, i.e. $p = 0.01$, $SINR = -10$ dB. On the other hand, the impulsive noise parameters vary in the second scenario to observe the robustness of the proposed blanking method. The impulsive noise occurrence probability is set as a random variable with a uniform distribution of 0.005 to 0.02. Similarly, the signal-to-impulse-noise ratio (SINR) also follows uniform distribution on the interval -5 dB to -15 dB. The thresholds for the proposed blanking preprocessor bank are selected as follows. The thresholds are given by $\{T_b\} = \{T_l + (i-1)\Delta T\}_{i=1}^{Q}$ [100]. The lower limit of the threshold is set at $T_l = 2.0$, and the higher limit of the threshold is set at $T_h = 3.0$. The threshold steps are set to be $\Delta T = 0.05$ and $\Delta T = 0.2$, which means $Q = 21$ and $Q = 6$, respectively. The preprocessor outputs is then sort based on the α_q values. Subsequently, 100%, 80%, and 50% of preprocessor outputs have been taken to combine with the highest α_q values.

Keep in mind that it wants the preprocessor outputs with $\alpha_q \approx 1$. In other words, the best 21, 16, and 10 preprocessor outputs are combined for $\Delta T = 0.05$ and 6, 4, and 3 outputs are combined for $\Delta T = 0.2$.

It is worth mentioning that the selection of T_b should be arbitrary. However, keep in mind that the lower threshold will cause lot of information loss, and a higher threshold will make many large samples left unblanked. The reasonable values of the threshold are between 2.0 and 3.5 based on the dynamic of the OFDM signal amplitude. On the other hand, the value of Q is determined by the threshold step selection, ΔT, which can be chosen between 0.05 and 0.2 and depends on the range of $_b$. The rule of thumb is when the range of T_b is large, smaller Q can be assigned, and vice versa.

3.3.1 PAPR Performance

PAPR is commonly analyzed using complementary cumulative distribution function (CCDF), which shows the probability of PAPR exceeds a certain level. The CCDF plot of the proposed system is shown in Fig. 3.3. It can be seen that the PAPR is reduced by about 0.5 dB at a probability of 10^{-3}. It is worth mentioning that the gain of the PAPR reduction method is proportional to the number of null subcarriers, i.e., the more the null subcarriers, the more the PAPR reduction.

3.3.2 BER Performance

The BER performance of the PLC system with the optimal blanking and the proposed blanking, along with and without peak amplitude clipping, for $\Delta T = 0.05$ and $\Delta T = 0.2$ is shown in Figs. 3.4 and 3.5, respectively. It can be observed from the two figures that the BER performance for the proposed blanking outperforms one of the optimal blankings. Note that the optimum threshold is obtained by optimizing the output SNR as $\min_T(E[|y_n|^2])/\alpha$, where the closed-form expressions of $E[|y_n|^2]$ and α for blanking nonlinearity are given in [79].

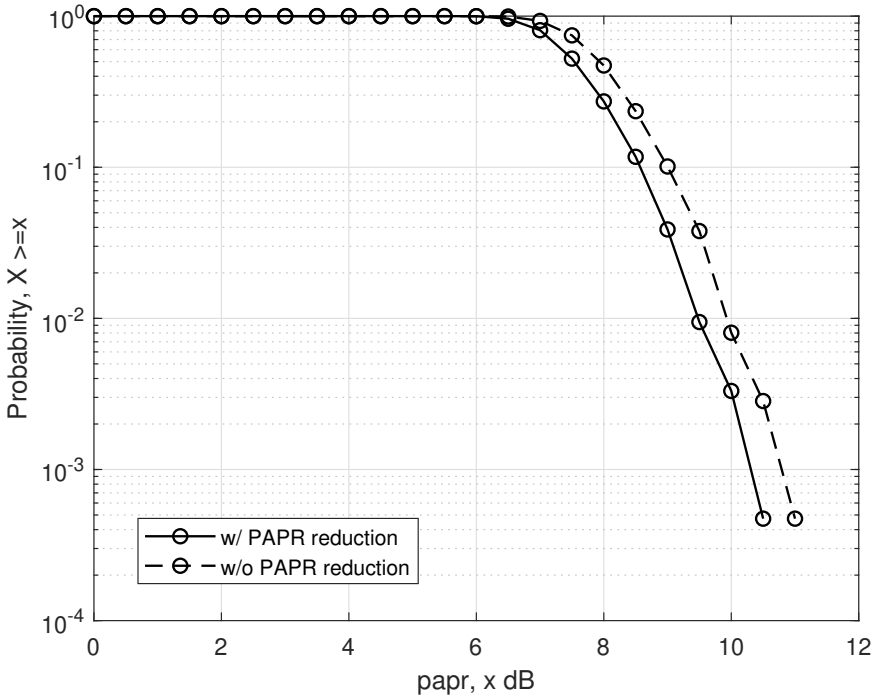

Figure 3.3: PAPR performance.

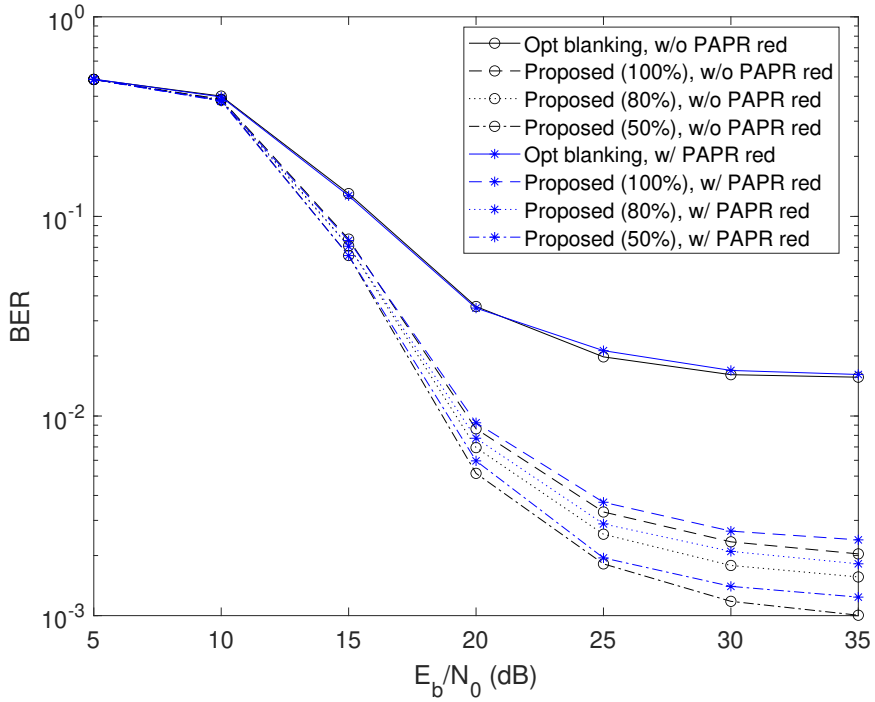

Figure 3.4: BER performance, $p = 0.01$, $SINR = -10$ dB, $\Delta T = 0.05$.

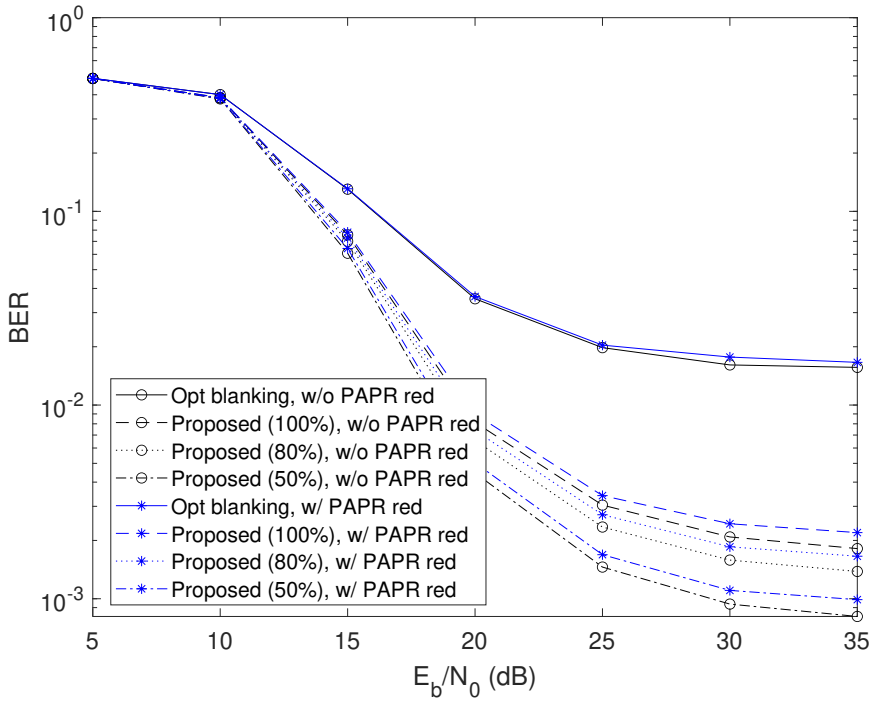

Figure 3.5: BER performance, $p = 0.01$, $SINR = -10$ dB, $\Delta T = 0.2$.

The results are understandable as some useful information is missing due to the optimal blanking. However, the missing information can be retrieved through multiple outputs (or "blanking channels") in the proposed blanking scheme. It can also be seen that the BER plots of the proposed blanking are relatively the same for 100%, 80%, and 50% schemes. Further, increasing ΔT from 0.05 to 0.2 shows little effect on the performance.

BER performance for random impulsive noise parameters $\Delta T = 0.05$ and $\Delta T = 0.2$ is shown in Figs. 3.6 and 3.7. It can be seen that the BER plots for the proposed blanking are significantly better compared with one of the optimal blanking. Furthermore, it can be seen that the peak amplitude clipping relatively does not deteriorate the BER performance. It is because the peak amplitude clipping is performed in the null subcarriers and $\mathcal{N} \cup \mathcal{N}^c = \emptyset$.

As null subcarriers are used, it is worth to compare the BER performance of the blanking method with the compressive sensing method. SL0 is employed as the impulsive noise reconstruction algorithm. The procedure of impulsive noise

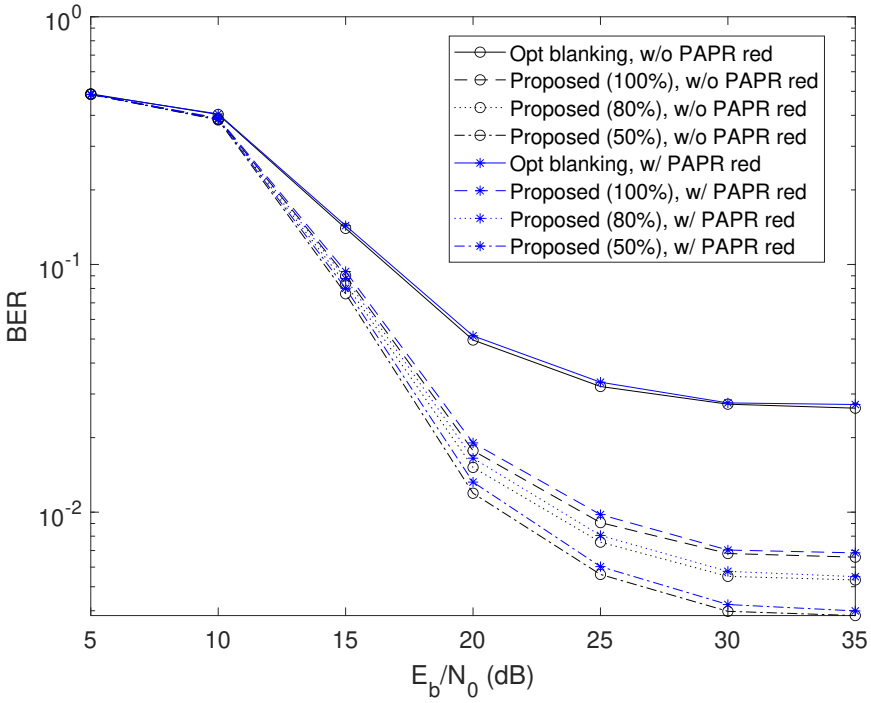

Figure 3.6: BER performance, random p, $SINR$, $\Delta T = 0.05$

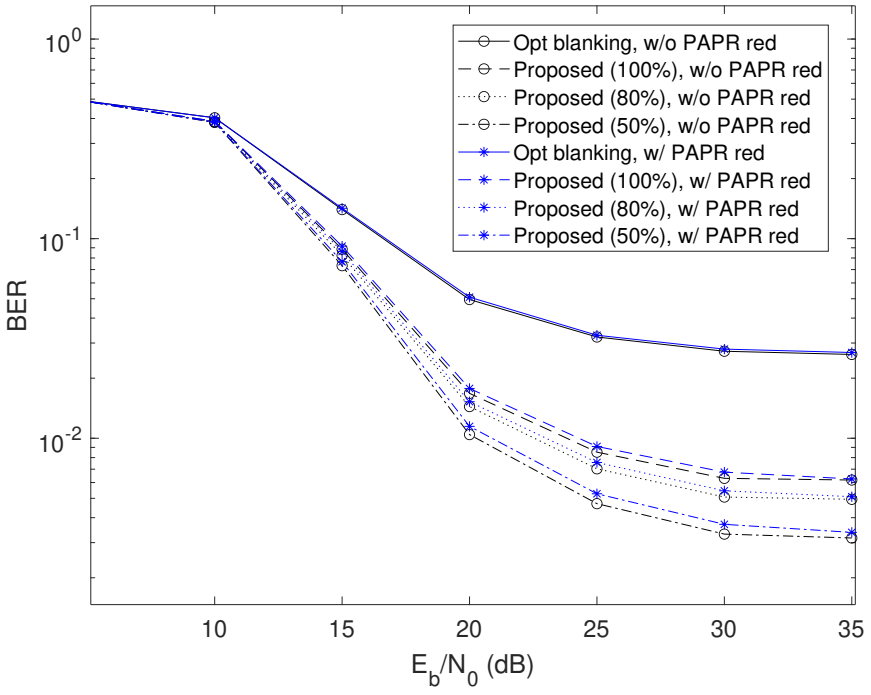

Figure 3.7: BER performance, random p, $SINR$, $\Delta T = 0.2$

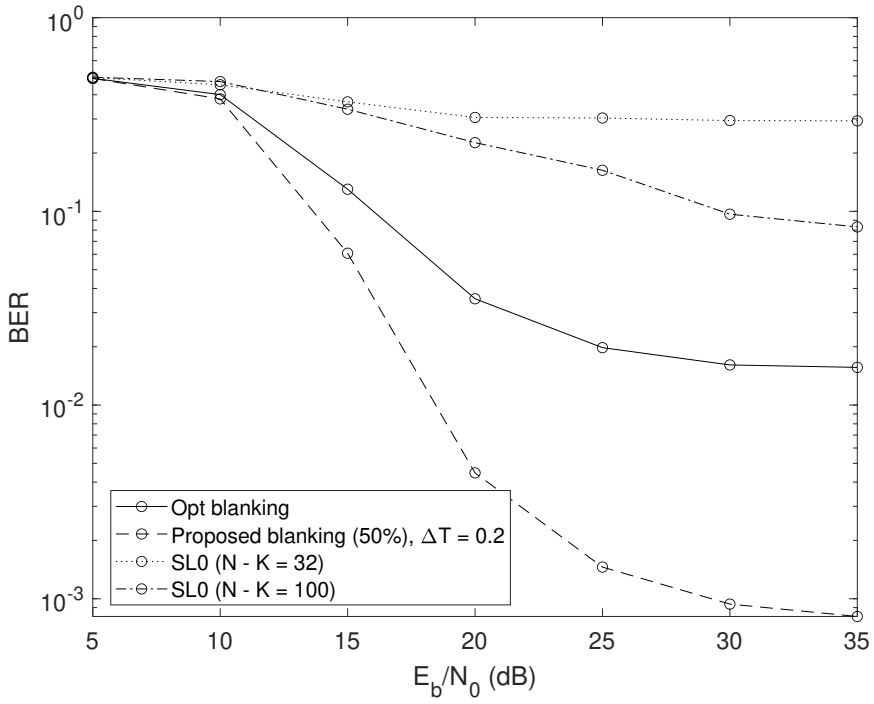

Figure 3.8: BER performance comparison

reconstruction and mitigation follows [78]. The SL0 algorithm is chosen as it has low complexity and performs better than the ℓ_1 algorithm [87], [101]. The BER plots are depicted in Fig. 3.8. It can be seen that using the same number of null subcarriers ($N - K = 32$), the clipping method yields better performance. Compressive sensing performance depends on the number of null subcarriers. In general, the more null subcarriers, the better the performance. Therefore, in order to obtain good performance, it needs to sacrifice the data rate.

3.3.3 Outage Probability

Outage probability can be used as a metric to measure the system performance related instantaneous output SNR of the blanking preprocessor(s). It is defined as the probability of mutual information, I less than the information rate, R_b [102].

Mathematically, it can be written as

$$\begin{aligned} P_{out} &= \Pr(I < R_b) \\ &= \Pr(\log_2(1+\gamma) < R_b) \\ &= \Pr(\gamma < 2^R - 1), \end{aligned} \tag{3.14}$$

where γ is the output SNR of the blanking preprocessor bank and the value of R_b is chosen as 3 bps/Hz because the SNR, energy and spectral efficiencies are much better compared with 1 and 2 bps/Hz [103].

The outage probability plot with varying SNR with fixed impulsive noise parameters for $\Delta T = 0.05$ and $\Delta T = 0.2$ is depicted in Figs. 3.9 and 3.10. It can be seen that the outage probability for the system with the blanking preprocessor bank outperforms the one with optimal blanking. It is further observed that the outage probability becomes better when a smaller portion of the blanking preprocessors is combined.

Figs. 3.11 and 3.12 show the outage probability for random impulsive noise parameters for $\Delta T = 0.05$ and $\Delta T = 0.2$, respectively. The general trends show the robustness of the proposed method compared to the optimal blanking. Furthermore, it can be observed that the PAPR reduction technique plays an important role in reducing the blanker's false alarm. As a result, the outage probabilities are reduced.

The blanking process for the proposed scheme has the same complexity as the optimal blanking scheme, i.e., $\mathcal{O}(N)$. The proposed method needs to perform a sorting algorithm, which gives an additional complexity of $\mathcal{O}(Q \log Q)$. This may have an effect on the computation time. However, in the optimal blanking scheme, it has an additional complexity for calculating the optimum threshold (although it can be estimated offline).

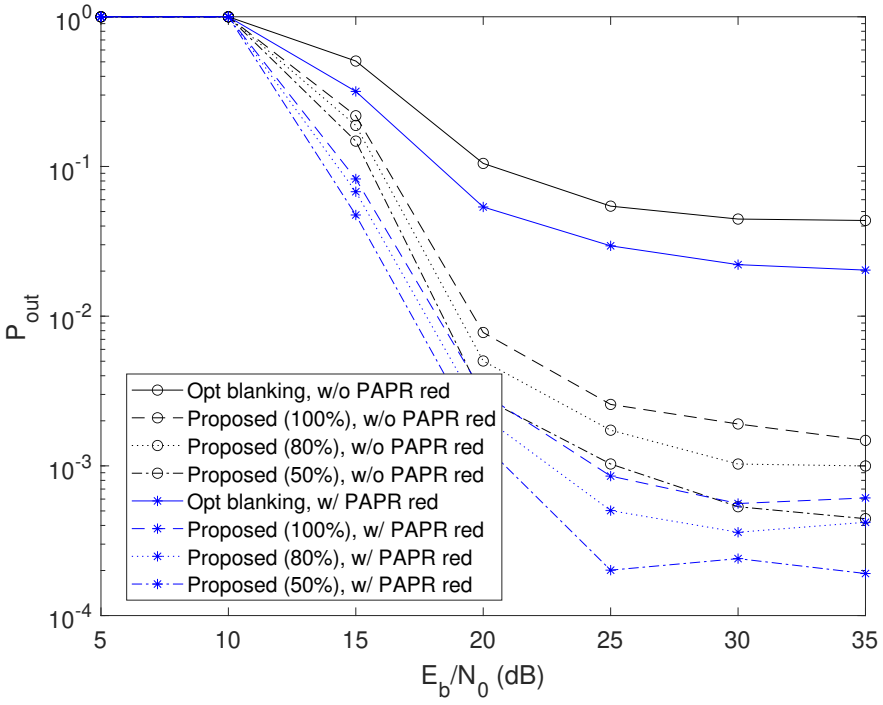

Figure 3.9: Outage probability, $p = 0.01$, $SINR = -10$ dB, $\Delta T = 0.05$

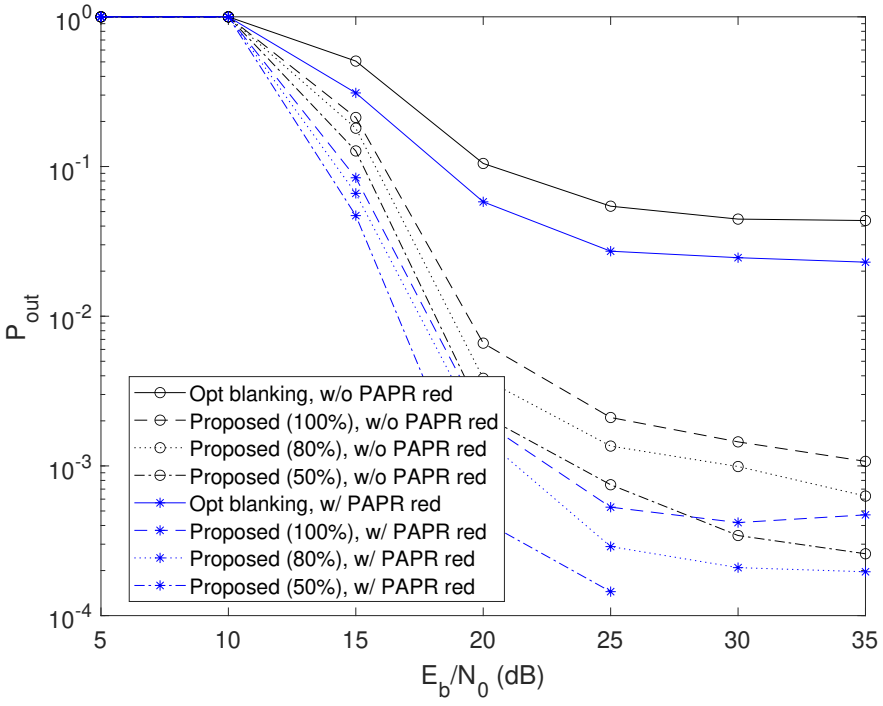

Figure 3.10: Outage probability, $p = 0.01$, $SINR = -10$ dB, $\Delta T = 0.2$

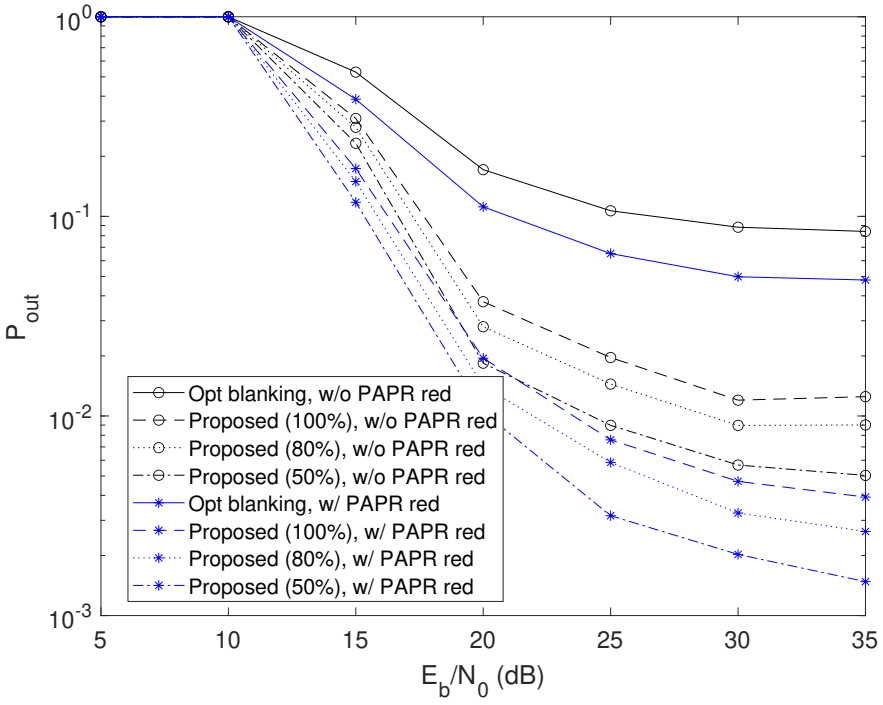

Figure 3.11: Outage probability, random p, $SINR$, $\Delta T = 0.05$

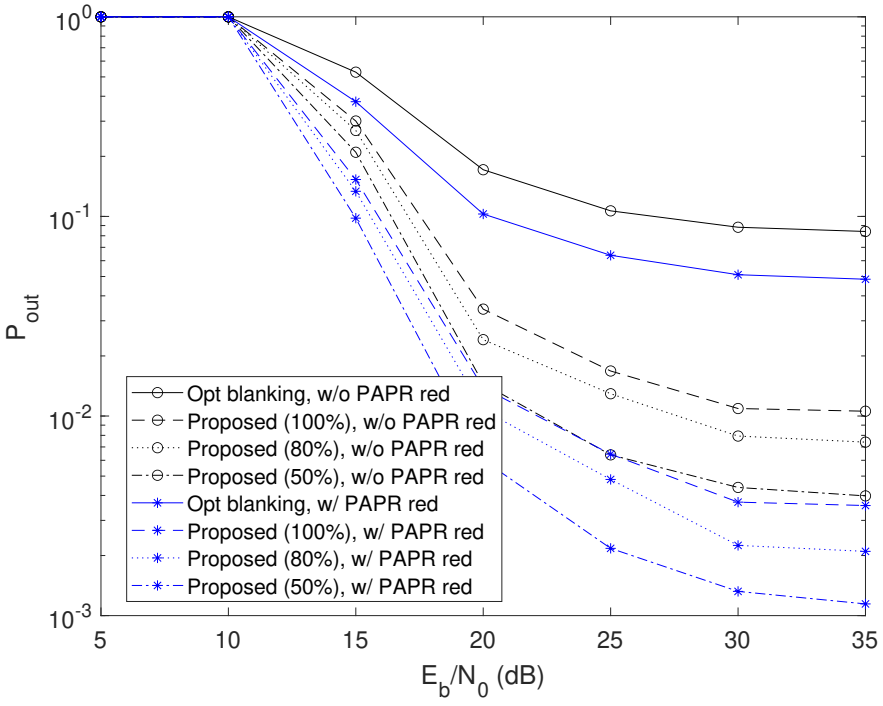

Figure 3.12: Outage probability, random p, $SINR$, $\Delta T = 0.2$

3.3.4 Effect of Thresholds Selection

The performance of the proposed method depends on the threshold selection of the blanking nonlinear preprocessors. To analyze the effect of the threshold selection, the second threshold setting is set to the lower limit of threshold to be $T_l = 2.6$ and higher limit of threshold to be $T_h = 3.4$ with the same ΔT and compared with the first (previous) threshold setting.

Figs. 3.13 and 3.14 show the comparison of BER plots using two different threshold sets for $\Delta T = 0.05$ and $\Delta T = 0.2$, respectively. It can be seen that using the second threshold setting gives performance degradation in both BER and outage performance. It may be caused by improper setting of the higher limit of threshold (too large) in the second set so that most of the samples are left unblanked. Moreover, it is noticed that BER and outage probability plots of the 100% scheme for the second threshold set are close to the optimal blanking plots. This can be explained as follows. When the thresholds are not properly set, poor outputs from a few blanking preprocessors may occur and may degrade the overall performance. However, the poor outputs' adverse effects can be eliminated by taking 80% and 50% of the best output. That's why the 80% and 50% schemes result in better performance compared with the optimal blanking scheme. Likewise, Figs. 3.15 and 3.16 shows the outage probability plots with similar trends.

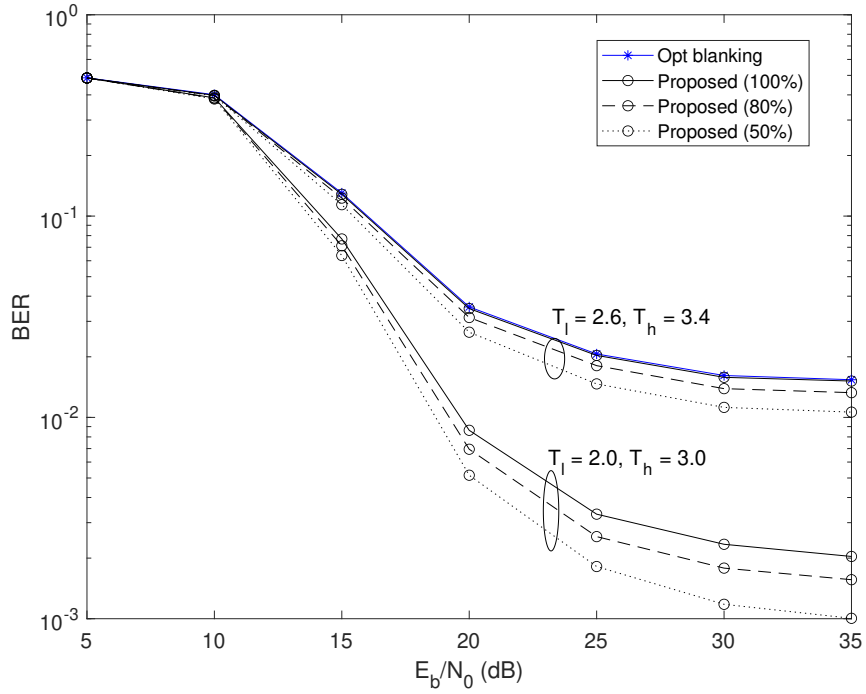

Figure 3.13: BER plots, $p = 0.01$ and $SINR = -10$ dB, $\Delta T = 0.05$

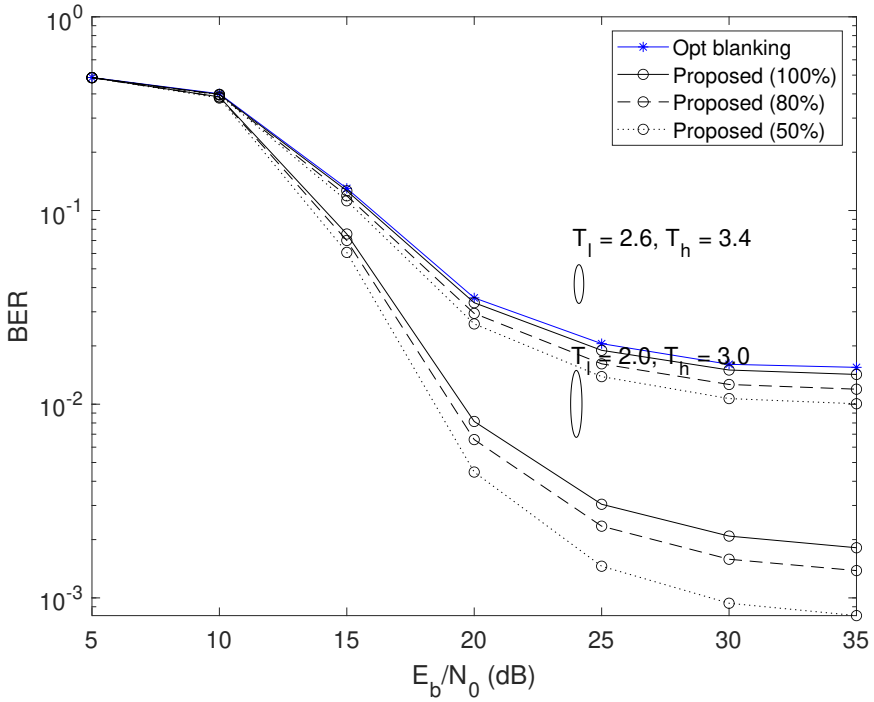

Figure 3.14: BER plots, $p = 0.01$ and $SINR = -10$ dB, $\Delta T = 0.2$

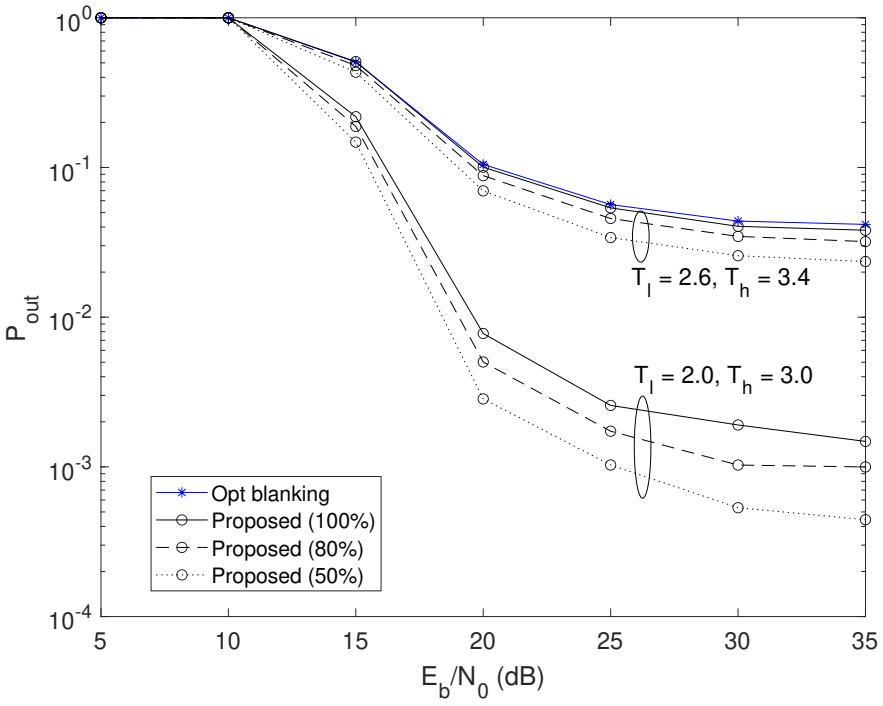

Figure 3.15: Outage probability, $p = 0.01$, $SINR = -10$ dB, $\Delta T = 0.05$

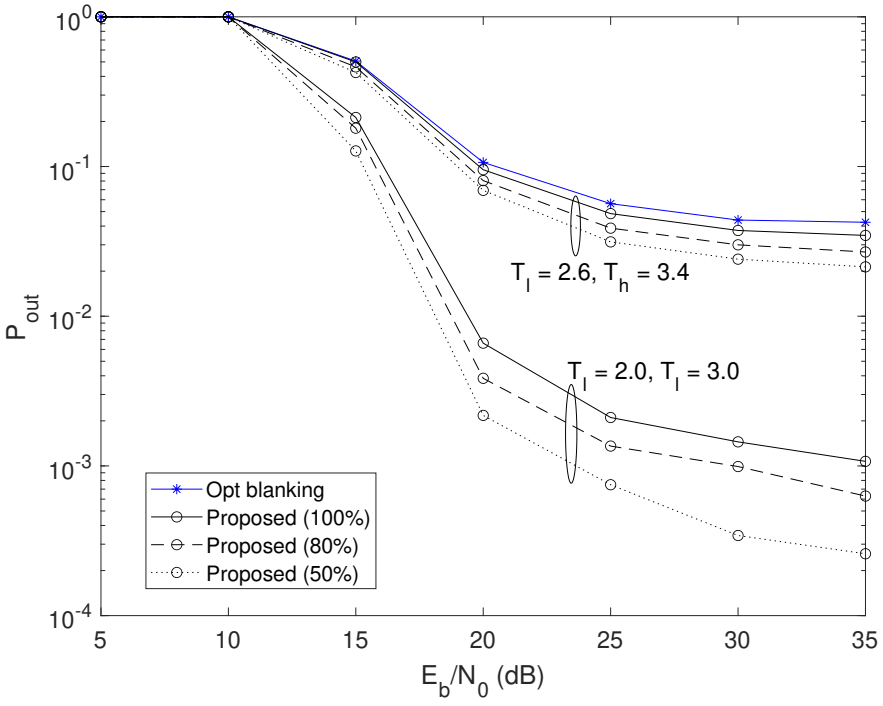

Figure 3.16: Outage probability, $p = 0.01$, $SINR = -10$ dB, $\Delta T = 0.2$

3.4 Chapter Summary

A blanking preprocessor blank, which consists of multiple blanking preprocessors with different thresholds has been proposed. The proposed method does not need prior information about the impulsive noise. Moreover, an expression regarding the output SNR of each blanking preprocessor has been derived. The proposed blanking preprocesor bank has been used to analyse the PLC system with a fixed or varying the impulsive noise. However, the threshold selection should be carefully considered. This means that the lower and higher limit of thresholds should not be set too small and large respectively, as the lower threshold will cause lot of information loss, and a higher threshold will make many large samples left unblanked. It has shown though simulations that the proposed method, in terms of BER and outage probability, outperforms one of the optimal blankings, even when 50% of the best values is taken.

Chapter 4

CTF of Two-way Relay-assisted PLC Systems

Although the previous chapter is able to mitigate the effect of impulsive noise in PLC system, the performance of the PLC system still degrade due to the harsh environment of the power-line. For example, the signalling paths are highly correlated to each other in PLC scenario as they use the same power cables. As a solution to this problem, relays are suggested to improve reliability. Yet, many PLC applications need two-way communication links. Thus, this chapter presents the modelling of a relay inside a P2P PLC channel as well as extending relay in two-way channel model. The rest of this chapter is organised as below. An introduction of PLC channel models is presented in Section 4.1. In Section 4.2, the circuit modelling of relay node and relay-assisted channels are discussed. In Section 4.3, the CTF expressions of a two-way relay-assisted PLC channel is derived. In Section 4.4 shows the numerical simulation which demonstrate the proposed two-way CTF have high correlated among the paths. Finally the chapter is briefly summarised in Section 4.5.

4.1 Introduction

PLC systems are often designed to be more reliable through the understanding of PLC channel characteristics. PLC bottom-up channel models are used to utilise the TL theory to obtain the CTF based on their network information such as network structure, cable parameters, and appliances impedance inorder to create a strong connection with the physical topology [43], [104]. However, PLC bottom-up channel models are hard to define a fixed structural model. Still, many researchers are able to model the PLC system.

Yet, the existing PLC channel models are still based on P2P links. The limitation of P2P PLC systems occur due to the harsh nature of the power line channel [105]. The relay cooperative communication scheme is used to improve system performance. A BMA three-node relay system consists of one source node, one relay node, and one destination node. The source node broadcasts the signal to the other two nodes in the first phase. In the second phase, the source node continues to broadcast, and at the same time, the relay node forwards its received signal to the destination node. In this scheme, the relay node uses TDD mode [106].

In all PLC scenario, the signalling paths are highly correlated to each other as they use the same power cables. The consideration of a relay device in a PLC system will influence the channel paths. Thus, the existing P2P PLC channel models cannot be directly used in the relay-assisted PLC system. In the literature, a single-relay, or sometimes called a three-node, one-way channel model has been proposed in [107]. However, many PLC smart grid applications need two-way communication links. To fill the gap, the three-node two-way relay-assisted PLC channel is modelled using a bottom-up approach in this chapter.

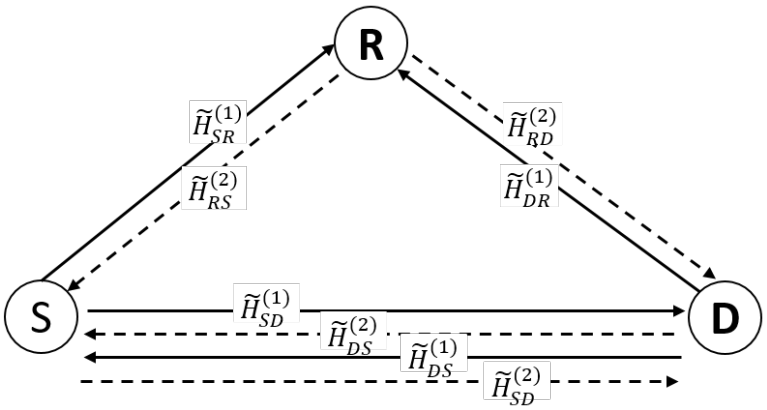

Figure 4.1: A three-node two-way relay-assisted PLC system model

4.2 Modelling of Circuit

The three-node two-way relay system is proposed in Fig. 4.1. Using Canate's P2P channel model, the network layout of the three-node relay-assisted PLC system model is shown in Fig. 4.2. The system is assumed to be half-duplex. $H(f)$ and $\tilde{H}(f)$ indicate the CTF of the signalling path before and after the relay node is introduced, respectively. Note that the load impedance at the branch, Z_b is assumed as frequency-dependent impedance given by [46]

$$Z_b = \frac{R'}{1 + jQ_f(\frac{\omega}{\omega_0} - \frac{\omega_0}{\omega})}, \tag{4.1}$$

where R', ω_0 and Q_f are the resistance at resonance, resonance angular frequency, and quality factor, respectively.

4.2.1 ABCD Matrix Channel Model

The calculation of CTF of the PLC P2P channel is made conveniently through the use of ABCD representation of a two-port circuit as shown in Fig. 4.3.

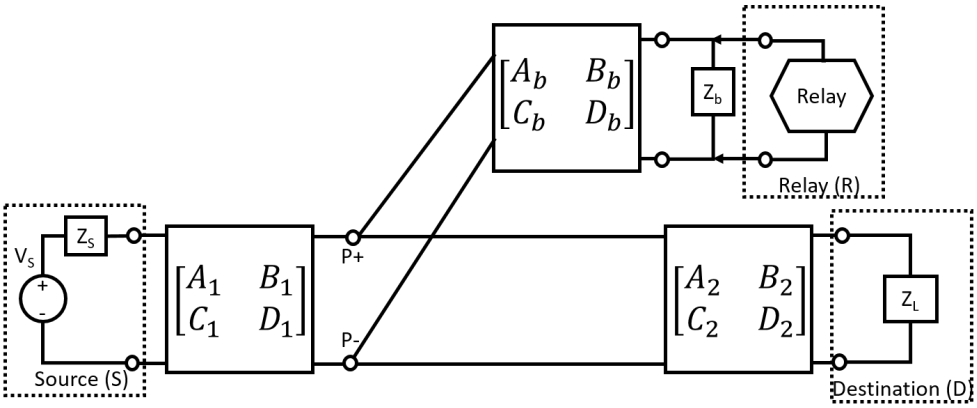

Figure 4.2: Network layout of the three-segment

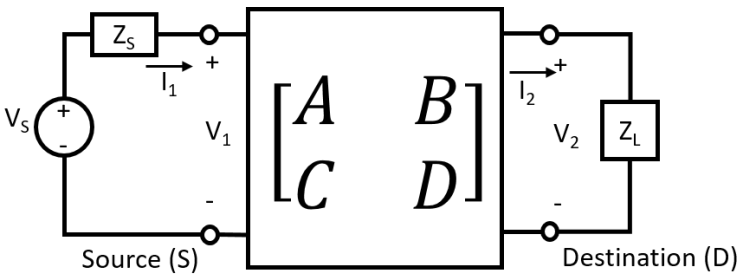

Figure 4.3: Two-port network of a P2P PLC system

The formulation is as follows [108], [109]

$$\begin{bmatrix} V_1 \\ I_1 \end{bmatrix} = \begin{bmatrix} A & B \\ C & D \end{bmatrix} \begin{bmatrix} V_2 \\ I_2 \end{bmatrix}. \tag{4.2}$$

Here are some common circuit configurations and their ABCD representations.

- A transmitter with voltage source, V_S and a inner impedance of source, Z_S gives the ABCD matrix

$$\Phi_S = \begin{bmatrix} 1 & Z_S \\ 0 & 1 \end{bmatrix}. \tag{4.3}$$

- A general impedance between the cables, Z gives the matrix

$$\Phi_Z = \begin{bmatrix} 1 & 0 \\ \frac{1}{Z} & 1 \end{bmatrix}. \tag{4.4}$$

- The ABCD matrix of two cascaded circuits is the product of two individual ABCD matrix, i.e Φ_1 and Φ_2.

$$\Phi_0 = \Phi_1 \Phi_2, \tag{4.5}$$

$$\begin{bmatrix} A_0 & B_0 \\ C_0 & D_0 \end{bmatrix} = \begin{bmatrix} A_1 & B_1 \\ C_1 & D_1 \end{bmatrix} \begin{bmatrix} A_2 & B_2 \\ C_2 & D_2 \end{bmatrix}. \tag{4.6}$$

- A cable line with characteristic impedance, Z_0 and propagation constant,γ and length, d gives the matrix

$$\Phi_C = \begin{bmatrix} \cosh(\gamma d) & Z_0 \sinh(\gamma d) \\ \frac{1}{Z_0} \sinh(\gamma d) & \cosh(\gamma d) \end{bmatrix}. \tag{4.7}$$

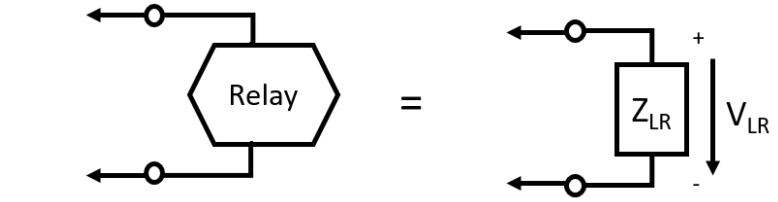

(a) First phase

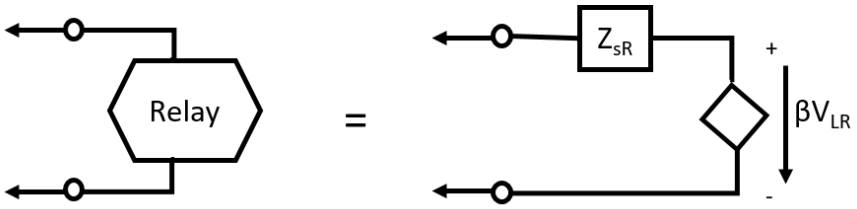

(b) Second phase

Figure 4.4: Relay node in two phases

4.2.2 Equivalent Input Impedance

For any two-port network, the equivalent input impedance, Z_{eqb} can be derived using its ABCD representation and the load impedance, Z_L as follows [49]

$$Z_{eqb} = \frac{V_1}{I_1} = \frac{AZ_L + B}{CZ_L + D}. \tag{4.8}$$

4.2.3 Relay Node

In the source node, the transmitter consists of a voltage source, V_S, and a inner impedance, Z_S. The relay node works in two phases, which are (1) the receiving relay node has a load impedance, Z_{LR} as in Fig. 4.4a, and (2) the transmitting relay node has a controlled voltage source, V_R and its inner impedance, Z_{SR} in Fig. 4.4b. The output voltage of the relay node is expressed as

$$V_R = \beta V_{LR}, \tag{4.9}$$

where β is the amplitude gain and V_{LR} is the received voltage of the relay node in the first phase. On the other hand, the destination node has a load of Z_L.

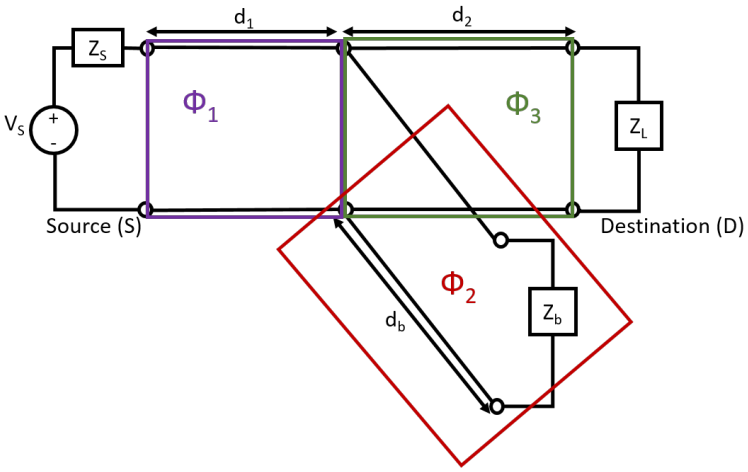

Figure 4.5: A transmission line with a branch circuit

4.2.4 Relay-assisted PLC Channels

The channel model of a transmission line with one branch/relay circuit is shown in Fig. 4.5. With the given circuit, the backbone segments and the branch segments can be identified. Backbone segment is the shortest path between the transmitter and receiver node and the branch segment is the section where relay can be introduced. The structure is divided into three cascaded two-port network sub-circuits, i.e. the main backbone transmission line segment, Φ_1, the branched-circuit segment Φ_2, and the second backbone transmission line segment, Φ_3. The CTF can be obtained with the following steps as illustrated in Fig. 4.6:

(a) Calculate Φ_1, Φ_2, and Φ_3. The backbone transmission line segments, Φ_1 and Φ_3 can be found directly from ABCD matrix. However, the branched circuit segment, Φ_2 needs the equivalent input impedance using (4.3) - (4.8) to calculate the ABCD matrix. They are

$$\begin{aligned} \Phi_1 &= \begin{bmatrix} A_1 & B_1 \\ C_1 & D_1 \end{bmatrix} \\ &= \begin{bmatrix} \cosh(\gamma_1 d_1) & Z_{0,1}\sinh(\gamma_1 d_1) \\ \frac{1}{Z_{0,1}}\sinh(\gamma_1 d_1) & \cosh(\gamma_1 d_1) \end{bmatrix}. \end{aligned} \tag{4.10}$$

$$\Phi_2 = \begin{bmatrix} A_b & B_b \\ C_b & D_b \end{bmatrix} = \begin{bmatrix} 1 & 0 \\ \frac{1}{Z_{eqb}} & 1 \end{bmatrix}. \tag{4.11}$$

$$\begin{aligned} \Phi_3 &= \begin{bmatrix} A_2 & B_2 \\ C_2 & D_2 \end{bmatrix} \\ &= \begin{bmatrix} \cosh(\gamma_2 d_2) & Z_{0,2}\sinh(\gamma_2 d_2) \\ \frac{1}{Z_{0,2}}\sinh(\gamma_2 d_2) & \cosh(\gamma_2 d_2) \end{bmatrix}. \end{aligned} \tag{4.12}$$

where $Z_{0,1}$, γ_1 and d_1 are the characteristic impedance, propagation constants and cable length of the main backbone transmission line segment respectively, Z_{eqb} denotes the equivalent input impedance of branched-circuit segment, and $Z_{0,2}$, γ_2 and d_2 are the characteristic impedance, propagation constants and cable length of the second backbone transmission line segment respectively.

(b) Calculate the ABCD matrix of the whole structure, Φ_T, by multiplying the ABCD matrix of each segment. The result is given by

$$\Phi_T = \prod_{i=1}^{3} \Phi_i = \begin{bmatrix} A_T & B_T \\ C_T & D_T \end{bmatrix}. \tag{4.13}$$

(c) Using (4.10) - (4.13), the CTF of the PLC channel with one branch can be calculated. The result is given by

$$\tilde{H}_T(f) = \frac{V_L}{V_S} = \frac{Z_L}{A_T Z_L + B_T + C_T Z_L Z_S + D_T Z_S}. \tag{4.14}$$

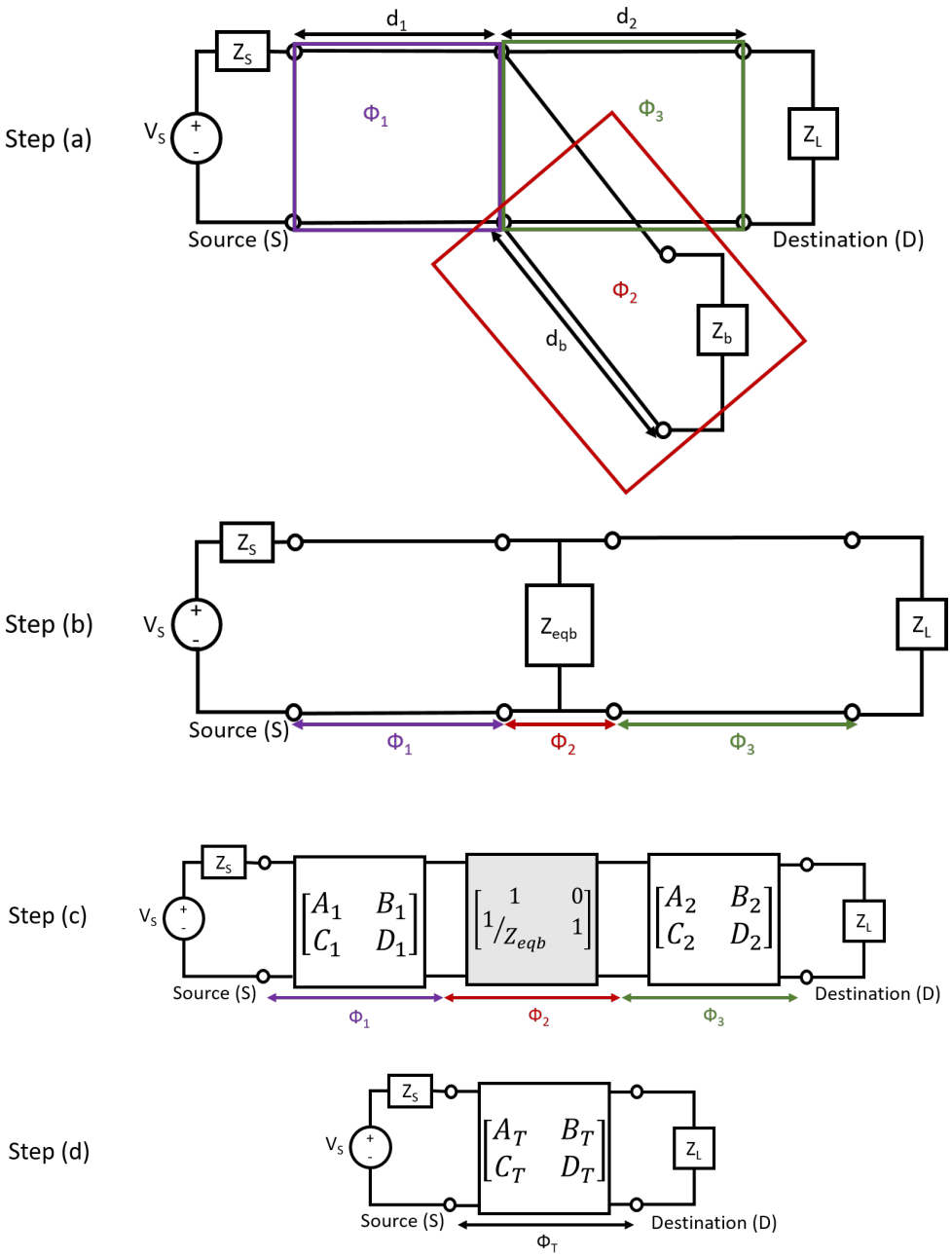

Figure 4.6: Steps for obtaining the CTF of a one-branched circuit

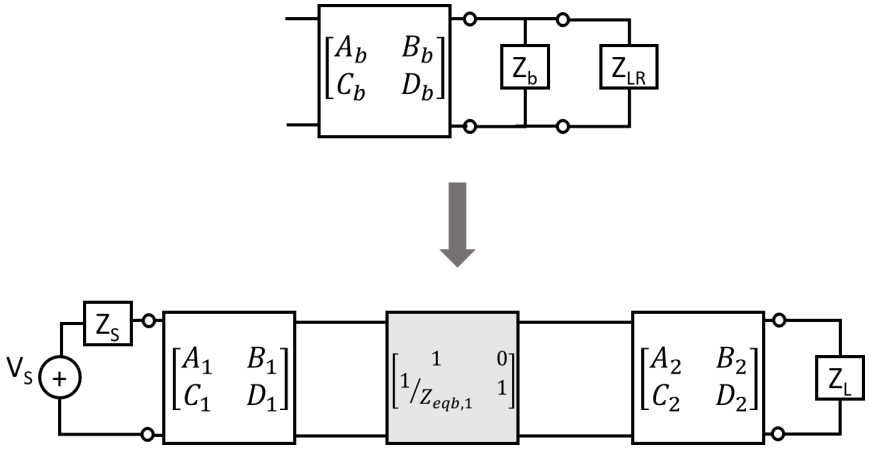

Figure 4.7: CTF from S to D in the first phase

4.3 CTF Derivation

In this session, the CTFs of the signalling paths are calculated using ABCD matrix as follows:

(a) From S to D in the first phase. In the first phase, the relay node is treated as a load. The CTF of the signaling path from the source to the destination node along the backbone or so called direct path, can be found using ABCD method as shown in Fig. 4.7. The equivalent input impedance of the relay branch is given by

$$Z_{eqb,1} = \frac{A_b Z'_{LR} + B_b}{C_b Z'_{LR} + D_b}, \tag{4.15}$$

where Z'_{LR} is the equivalent impedance of Z_b parallel to Z_{LR} as given by

$$Z'_{LR} = Z_b || Z_{LR} = \frac{Z_b Z_{LR}}{Z_b + Z_{LR}}. \tag{4.16}$$

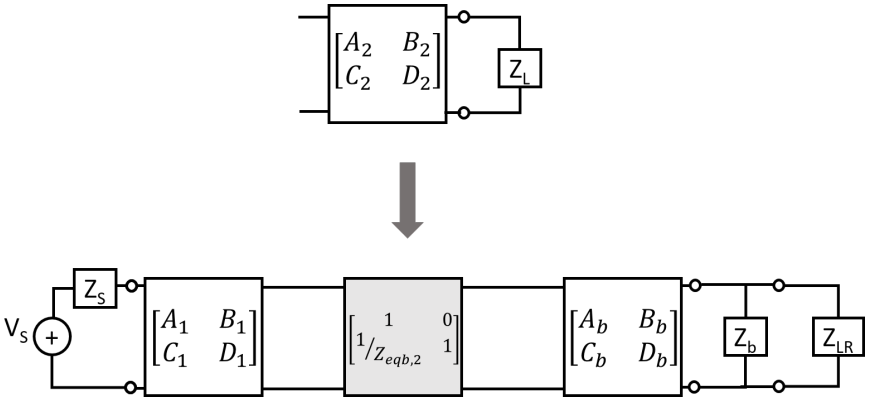

Figure 4.8: CTF from S to R in the first phase

The matrix between S and D in the first phase is given by

$$\begin{aligned}\Phi_{SD}^{(1)} &= \begin{bmatrix} A_{SD}^{(1)} & B_{SD}^{(1)} \\ C_{SD}^{(1)} & D_{SD}^{(1)} \end{bmatrix} \\ &= \begin{bmatrix} A_1 & B_1 \\ C_1 & D_1 \end{bmatrix} \begin{bmatrix} 1 & 0 \\ \frac{1}{Z_{eqb,1}} & 1 \end{bmatrix} \begin{bmatrix} A_2 & B_2 \\ C_2 & D_2 \end{bmatrix}. \end{aligned} \tag{4.17}$$

As a result, the CTF between S and D in the first phase is

$$\tilde{H}_{SD}^{(1)} = \frac{Z_L}{A_{SD}^{(1)} Z_L + B_{SD}^{(1)} + C_{SD}^{(1)} Z_L Z_S + D_{SD}^{(1)} Z_S}. \tag{4.18}$$

(b) From S to R in the first phase. The relay node receives signal from Φ_1 to Φ_2 in the first phase as shown in Fig. 4.8. In this case, the second segment, Φ_3 along the backbone is treated as branch. The equivalent input impedance of Φ_3 is given by

$$Z_{eqb,2} = \frac{A_2 Z_L + B_2}{C_2 Z_L + D_2}. \tag{4.19}$$

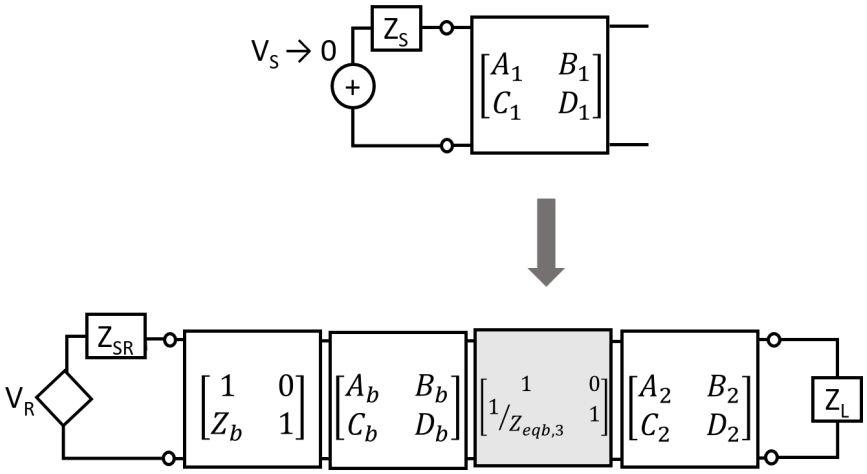

Figure 4.9: CTF from R to D in the second phase

The matrix between S and R in the first phase is

$$\begin{aligned}\Phi_{SR}^{(1)} &= \begin{bmatrix} A_{SR}^{(1)} & B_{SR}^{(1)} \\ C_{SR}^{(1)} & D_{SR}^{(1)} \end{bmatrix} \\ &= \begin{bmatrix} A_1 & B_1 \\ C_1 & D_1 \end{bmatrix} \begin{bmatrix} 1 & 0 \\ \frac{1}{Z_{eqb,2}} & 1 \end{bmatrix} \begin{bmatrix} A_b & B_b \\ C_b & D_b \end{bmatrix}. \end{aligned} \tag{4.20}$$

Thus, the CTF between S and R in the first phase is

$$\tilde{H}_{SR}^{(1)} = \frac{Z'_{LR}}{A_{SR}^{(1)} Z'_{LR} + B_{SR}^{(1)} + C_{SR}^{(1)} Z'_{LR} Z_S + D_{SR}^{(1)} Z_S}, \tag{4.21}$$

where Z_{SR} is the inner impedance of the relay node at the transmission node.

(c) From R to D in the second phase. In the second phase, the relay node is being treated as the transmitter. According to Fig. 4.9, the relay node forwards signal from Φ_2 to Φ_3. Thus, the first segment, Φ_1 is treated as branch. The equivalent input impedance of Φ_1 is formulated as

$$Z_{eqb,3} = \frac{A_1 Z_S + B_1}{C_1 Z_S + D_1}. \tag{4.22}$$

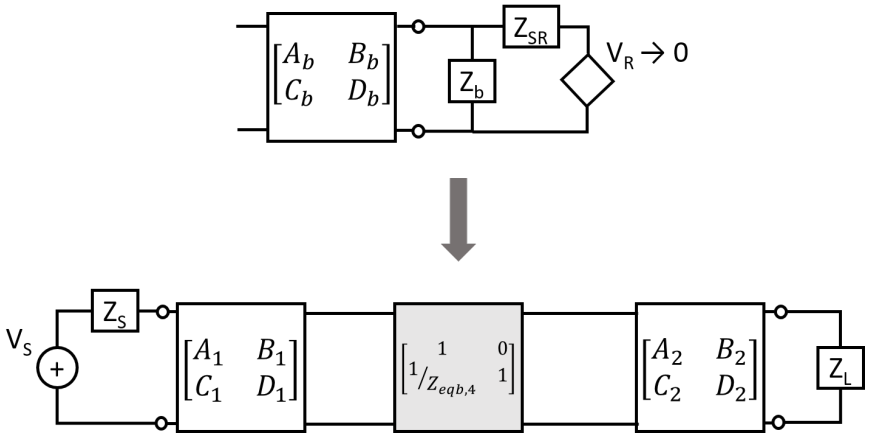

Figure 4.10: CTF from S to D in the second phase

The matrix between R and D in the second phase is

$$\begin{aligned}\Phi_{RD}^{(2)} &= \begin{bmatrix} A_{RD}^{(2)} & B_{RD}^{(2)} \\ C_{RD}^{(2)} & D_{RD}^{(2)} \end{bmatrix} \\ &= \begin{bmatrix} 1 & 0 \\ Z_b & 1 \end{bmatrix} \begin{bmatrix} A_b & B_b \\ C_b & D_b \end{bmatrix} \begin{bmatrix} 1 & 0 \\ \frac{1}{Z_{eqb,3}} & 1 \end{bmatrix} \begin{bmatrix} A_2 & B_2 \\ C_2 & D_2 \end{bmatrix}. \end{aligned} \tag{4.23}$$

Thus, the CTF between R and D in the second phase is

$$\tilde{H}_{RD}^{(2)} = \frac{Z_L}{A_{RD}^{(2)} Z_L + B_{RD}^{(2)} + C_{DR}^{(2)} Z_{SR} Z_L + D_{DR}^{(2)} Z_{SR}}. \tag{4.24}$$

(d) From S to D in the second phase. In the second phase (Fig. 4.10), the relay node is being treated as the load in the second phase. Similarly to the first phase method, the equivalent input impedance of the relay branch is

$$Z_{eqb,4} = \frac{A_b Z''_{LR} + B_b}{C_b Z''_{LR} + D_b} \tag{4.25}$$

where Z''_{LR} is the equivalent impedance of Z_b parallel to Z_{SR}

$$Z''_{LR} = Z_b || Z_{SR} = \frac{Z_b Z_{SR}}{Z_b + Z_{SR}} \tag{4.26}$$

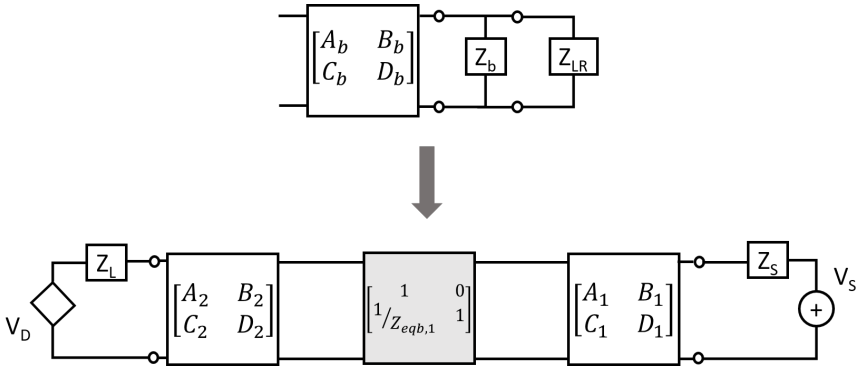

Figure 4.11: CTF from D to S in the first phase

Therefore, the matrix between S and D in the second phase is

$$\begin{aligned}\Phi_{SD}^{(2)} &= \begin{bmatrix} A_{SD}^{(2)} & B_{SD}^{(2)} \\ C_{SD}^{(2)} & D_{SD}^{(2)} \end{bmatrix} \\ &= \begin{bmatrix} A_1 & B_1 \\ C_1 & D_1 \end{bmatrix} \begin{bmatrix} 1 & 0 \\ \frac{1}{Z_{eqb,4}} & 1 \end{bmatrix} \begin{bmatrix} A_2 & B_2 \\ C_2 & D_2 \end{bmatrix} \end{aligned} \tag{4.27}$$

Thus, the CTF between S and D in the second phase is

$$\tilde{H}_{SD}^{(2)} = \frac{Z_L}{A_{SD}^{(2)} Z_L + B_{SD}^{(2)} + C_{SD}^{(2)} Z_S Z_L + D_{SD}^{(2)} Z_S}. \tag{4.28}$$

(e) From D to S in the first phase. In the first phase, the relay node is treated as the load. The CTF for the signaling path from the destination to the source node along the backbone, can be calculated using (4.15) which is shown in Fig. 4.11. Therefore, the matrix between D and S in the first phase is

$$\begin{aligned}\Phi_{DS}^{(1)} &= \begin{bmatrix} A_{DS}^{(1)} & B_{DS}^{(1)} \\ C_{DS}^{(1)} & D_{DS}^{(1)} \end{bmatrix} \\ &= \begin{bmatrix} A_2 & B_2 \\ C_2 & D_2 \end{bmatrix} \begin{bmatrix} 1 & 0 \\ \frac{1}{Z_{eqb,1}} & 1 \end{bmatrix} \begin{bmatrix} A_1 & B_1 \\ C_1 & D_1 \end{bmatrix}. \end{aligned} \tag{4.29}$$

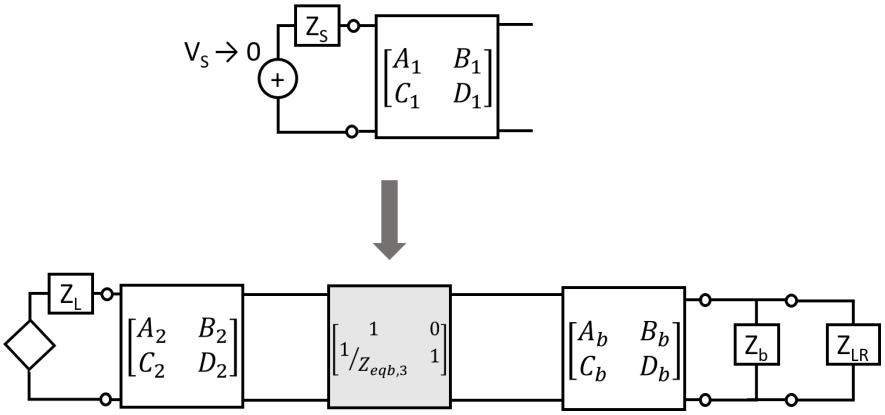

Figure 4.12: CTF from D to R in the first phase

Thus, the CTF between D and S in the first phase is

$$\tilde{H}_{DS}^{(1)} = \frac{Z_S}{A_{DS}^{(1)} Z_S + B_{DS}^{(1)} + C_{DS}^{(1)} Z_S Z_L + D_{DS}^{(1)} Z_L}. \tag{4.30}$$

(f) From D to R in the first phase. In Fig. 4.12, the relay node receives signal from Φ_3 to Φ_2 in the first phase. The first segment, Φ_1 on the backbone is treated as branch which its equivalent input impedance is (4.22). The matrix between D and R in the first phase is

$$\begin{aligned} \Phi_{DR}^{(1)} &= \begin{bmatrix} A_{DR}^{(1)} & B_{DR}^{(1)} \\ C_{DR}^{(1)} & D_{DR}^{(1)} \end{bmatrix} \\ &= \begin{bmatrix} A_2 & B_2 \\ C_2 & D_2 \end{bmatrix} \begin{bmatrix} 1 & 0 \\ \frac{1}{Z_{eqb,3}} & 1 \end{bmatrix} \begin{bmatrix} A_b & B_b \\ C_b & D_b \end{bmatrix}. \end{aligned} \tag{4.31}$$

Thus, the CTF between D and R in the first phase is

$$\tilde{H}_{DR}^{(1)} = \frac{Z'_{LR}}{A_{DR}^{(1)} Z'_{LR} + B_{DR}^{(1)} + C_{DR}^{(1)} Z'_{LR} Z_L + D_{DR}^{(1)} Z_L}. \tag{4.32}$$

(g) From D to S in the second phase. In Fig. 4.13, the relay node is being treated as the load in the second phase. Thus, the equivalent input impedance of the relay branch is (4.25). Therefore, the matrix between D

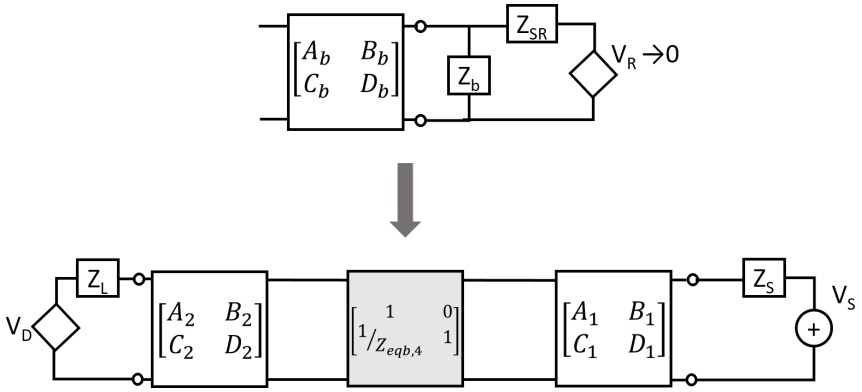

Figure 4.13: CTF from D to S in the second phase

and S in the second phase is

$$\begin{aligned} \Phi_{DS}^{(2)} &= \begin{bmatrix} A_{DS}^{(2)} & B_{DS}^{(2)} \\ C_{DS}^{(2)} & D_{DS}^{(2)} \end{bmatrix} \\ &= \begin{bmatrix} A_2 & B_2 \\ C_2 & D_2 \end{bmatrix} \begin{bmatrix} 1 & 0 \\ \frac{1}{Z_{eqb,4}} & 1 \end{bmatrix} \begin{bmatrix} A_1 & B_1 \\ C_1 & D_1 \end{bmatrix}. \end{aligned} \tag{4.33}$$

Thus, the CTF between D and S in the second phase is

$$\tilde{H}_{DS}^{(2)} = \frac{Z_S}{A_{DS}^{(2)} Z_L + B_{DS}^{(2)} + C_{DS}^{(2)} Z_S Z_L + D_{DS}^{(2)} Z_L}. \tag{4.34}$$

(h) From R to S in the second phase. In Fig. 4.14, the relay node is being treated as the transmitter. The relay node forwards signal from Φ_2 to Φ_1. Thus, the Φ_3 is treated as branch and its equivalent input impedance is (4.19). The matrix between R and S in the second phase is

$$\begin{aligned} \Phi_{RS}^{(2)} &= \begin{bmatrix} A_{RS}^{(2)} & B_{RS}^{(2)} \\ C_{RS}^{(2)} & D_{RS}^{(2)} \end{bmatrix} \\ &= \begin{bmatrix} 1 & 0 \\ Z_b & 1 \end{bmatrix} \begin{bmatrix} A_b & B_b \\ C_b & D_b \end{bmatrix} \begin{bmatrix} 1 & 0 \\ \frac{1}{Z_{eqb,2}} & 1 \end{bmatrix} \begin{bmatrix} A_1 & B_1 \\ C_1 & D_1 \end{bmatrix}. \end{aligned} \tag{4.35}$$

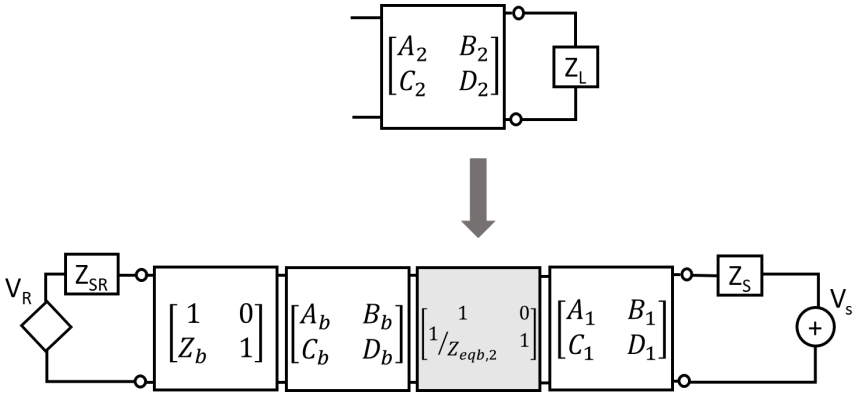

Figure 4.14: CTF from R to S in the second phase

Thus, the CTF between R and S in the second phase is

$$\tilde{H}_{RS}^{(2)} = \frac{Z_S}{A_{RS}^{(2)} Z_S + B_{RS}^{(2)} + C_{RS}^{(2)} Z_S Z_{SR} + D_{RS}^{(2)} Z_{SR}}. \tag{4.36}$$

4.4 Numerical Examples

The topology of a three-node two-way relay-assisted PLC channel is depicted in Fig. 4.15 where each segment of the network used different type of cables. Table 4.1 shows the complete parameters of the three-segment PLC channel realisation.

The relay node is assumed to have different impedance in two different modes, i.e., inner impedance, $Z_{SR} = 50\Omega$ in transmit mode, and load impedance $Z_{LR} = 150\Omega$ in receive mode. Moreover, R', $\omega_0/2\pi$, and Q_f of Z_b are drawn from uniform distributions on $\{200, 1800\}\Omega$, $\{2, 28\}MHz$, and $\{5, 25\}$, respectively [46]. Fig. 4.16 shows the characteristics of a relay load impedance, Z_b, to which the relay is attached to the branch.

The comparison of the CTFs from S to D with and without relay is depicted in Fig. 4.17. It can be seen that the backbone channel gain greatly improved with the assist of relay inside a PLC channel. The CTFs of the three-node two-way relay-assisted PLC are addressed sequentially with different parameter configurations, as shown in (a) - (f) on page 69.

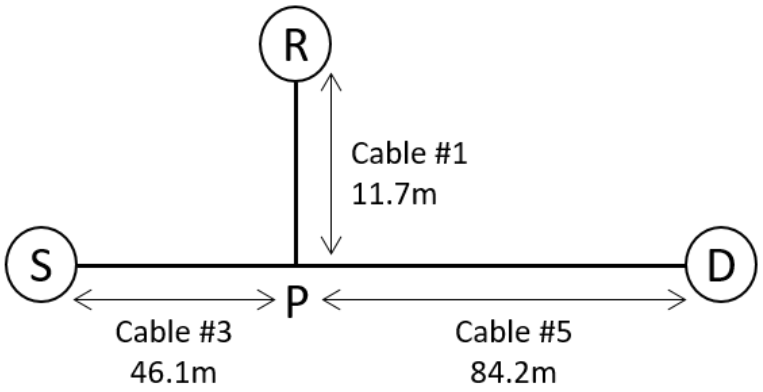

Figure 4.15: A simple three-node two-way channel topology

Table 4.1: Parameters for the three-segment channel realisation

Line section	Length	Cable type	Terminated load
Backbone 1	$d_1 = 46.1m$	$n_{d_1} = 3$	N/A
Branch-tap 1	$d_{b,1} = 11.7m$	$n_{d_{b,1}} = 1$	$Z_b(f,t)$
Backbone 2	$d_2 = 84.2m$	$n_{d_2} = 5$	N/A
Branch-tap 2	$d_{b,2} = 0$	N/A	$Z_{b,2} = \infty$
Backbone 3	$d_3 = 0$	N/A	N/A
Branch-tap 3	$d_{d,3} = 0$	N/A	$Z_{b,3} = \infty$
Backbone 4	$d_4 = 0$	N/A	N/A
Transmitting inner impedance: $Z_S = 50\Omega$			
Receiving load impedance: $Z_L = 150\Omega$			

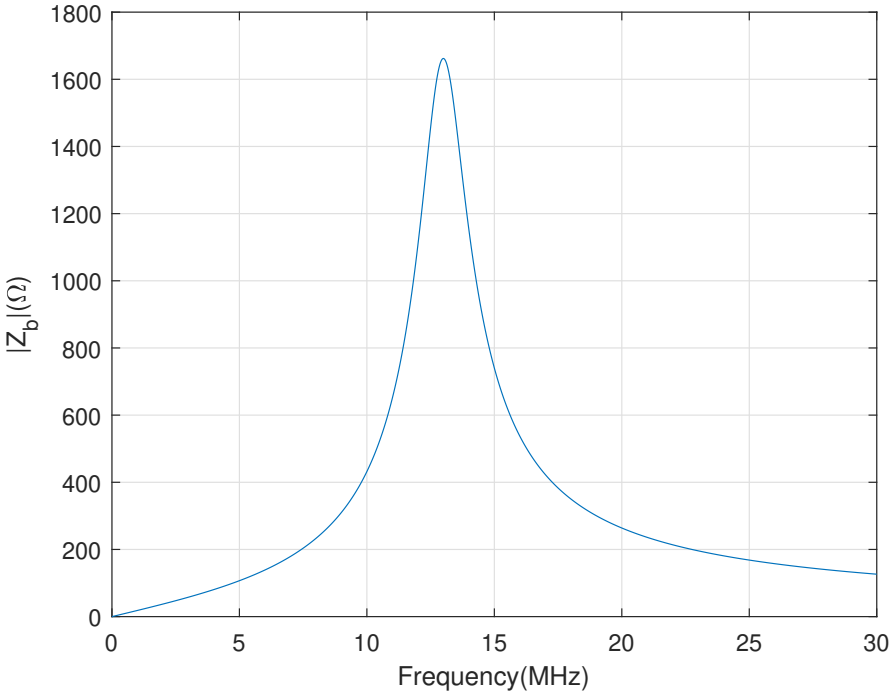

Figure 4.16: Frequency response of $Z_b(f)$

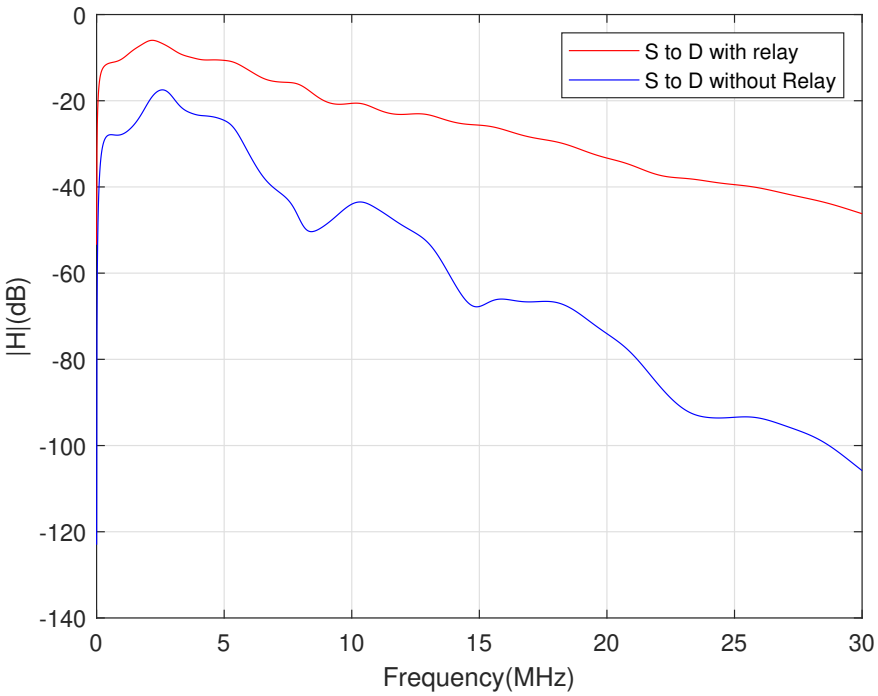

Figure 4.17: CTF of S to D with and without Relay

(a) Transfer function from S to D in the first phase. Parameters are set according to Table 4.2. It is assumed the received impedance of the relay node and the destination node are the same, $Z_{LR} = Z_L$. Thus, the paralleling equivalent impedance of Z_b and Z_{LR} can be calculated. The CTF of $\tilde{H}_{SD}^{(1)}$ can be obtained at Fig. 4.18.

(b) Transfer function from S to R in the first phase. Parameters are set according to Table 4.3. The paralleling equivalent impedance of Z_b and Z_{LR} is treated as the receiving load and the backbone 2 is treated as a "branch". The CTF of $\tilde{H}_{SR}^{(1)}$ is shown in Fig. 4.19.

(c) Transfer function from R to D in the second phase. Parameters are set according to Table 4.4. Since the relay node in the second phase works in transmitting mode, the inner impedance of the relay node and the source node are the same, $Z_{SR} = Z_S$. Backbone 1 is treated as a "branch", and the source voltage, V_S, becomes zero based on the superposition theorem. The CTF of $\tilde{H}_{RD}^{(2)}$ is shown in Fig. 4.20.

(d) Transfer function from S to D in the second phase. Parameters are set according to Table 4.5. The parallel equivalent impedance of Z_b and Z_{SR} is treated as the terminated load on the branch, whereas the relay voltage, V_R, becomes zero based on the superposition theorem. The CTF of $\tilde{H}_{SD}^{(2)}$ is depicted in Fig. 4.21.

(e) Transfer function from D to S in the first phase. Parameters are set according to Table 4.6. It is assumed the received impedance of the relay node and the destination node are the same, $Z_{LR} = Z_L$. Thus, the paralleling equivalent impedance of Z_b and Z_{LR} can be calculated. The CTF of $\tilde{H}_{DS}^{(1)}$ is shown in Fig. 4.22.

(f) Transfer function from D to R in the first phase. Parameters are set according to Table 4.7. The paralleling equivalent impedance of Z_b and Z_{LR} is treated as the receiving load, and the backbone one is treated as a "branch". The CTF of $\tilde{H}_{DR}^{(1)}$ is shown in Fig. 4.23.

Table 4.2: Parameters for generating $\tilde{H}_{SD}^{(1)}$

Line section	Length	Cable type	Terminated load
Backbone 1	$d_1 = 46.1m$	$n_{d_1} = 3$	N/A
Branch-tap 1	$d_{b,1} = 11.7m$	$n_{d_{b,1}} = 1$	$Z_b(f)\|\|Z_{LR}$
Backbone 2	$d_2 = 84.2m$	$n_{d_2} = 5$	N/A
Branch-tap 2	$d_{b,2} = 0$	N/A	$Z_{b,2} = \infty$
Backbone 3	$d_3 = 0$	N/A	N/A
Branch-tap 3	$d_{d,3} = 0$	N/A	$Z_{b,3} = \infty$
Backbone 4	$d_4 = 0$	N/A	N/A
Transmitting inner impedance: $Z_S = 50\Omega$			
Receiving load impedance: $Z_L = 150\Omega$			

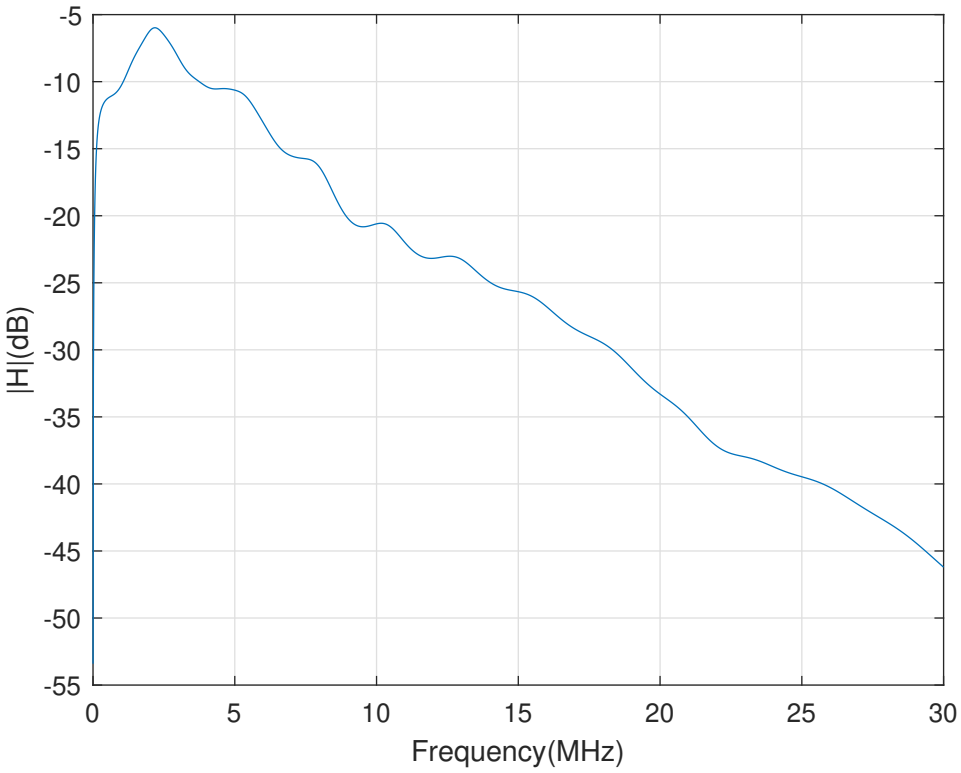

Figure 4.18: CTF of S to D in first phase

Table 4.3: Parameters for generating $\tilde{H}_{SR}^{(1)}$

Line section	Length	Cable type	Terminated load
Backbone 1	$d_1 = 46.1m$	$n_{d_1} = 3$	N/A
Branch-tap 1	$d_2 = 84.2m$	$n_{d_2} = 5$	Z_L
Backbone 2	$d_{b,1} = 11.7m$	$n_{d_{b,1}} = 1$	N/A
Branch-tap 2	$d_{b,2} = 0$	N/A	$Z_{b,2} = \infty$
Backbone 3	$d_3 = 0$	N/A	N/A
Branch-tap 3	$d_{d,3} = 0$	N/A	$Z_{b,3} = \infty$
Backbone 4	$d_4 = 0$	N/A	N/A
Transmitting inner impedance: $Z_S = 50\Omega$			
Receiving load impedance: $Z_b \| \| Z_{LR}$			

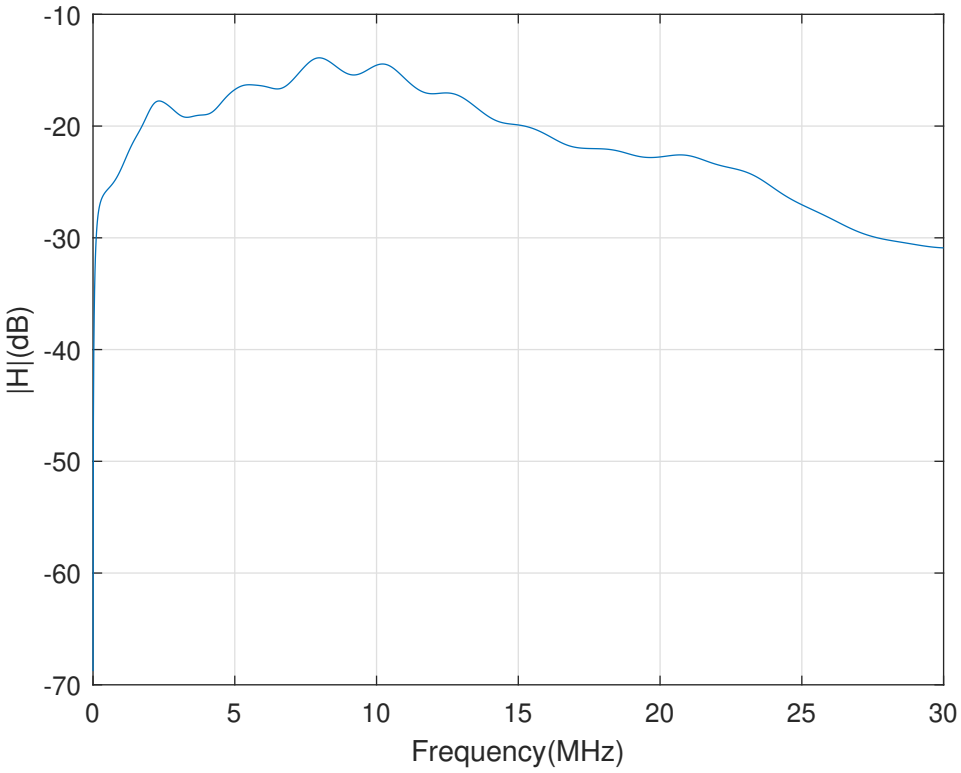

Figure 4.19: CTF of S to R in first phase

Table 4.4: Parameters for generating $\tilde{H}_{RD}^{(2)}$

Line section	Length	Cable type	Terminated load
Backbone 1	$d_0 = 0$	N/A	N/A
Branch-tap 1	$d_{b,0} = 0$	N/A	$Z_b(f)$
Backbone 2	$d_{b,1} = 11.7m$	$n_{d_{b,1}} = 1$	N/A
Branch-tap 2	$d_1 = 46.1m$	$n_{d_1} = 3$	$Z_S = 50\Omega$
Backbone 3	$d_2 = 84.2m$	$n_{d_2} = 5$	N/A
Branch-tap 3	$d_{d,3} = 0$	N/A	$Z_{b,3} = \infty$
Backbone 4	$d_4 = 0$	N/A	N/A
Transmitting inner impedance: $Z_S R = 50\Omega$			
Receiving load impedance: $Z_L = 150\Omega$			

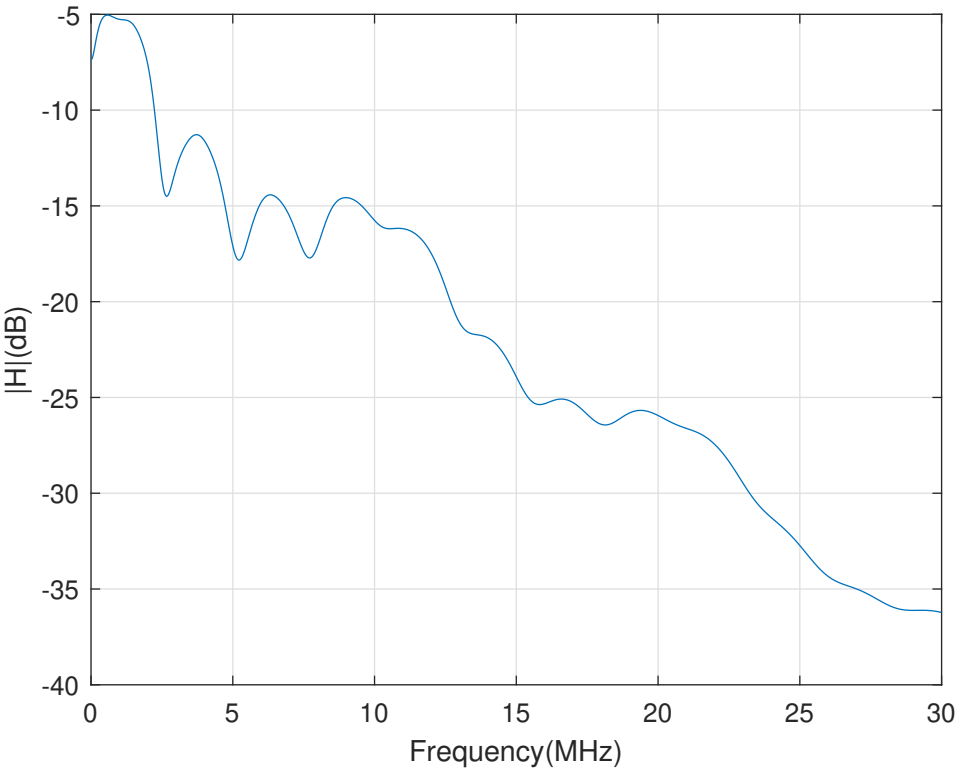

Figure 4.20: CTF of S to D in second phase

Table 4.5: Parameters for generating $\tilde{H}_{SD}^{(2)}$

Line section	Length	Cable type	Terminated load
Backbone 1	$d_1 = 46.1m$	$n_{d_1} = 3$	N/A
Branch-tap 1	$d_{b,1} = 11.7m$	$n_{d_{b,1}} = 1$	$Z_b \| \| Z_{LR}$
Backbone 2	$d_2 = 84.2m$	$n_{d_2} = 5$	N/A
Branch-tap 2	$d_{b,2} = 0$	N/A	$Z_{b,2} = \infty$
Backbone 3	$d_3 = 0$	N/A	N/A
Branch-tap 3	$d_{d,3} = 0$	N/A	$Z_{b,3} = \infty$
Backbone 4	$d_4 = 0$	N/A	N/A
Transmitting inner impedance: $Z_S = 50\Omega$			
Receiving load impedance: $Z_L = 150\Omega$			

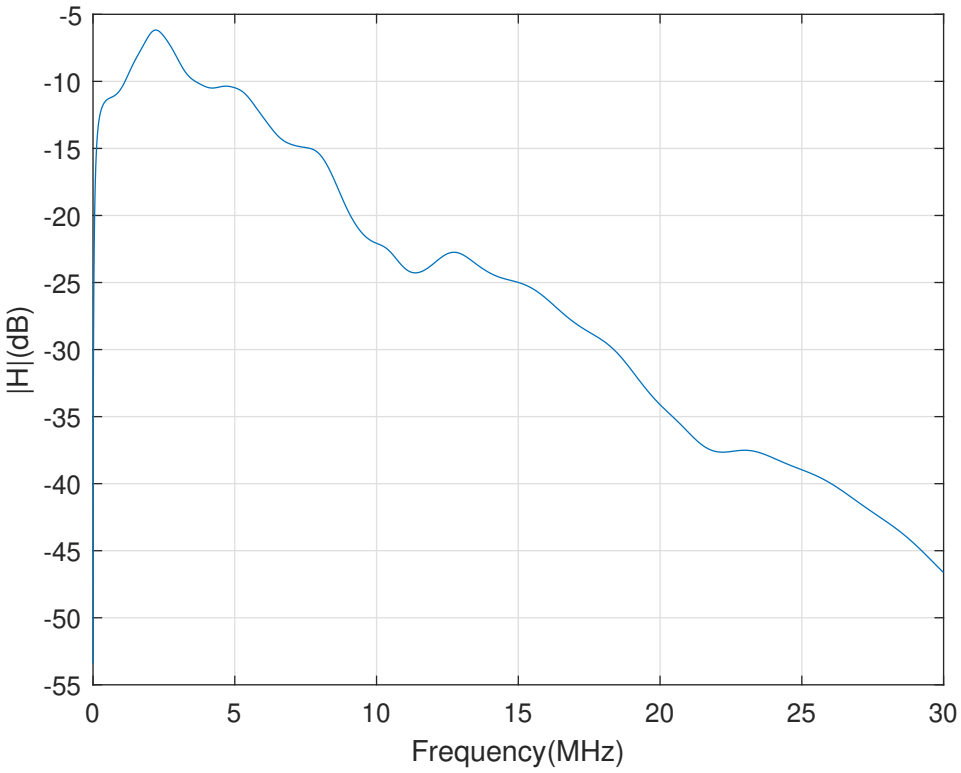

Figure 4.21: CTF of S to D in second phase

Table 4.6: Parameters for generating $\tilde{H}_{DS}^{(1)}$

Line section	Length	Cable type	Terminated load
Backbone 1	$d_2 = 84.2m$	$n_{d_2} = 5$	N/A
Branch-tap 1	$d_{b,1} = 11.7m$	$n_{d_{b,1}} = 1$	$Z_b \| \| Z_{LR}$
Backbone 2	$d_1 = 46.1m$	$n_{d_1} = 3$	N/A
Branch-tap 2	$d_{b,2} = 0$	N/A	$Z_{b,2} = \infty$
Backbone 3	$d_3 = 0$	N/A	N/A
Branch-tap 3	$d_{d,3} = 0$	N/A	$Z_{b,3} = \infty$
Backbone 4	$d_4 = 0$	N/A	N/A
Transmitting inner impedance: $Z_S = 50\Omega$			
Receiving load impedance: $Z_L = 150\Omega$			

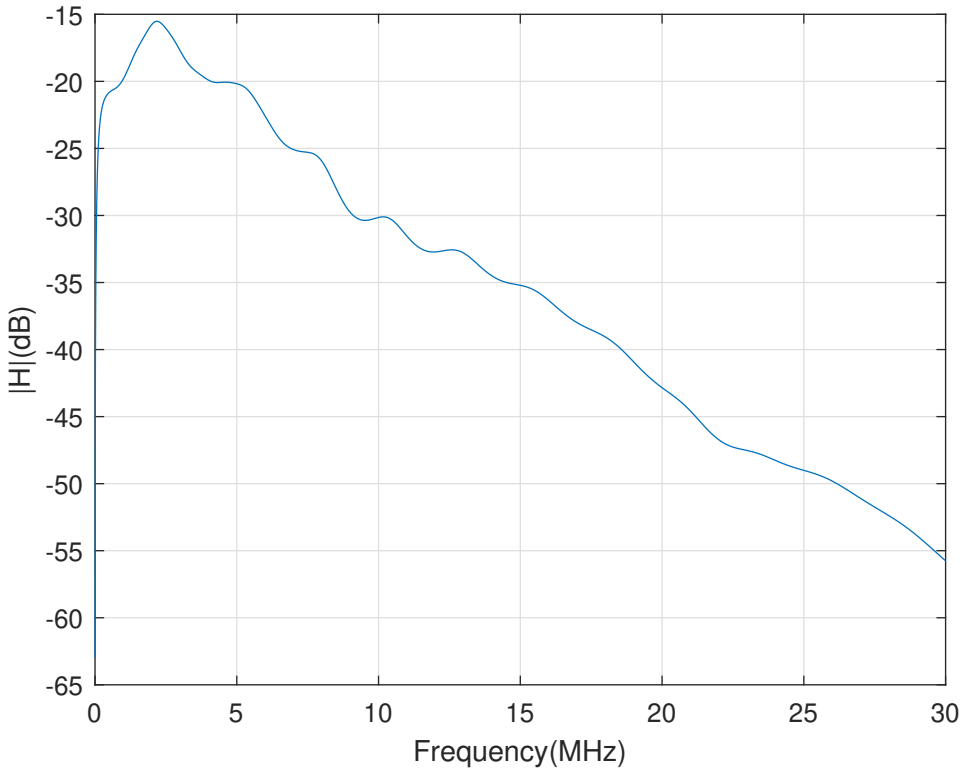

Figure 4.22: CTF of D to S in first phase

Table 4.7: Parameters for generating $\tilde{H}_{DR}^{(1)}$

Line section	Length	Cable type	Terminated load
Backbone 1	$d_2 = 84.2m$	$n_{d_2} = 5$	N/A
Branch-tap 1	$d_1 = 46.1m$	$n_{d_1} = 3$	Z_S
Backbone 2	$d_{b,1} = 11.7m$	$n_{d_{b,1}} = 1$	N/A
Branch-tap 2	$d_{b,2} = 0$	N/A	$Z_{b,2} = \infty$
Backbone 3	$d_3 = 0$	N/A	N/A
Branch-tap 3	$d_{d,3} = 0$	N/A	$Z_{b,3} = \infty$
Backbone 4	$d_4 = 0$	N/A	N/A
Transmitting inner impedance: $Z_L = 150\Omega$			
Receiving load impedance: $Z_b \| \| Z_{LR}$			

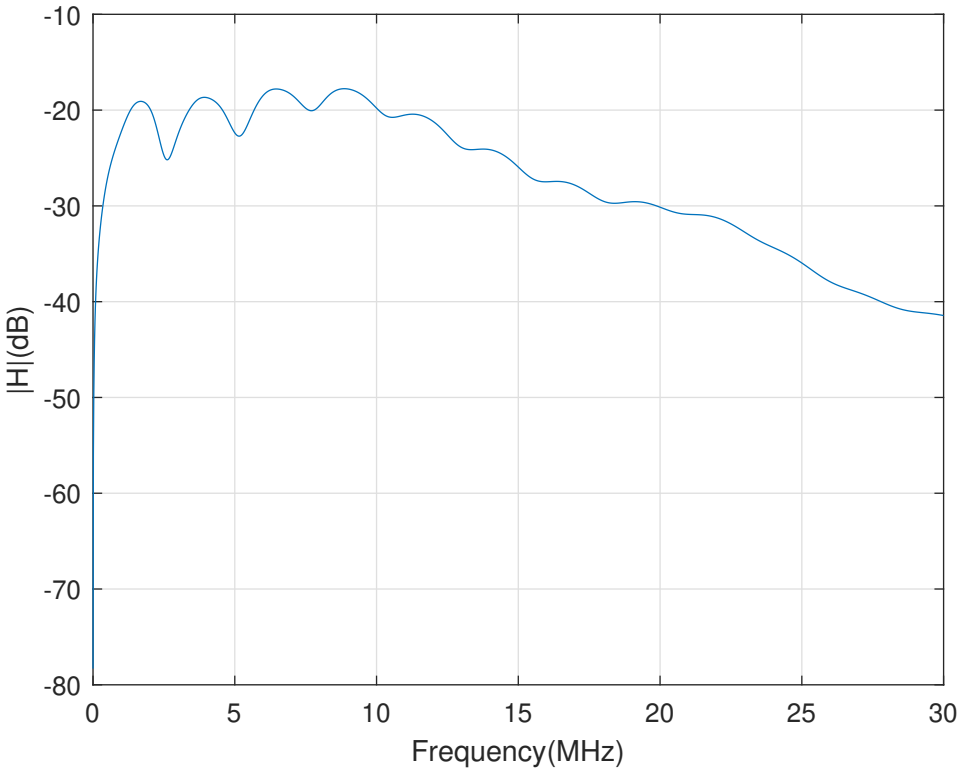

Figure 4.23: CTF of D to R in first phase

Table 4.8: Parameters for generating $\tilde{H}_{DS}^{(2)}$

Line section	Length	Cable type	Terminated load
Backbone 1	$d_2 = 84.2m$	$n_{d_2} = 5$	N/A
Branch-tap 1	$d_{b,1} = 11.7m$	$n_{d_{b,1}} = 1$	$Z_b \| \| Z_{SR}$
Backbone 2	$d_1 = 46.1m$	$n_{d_1} = 3$	N/A
Branch-tap 2	$d_{b,2} = 0$	N/A	$Z_{b,2} = \infty$
Backbone 3	$d_3 = 0$	N/A	N/A
Branch-tap 3	$d_{d,3} = 0$	N/A	$Z_{b,3} = \infty$
Backbone 4	$d_4 = 0$	N/A	N/A
Transmitting inner impedance: $Z_L = 150\Omega$			
Receiving load impedance: $Z_S = 50\Omega$			

(g) Transfer function for D to S in the second phase. Parameters are set according to Table 4.8. The paralleling equivalent impedance of Z_b and Z_{sR} is treated as the terminated load on the branch, whereas the relay voltage, V_R, becomes zero based on the superposition theorem. The CTF of $\tilde{H}_{DS}^{(2)}$ is shown in Fig. 4.24.

(h) Transfer function from R to S in the second phase. Parameters are set according to Table 4.9. Since the relay node in the second phase works in transmitting mode, the inner impedance of the relay node and the source node are the same, $Z_{SR} = Z_S$. Backbone 2 is treated as a "branch". The CTF of $\tilde{H}_{RS}^{(2)}$ is shown in Fig. 4.25.

All the transfer function results of Figs. 4.18-4.25 are combined together to give the overall CTFs of the three-node two-way relay-assisted PLC in Fig. 4.26.

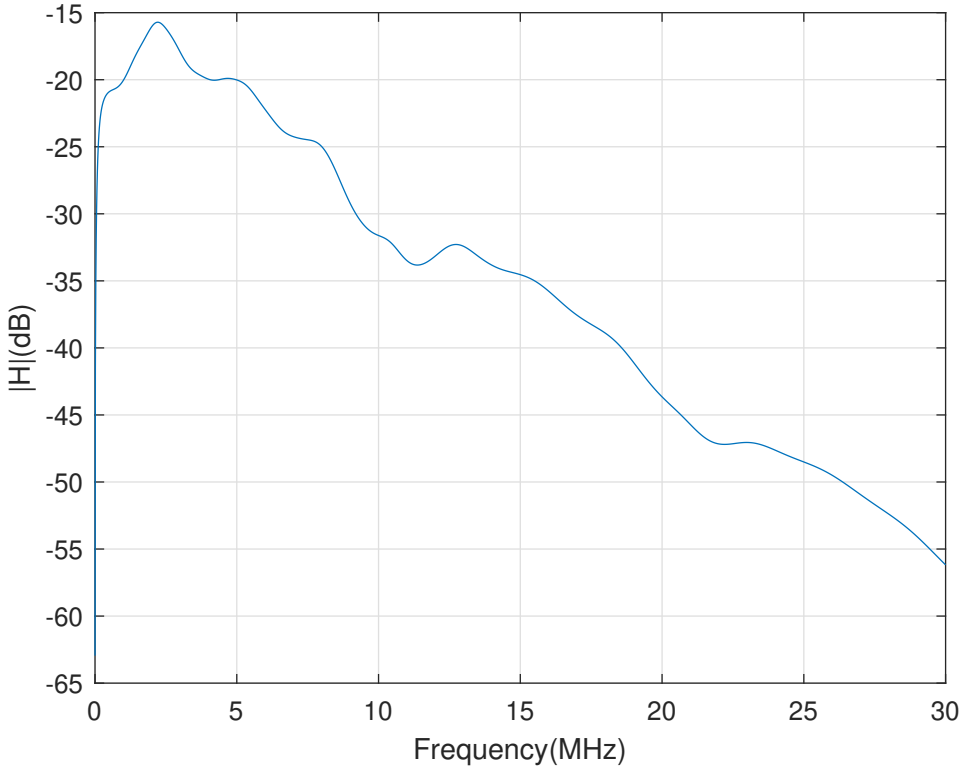

Figure 4.24: CTF of D to S in second phase

Table 4.9: Parameters for generating $\tilde{H}_{RS}^{(2)}$

Line section	Length	Cable type	Terminated load
Backbone 1	$d_0 = 0$	N/A	N/A
Branch-tap 1	$d_b = 0$	N/A	Z_b
Backbone 2	$d_{b,1} = 11.7m$	$n_{d_{b,1}} = 1$	N/A
Branch-tap 2	$d_2 = 84.2m$	$n_{d_2} = 5$	Z_L
Backbone 3	$d_1 = 46.1m$	$n_{d_1} = 3$	N/A
Branch-tap 3	$d_{d,3} = 0$	N/A	$Z_{b,3} = \infty$
Backbone 4	$d_4 = 0$	N/A	N/A
Transmitting inner impedance: $Z_{SR} = 50\Omega$			
Receiving load impedance: $Z_S = 50\Omega$			

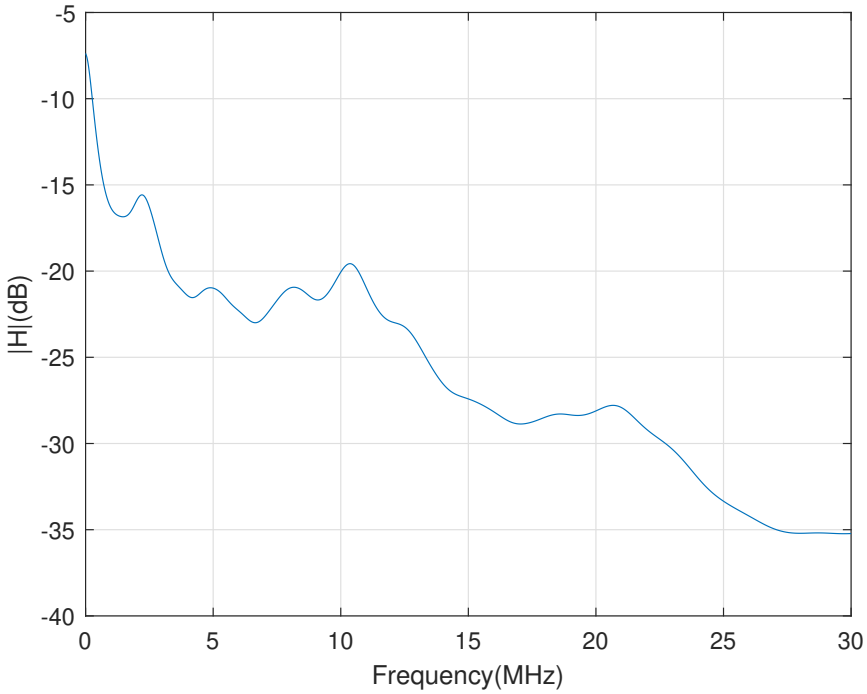

Figure 4.25: CTF of R to S in second phase

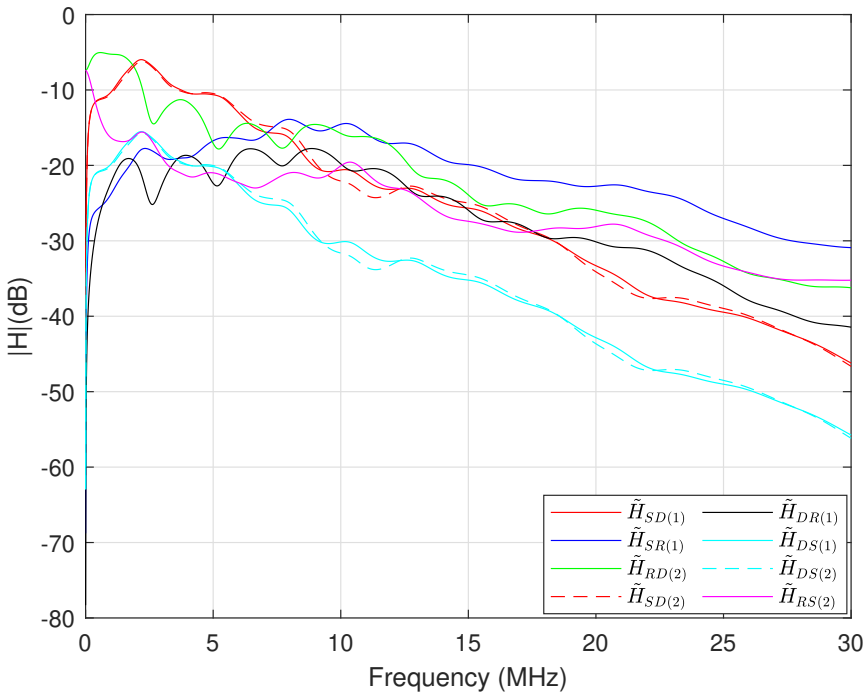

Figure 4.26: CTF of a three-hop two-way relay system

In the literature [107], the numerical results of the forward channel are compared and justified with the experimental result. Hereby, the backward CTF is derived using the same methodology to justify the numerical results. It can be seen that

$$H_{SD} \neq \tilde{H}_{SD}^{(1)} \neq \tilde{H}_{SD}^{(2)}, \tag{4.37}$$

$$H_{DS} \neq \tilde{H}_{DS}^{(1)} \neq \tilde{H}_{DS}^{(2)}, \tag{4.38}$$

$$\tilde{H}_{SD}^{(1)} \neq \tilde{H}_{SR}^{(1)}\tilde{H}_{RD}^{(2)}, \tag{4.39}$$

$$\tilde{H}_{SD}^{(2)} \neq \tilde{H}_{SR}^{(1)}\tilde{H}_{RD}^{(2)}, \tag{4.40}$$

$$\tilde{H}_{DS}^{(1)} \neq \tilde{H}_{DR}^{(1)}\tilde{H}_{RS}^{(2)}, \tag{4.41}$$

$$\tilde{H}_{DS}^{(2)} \neq \tilde{H}_{DR}^{(1)}\tilde{H}_{RS}^{(2)}. \tag{4.42}$$

In this part, the path gains in the relay-assisted PLC are prove to be correlated to each other. The magnitude of the two-way path gains, $\{\tilde{H}_{SD}^{(1)}, \tilde{H}_{SR}^{(1)}, \tilde{H}_{RD}^{(2)}, \tilde{H}_{SD}^{(2)}, \tilde{H}_{DR}^{(1)}, \tilde{H}_{DS}^{(1)}, \tilde{H}_{DS}^{(2)}, \tilde{H}_{RS}^{(2)}\}$, is denoted to be $\{x_1, \cdots, x_8\}$. The magnitude of the forward and backward channels are given by $\{x_1, \cdots, x_4\}$ and $\{x_5, \cdots, x_8\}$. The degree of correlation is calculated by [110]

$$d_c = \sqrt{\frac{\sum_{i,j}(\rho_{i,j})^2}{N_\rho}}, \tag{4.43}$$

for $i > j$ and $i, j = 1, \cdots, 8$, where N_ρ is the number of $\rho_{i,j}$ and

$$\rho_{i,j} = \frac{Cov(x_i, x_j)}{STD(x_i)STD(x_j)}. \tag{4.44}$$

In (4.44), $Cov(\cdot)$ and $STD(\cdot)$ denote the covariance and standard deviation, respectively.

As a result, the channels are highly correlated to each other as the realisation of the degree of correlation of forward, backward, and two-way channels are 0.6674, 0.6672, and 0.6997, respectively.

4.5 Chapter Summary

In this chapter, the channel model of a three-node two-way relay-assisted PLC system has been proposed to fulfill the two-way communication links for all PLC application. Based on the transmission line theory analysis, the CTFs of a three-node two-way relay-assisted PLC system is derived using ABCD method. It is a straight forward application to verify the Canate's PLC channel model. Simulation results show that the CTFs of the proposed relay-assisted PLC channels can be obtained by dividing them into group of an equivalent P2P PLC channels. Moreover, the reliability of this model has been verified using deterministic channel samples. From the degree of correlation, a two-way PLC channels is proved to have higher correlation of about 5% more compared to one-way PLC channel. The generated relay-assisted channel samples offer a good realistic testing platform for the relay schemes mentioned in subsequent chapters.

Chapter 5

CTFs of Two-way Two-relay PLC Systems

In this chapter, the channel model in a two-way PLC system, which is discussed in Chapter 4 is extended to two-relay PLC forward and backward CTFs using ABCD matrix. In the proposed design scheme, composite CTF for a certain link is also discussed and compared with the single-relay system. An introduction of a relay-assisted PLC systems is described in Section 5.1. The technique of modelling the channel are presented in Section 5.2. In Section 5.3, the CTFs of a two-way two-relay are derived. Numerical examples are shown in Section 5.4 to verify the the results. Finally, the chapter summary is highlighted in Section 5.5.

5.1 Introduction

A single-relay, or sometimes called as three-nodes, one-way channel model has been proposed in [107]. However, many PLC applications need two-way communication links. In [111], the system performance of two-way relay-assisted PLC was evaluated. Furthermore, an extended channel model of the one in [107] for two-way scheme relay-assisted PLC was presented in the previous chapter. It has

been shown that the links in the two-way channels are highly correlated to each other. Additionally, the CTF of the forward and backward channels are different.

It is obvious that the performance of the system can be further improved by adding more relays. In particular, it has been shown that the average capacity, coverage, and throughput improve with the increase in the number of relays [71], [112]. However, increasing the number of relays increases the total power consumption due to the static power of modem [113].

A bottom-up channel model for two-relay one-way PLC network has been derived in [112]. It has been found that in the two-relay system, the use of both relays degrades the CTF when compared to the use of one relay only. It has been stated that the physical topology affects the channel characteristics [114]. Therefore, the channel characteristics of both systems need to be observed when opting for using a single-relay or two-relay two-way PLC system. Nevertheless, the comparison of the channel transfer function of single-relay and two-relay two-way PLC system is not available in the literature. This chapter fills this gap by first extending the one-way channel model in [112] into a two-way channel model. Next, a few comparable topologies and scenarios are deployed to simulate the CTFs.

5.2 Modelling of Circuit

In this chapter, Canate's hybrid P2P channel model is used, which consists of four segments and three branches, where each branch is terminated by a load impedance [46]. In each segment, the cable is characterised by its parameters and length. For the sake of simplicity and fairness, the three terminated loads are assumed to have the same impedances.

A general channel model of a two-branch transmission circuit consists of five cascaded two-port sub-circuits, i.e., three backbone transmission line segments, Φ_1, Φ_3, Φ_5, and two branched-circuit segments, Φ_2, Φ_4, is depicted in Fig. 5.1.

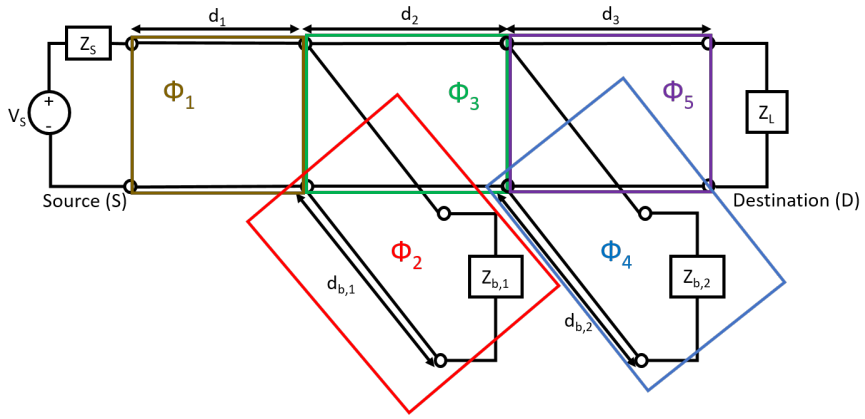

Figure 5.1: A transmission line with two-branch circuit

Further, Fig. 5.2 shows the two-port network layout of the proposed two-relay PLC system model consisting of source (S), relay 1 (R_1), relay 2 (R_2), and destination (D). Its simplification along with the possible communication links is shown in Fig. 5.3.

The simple steps to obtain the composite CTF for a certain link are as follows:

1. Calculate the equivalent input impedance, which depends on cable types, parameters, and lengths.
2. The ABCD matrix of each segment can be obtained using the equivalent impedance.
3. The overall ABCD matrix for the whole structure is the product of the ABCD matrix of each segment.
4. The transfer function can be obtained and expressed as the ratio of the load voltage to the source voltage [115], [116].
5. Lastly, the composite CTF for a certain link can be found by summing the respective CTFs of the segments which constitute the link. For example, the composite CTF of the entire S-R_1-D link is the sum of CTF of S-R_1 segment and CTF of R_1-D segment. If AF relay is used, there will be an amplifying constant in each segment except the last ABCD matrix [112].

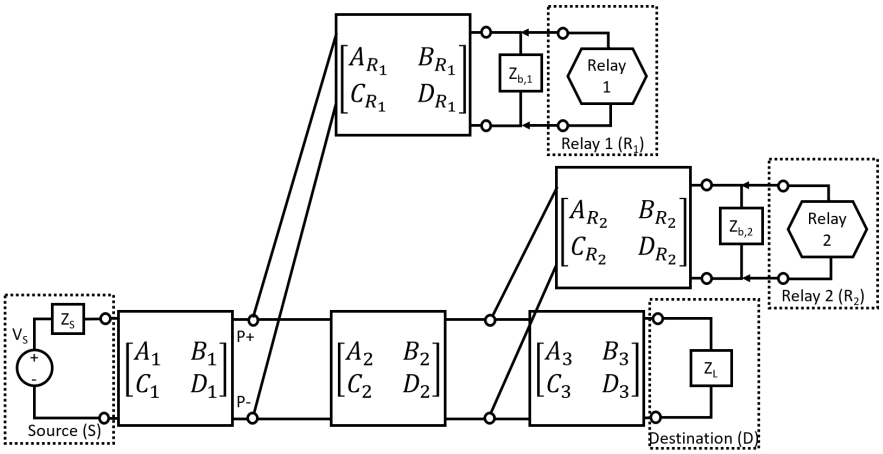

Figure 5.2: Network layout of four-segment

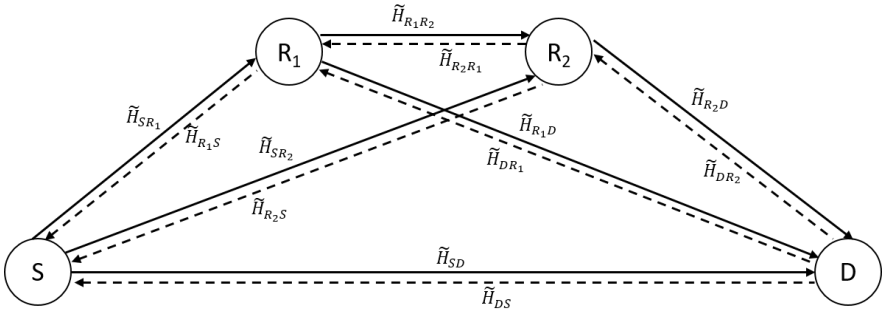

Figure 5.3: A four-node two-way relay-assisted PLC system model

5.3 CTF Derivation

In this section, the CTFs of all possible signalling path shown in Fig. 5.3 are derived. It is assumed that there is an ABCD matrix of transmitter source.

(a) Transfer function of direct path from S to D. Considering Fig. 5.2, the direct path from source to destination, the relay nodes, R_1 and R_2 are treated as the loads. The signaling of the direct path can be found by first calculating the equivalent impedance of the two relay branches as follows

$$Z_{eqb,1} = \frac{A_{R_1} Z'_{LR_1} + B_{R_1}}{C_{R_1} Z'_{LR_1} + D_{R_1}}, \tag{5.1}$$

$$Z_{eqb,2} = \frac{A_{R_2} Z'_{LR_2} + B_{R_2}}{C_{R_2} Z'_{LR_2} + D_{R_2}}, \tag{5.2}$$

where Z'_{LR_1} and Z'_{LR_2} is the equivalent impedance of Z_b parallel to Z_{LR_1} and Z_{LR_2}, respectively.

$$Z'_{LR_1} = Z_{b_1} || Z_{LR_1} = \frac{Z_{b_1} Z_{LR_1}}{Z_{b_1} + Z_{LR_1}}, \tag{5.3}$$

$$Z'_{LR_2} = Z_{b_2} || Z_{LR_2} = \frac{Z_{b_2} Z_{LR_2}}{Z_{b_2} + Z_{LR_2}}. \tag{5.4}$$

Therefore, the ABCD matrix of the direct path from S to D is given by

$$\begin{aligned} \Phi_{SD}^{(D)} &= \begin{bmatrix} A_{SD}^{(D)} & B_{SD}^{(D)} \\ C_{SD}^{(D)} & D_{SD}^{(D)} \end{bmatrix} \\ &= \begin{bmatrix} 1 & Z_S \\ 0 & 1 \end{bmatrix} \begin{bmatrix} A_1 & B_1 \\ C_1 & D_1 \end{bmatrix} \begin{bmatrix} 1 & 0 \\ \frac{1}{Z_{eqb,1}} & 1 \end{bmatrix} \begin{bmatrix} A_2 & B_2 \\ C_2 & D_2 \end{bmatrix} \\ &\times \begin{bmatrix} 1 & 0 \\ \frac{1}{Z_{eqb,2}} & 1 \end{bmatrix} \begin{bmatrix} A_3 & B_3 \\ C_3 & D_3 \end{bmatrix}. \end{aligned} \tag{5.5}$$

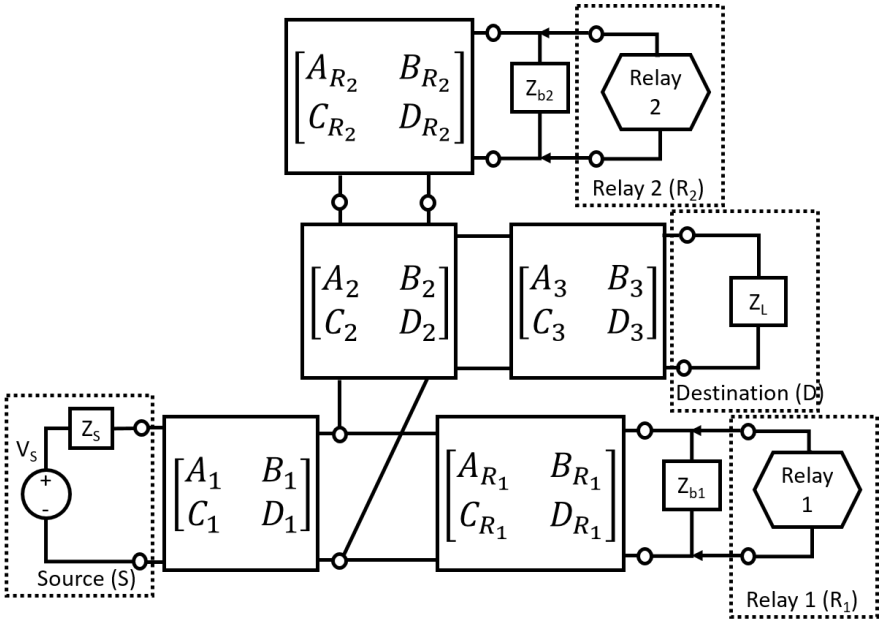

Figure 5.4: Network layout of the path S to R_1

As a result, the CTF of the direct path from S to D can be expressed as

$$\tilde{H}_{SD}^{(D)} = \frac{Z_L}{A_{SD}^{(D)} Z_L + B_{SD}^{(D)} + C_{SD}^{(D)} Z_L Z_S + D_{SD}^{(D)} Z_S}. \tag{5.6}$$

(b) Transfer function of the path S to D through R_1.

The section describes the connection between two paths, i.e. S to R_1 and R_1 to D.

- In Fig. 5.4, the signal travels from S - R_1, as always, R_1 is considered as the destination while R_2 and D behave as branches. The branch impedance is calculated first where R_2 is parallel to D. The equivalent input impedance of the branch is calculated by the impedance sum of R_2 and D, given by

$$Z_{R_2D} = \frac{A_2 Z'_{R_2D} + B_2}{C_2 Z'_{R_2D} + D_2}, \tag{5.7}$$

where Z'_{R_2D} is the equivalent impedance of $Z_{eq2}||Z_{Deq}$, and Z_{Deq} is the equivalent impedance of the D branch.

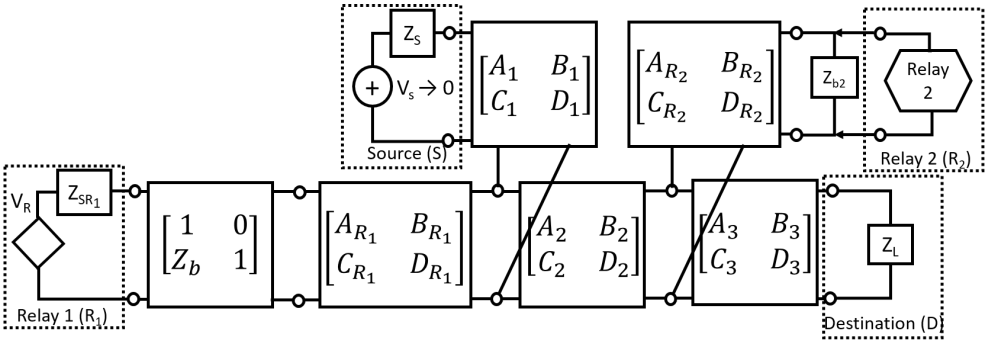

Figure 5.5: Network layout of the path R_1 to D

Their expressions are given by

$$Z'_{R_2D} = Z_{eq2}||Z_{Deq} = \frac{Z_{eq2}Z_{Deq}}{Z_{eq2}+Z_{Deq}}, \tag{5.8}$$

$$Z_{Deq} = \frac{A_3Z_L+B_3}{C_3Z_L+D_3}. \tag{5.9}$$

Second, the ABCD matrix of the direct path from S to R_1 is expressed as follows

$$\begin{aligned}\Phi^{(1)}_{SR_1} &= \begin{bmatrix} A^{(1)}_{SR_1} & B^{(1)}_{SR_1} \\ C^{(1)}_{SR_1} & D^{(1)}_{SR_1} \end{bmatrix} \\ &= \begin{bmatrix} 1 & Z_S \\ 0 & 1 \end{bmatrix} \begin{bmatrix} A_1 & B_1 \\ C_1 & D_1 \end{bmatrix} \begin{bmatrix} 1 & 0 \\ \frac{1}{Z_{R_2D}} & 1 \end{bmatrix} \begin{bmatrix} A_{R_1} & B_{R_1} \\ C_{R_1} & D_{R_1} \end{bmatrix}. \end{aligned} \tag{5.10}$$

Third, the CTF of S - R_1 can be calculated by

$$\tilde{H}^{(1)}_{SR_1} = \frac{Z'_{LR_1}}{A^{(1)}_{SR_1}Z'_{LR_1} + B^{(1)}_{SR_1} + C^{(1)}_{SR_1}Z_SZ'_{LR_1} + D^{(1)}_{SR_1}Z_S}. \tag{5.11}$$

- The path R_1 - D is considered as in Fig. 5.5. Here, R_1 behaves as the source and D behaves as the destination while S and R_2 become the branches. The equivalent input impedance of the branch is given by

$$Z_{Seq} = \frac{A_1Z_S+B_1}{C_1Z_S+D_1}. \tag{5.12}$$

With the second relay impedance and the source impedance, the path matrix from R_1 - D can be expressed as

$$\begin{aligned}\Phi^{(2)}_{R_1D} &= \begin{bmatrix} A^{(2)}_{R_1D} & B^{(2)}_{R_1D} \\ C^{(2)}_{R_1D} & D^{(2)}_{R_1D} \end{bmatrix} \\ &= \begin{bmatrix} 1 & 0 \\ Z_{b,1} & 1 \end{bmatrix} \begin{bmatrix} A_{R_1} & B_{R_1} \\ C_{R_1} & D_{R_1} \end{bmatrix} \begin{bmatrix} 1 & 0 \\ \frac{1}{Z_{Seq}} & 1 \end{bmatrix} \begin{bmatrix} A_2 & B_2 \\ C_2 & D_2 \end{bmatrix} \\ &\times \begin{bmatrix} 1 & 0 \\ \frac{1}{Z_{eq2}} & 1 \end{bmatrix} \begin{bmatrix} A_3 & B_3 \\ C_3 & D_3 \end{bmatrix}. \end{aligned} \tag{5.13}$$

Therefore, the CTF of R_1 - D path is

$$\tilde{H}^{(2)}_{R_1D} = \frac{Z_L}{A^{(2)}_{R_1D}Z_L + B^{(2)}_{R_1D} + C^{(2)}_{R_1D}Z_LZ_{SR_1} + D^{(2)}_{R_1D}Z_{SR_1}}. \tag{5.14}$$

Lastly, the composite path gain of the entire S - R_1 - D link is given by

$$\tilde{H}^{(R_1)}_{SD} = (\tilde{H}^{(1)}_{SR_1}A) + \tilde{H}^{(2)}_{R_1D}, \tag{5.15}$$

where A is the amplification factor when AF relay is employed.

(c) Transfer function of the path S to D through R_2. Similarly, the link S to D through R_2 consists of 2 paths, i.e. S - R_2 and R_2 - D.

- For the first path, the signal travels from S to R_2 is depicted in Fig. 5.6. R_2 is considered as the destination while R_1 and D are treated as branches. The path matrix from S to R_2 is

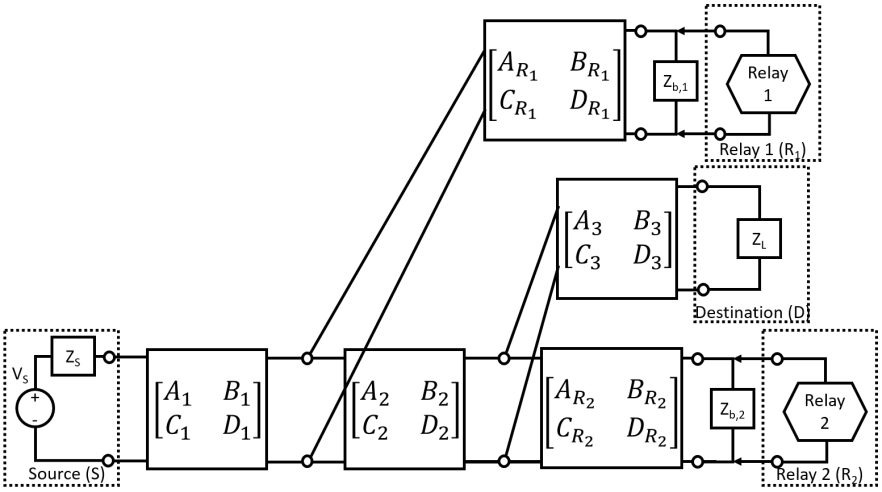

Figure 5.6: Network layout of the path S to R_2

$$\begin{aligned} \Phi^{(1)}_{SR_2} &= \begin{bmatrix} A^{(1)}_{SR_2} & B^{(1)}_{SR_2} \\ C^{(1)}_{SR_2} & D^{(1)}_{SR_2} \end{bmatrix} \\ &= \begin{bmatrix} 1 & Z_S \\ 0 & 1 \end{bmatrix} \begin{bmatrix} A_1 & B_1 \\ C_1 & D_1 \end{bmatrix} \begin{bmatrix} 1 & 0 \\ \frac{1}{Z_{eqb,1}} & 1 \end{bmatrix} \begin{bmatrix} A_2 & B_2 \\ C_2 & D_2 \end{bmatrix} \\ &\times \begin{bmatrix} 1 & 0 \\ \frac{1}{Z_{Deq}} & 1 \end{bmatrix} \begin{bmatrix} A_{R_2} & B_{R_2} \\ C_{R_2} & D_{R_2} \end{bmatrix}. \end{aligned} \tag{5.16}$$

Therefore, the CTF for S - R_2 can be expressed as

$$\tilde{H}^{(1)}_{SR_2} = \frac{Z'_{LR_2}}{A^{(1)}_{SR_2} Z'_{LR_2} + B^{(1)}_{SR_2} + C^{(1)}_{SR_2} Z'_{LR_2} Z_S + D^{(1)}_{SR_2} Z_S}. \tag{5.17}$$

- In the second path, i.e. R_2 to D, S and R_1 become the branches. The equivalent input impedance of the S - R_1 branch is

$$Z_{SR_1} = \frac{A_2 Z'_{SR_1} + B_2}{C_2 Z'_{SR_1} + D_2}, \tag{5.18}$$

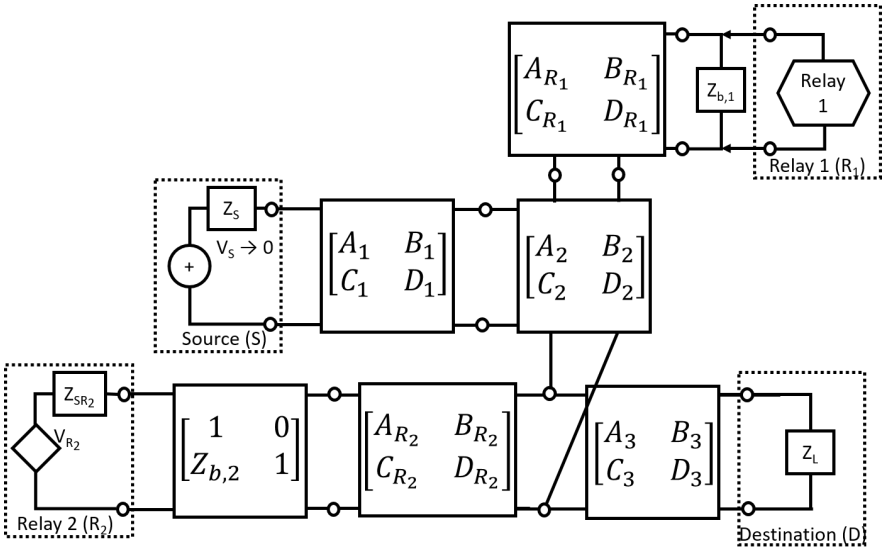

Figure 5.7: Network layout of the path R_2 to D

where Z'_{SR_1} is given by

$$Z'_{SR_1} = Z_{eqb,1}||Z_{Seq} = \frac{Z_{eqb,1}Z_{Seq}}{Z_{eqb,1}+Z_{Seq}}. \tag{5.19}$$

The matrix for R_2 - D path is given by

$$\begin{aligned}\Phi^{(2)}_{R_2D} &= \begin{bmatrix} A^{(2)}_{R_2D} & B^{(2)}_{R_2D} \\ C^{(2)}_{R_2D} & D^{(2)}_{R_2D}\end{bmatrix} \\ &= \begin{bmatrix} 1 & 0 \\ Z_{b_2} & 1\end{bmatrix}\begin{bmatrix} A_{R_2} & B_{R_2} \\ C_{R_2} & D_{R_2}\end{bmatrix}\begin{bmatrix} 1 & 0 \\ \frac{1}{Z_{SR_1}} & 1\end{bmatrix}\begin{bmatrix} A_3 & B_3 \\ C_3 & D_3\end{bmatrix}.\end{aligned} \tag{5.20}$$

Therefore, the CTF for R_2 - D path is

$$\tilde{H}^{(2)}_{R_2D} = \frac{Z_L}{A^{(2)}_{R_2D}Z_L + B^{(2)}_{R_2S} + C^{(2)}_{R_2D}Z_LZ_{SR_2} + D^{(2)}_{R_2D}Z_{SR_2}}. \tag{5.21}$$

Finally, the composite path gain of the entire S - R_2 - D link is given by

$$\tilde{H}^{(R_2)}_{SD} = (\tilde{H}^{(1)}_{SR_2}A) + \tilde{H}^{(2)}_{R_2D}. \tag{5.22}$$

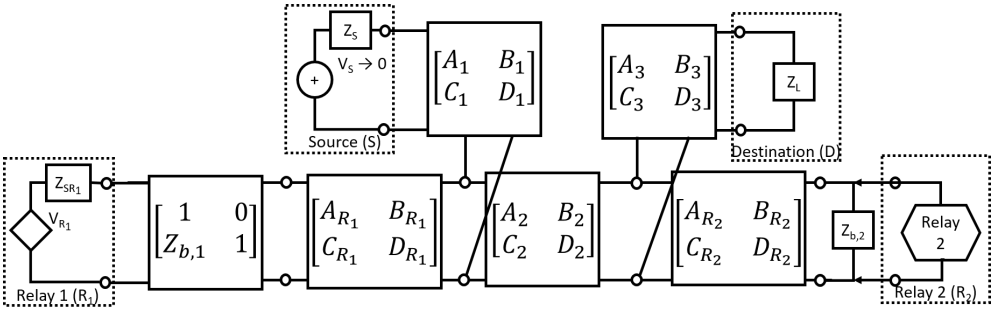

Figure 5.8: Network layout of the path R_1 - R_2

(d) Transfer function of the path S to D through R_1 - R_2. This section consists of three paths, i.e S to R_1, R_1 to R_2 and R_2 to D. The paths, S to R_1 and R_2 to D have been discussed earlier. The path R_1 to R_2 is shown in Fig. 5.8. The matrix for R_1 - R_2 path is given by

$$\begin{aligned}\Phi^{(2)}_{R_1R_2} &= \begin{bmatrix} A^{(2)}_{R_1R_2} & B^{(2)}_{R_1R_2} \\ C^{(2)}_{R_1R_2} & D^{(2)}_{R_1R_2} \end{bmatrix} \\ &= \begin{bmatrix} 1 & 0 \\ Z_{b_1} & 1 \end{bmatrix} \begin{bmatrix} A_{R_1} & B_{R_1} \\ C_{R_1} & D_{R_1} \end{bmatrix} \begin{bmatrix} 1 & 0 \\ \frac{1}{Z_{Seq}} & 1 \end{bmatrix} \begin{bmatrix} A_2 & B_2 \\ C_2 & D_2 \end{bmatrix} \\ &\times \begin{bmatrix} 1 & 0 \\ Z_{Deq} & 1 \end{bmatrix} \begin{bmatrix} A_{R_2} & B_{R_2} \\ C_{R_2} & D_{R_2} \end{bmatrix}. \end{aligned} \tag{5.23}$$

Therefore, the CTF for R_1 - R_2 path is

$$\tilde{H}^{(2)}_{R_1R_2} = \frac{Z'_{LR_2}}{A^{(2)}_{R_1R_2}Z'_{LR_2} + B^{(2)}_{R_1R_2} + C^{(2)}_{R_1R_2}Z'_{LR_2}Z_{SR_1} + D^{(2)}_{R_1R_2}Z_{SR_1}}. \tag{5.24}$$

Finally, the composite path gain of the entire S - R_1 - R_2 - D link is given by

$$\tilde{H}^{(R_1R_2)}_{SD} = (\tilde{H}^{(1)}_{SR_1}A) + (\tilde{H}^{(2)}_{R_1R_2}A) + \tilde{H}^{(2)}_{R_2D}. \tag{5.25}$$

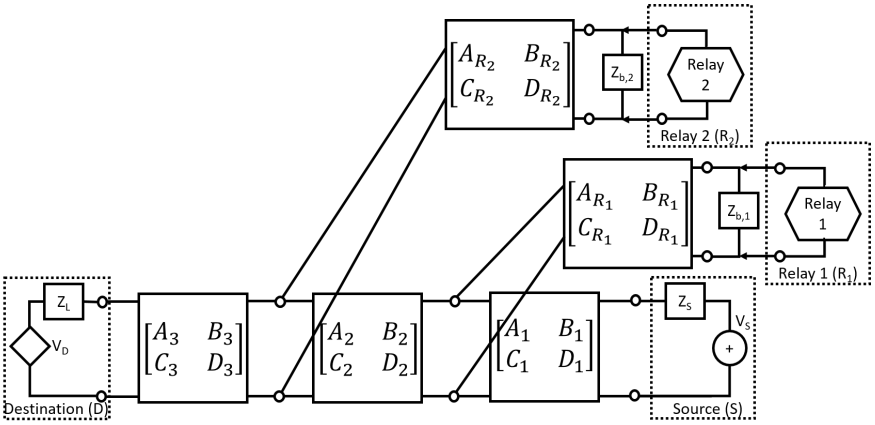

Figure 5.9: Network layout of the path D - S

(e) Transfer function of the direct path D to S. Considering the direct path from destination to source as shown in Fig. 5.9, the relay nodes, R_1 and R_2 are treated as the loads. The matrix of the direct path from D to S is given by

$$\begin{aligned} \Phi_{DS}^{(D)} &= \begin{bmatrix} A_{DS}^{(D)} & B_{DS}^{(D)} \\ C_{DS}^{(D)} & D_{DS}^{(D)} \end{bmatrix} \\ &= \begin{bmatrix} A_3 & B_3 \\ C_3 & D_3 \end{bmatrix} \begin{bmatrix} 1 & 0 \\ \frac{1}{Z_{eqb,2}} & 1 \end{bmatrix} \begin{bmatrix} A_2 & B_2 \\ C_2 & D_2 \end{bmatrix} \\ &\times \begin{bmatrix} 1 & 0 \\ \frac{1}{Z_{eqb,1}} & 1 \end{bmatrix} \begin{bmatrix} A_1 & B_1 \\ C_1 & D_1 \end{bmatrix}. \end{aligned} \tag{5.26}$$

As a result, the CTF of the direct path from D to S can be expressed as

$$\tilde{H}_{DS}^{(D)} = \frac{Z_S}{A_{DS}^{(D)} Z_S + B_{DS}^{(D)} + C_{DS}^{(D)} Z_S Z_L + D_{DS}^{(D)} Z_L}. \tag{5.27}$$

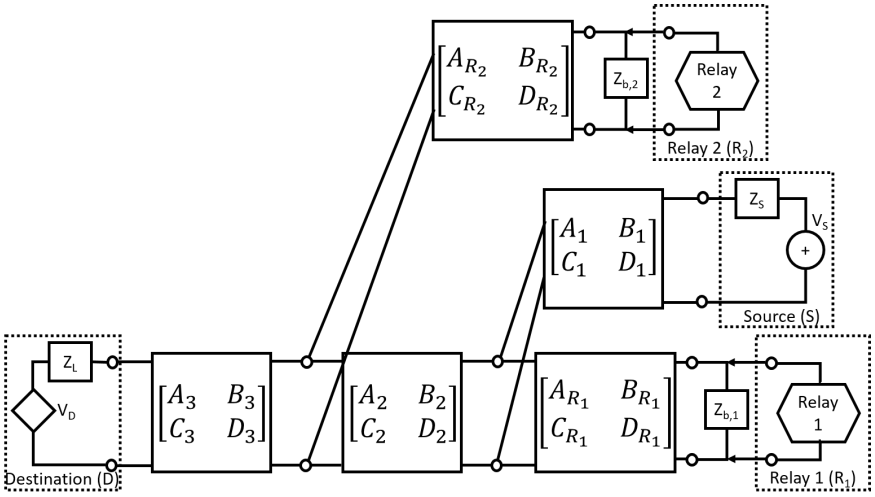

Figure 5.10: Network layout of the path D - R_1

(f) Transfer function of the path D to S through R_1 This section describes the connection between two paths, i.e. D to R_1 and R_1 to S.

- When the signal travels from D to R_1 as shown in Fig. 5.10, as always, R_1 is considered as the destination while S and R_2 behave as branches. Combining with the second relay impedance and the source impedance, the path matrix from D to R_1 can be expressed as

$$\begin{aligned} \Phi^{(1)}_{DR_1} &= \begin{bmatrix} A^{(1)}_{DR_1} & B^{(1)}_{DR_1} \\ C^{(1)}_{DR_1} & D^{(1)}_{DR_1} \end{bmatrix} \\ &= \begin{bmatrix} A_3 & B_3 \\ C_3 & D_3 \end{bmatrix} \begin{bmatrix} 1 & 0 \\ \frac{1}{Z_{eqb,2}} & 1 \end{bmatrix} \begin{bmatrix} A_2 & B_2 \\ C_2 & D_2 \end{bmatrix} \\ &\times \begin{bmatrix} 1 & 0 \\ \frac{1}{Z_{Seq}} & 1 \end{bmatrix} \begin{bmatrix} A_{R_1} & B_{R_1} \\ C_{R_1} & D_{R_1} \end{bmatrix}. \end{aligned} \tag{5.28}$$

Therefore, the CTF for D - R_1 path is

$$\tilde{H}^{(1)}_{DR_1} = \frac{Z'_{LR_1}}{A^{(1)}_{DR_1} Z'_{LR_1} + B^{(1)}_{DR_1} + C^{(1)}_{DR_1} Z'_{LR_1} Z_L + D^{(1)}_{DR_1} Z_L}. \tag{5.29}$$

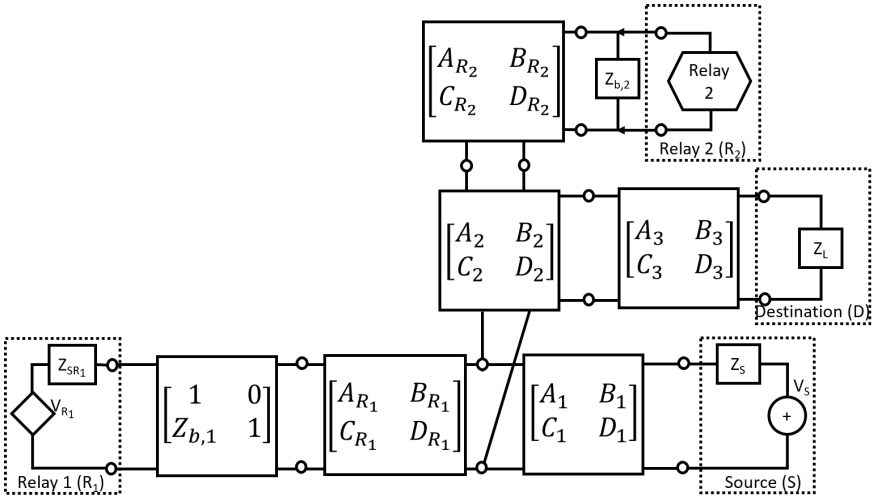

Figure 5.11: Network layout of the path R_1 - S

- In Fig. 5.11, the path from R_1 to S, R_1 behaves as the source and S behaves as the destination while R_2 and D become the branches. The path matrix for R_1 - S path is

$$\begin{aligned} \Phi^{(2)}_{R_1S} &= \begin{bmatrix} A^{(2)}_{R_1S} & B^{(2)}_{R_1S} \\ C^{(2)}_{R_1S} & D^{(2)}_{R_1S} \end{bmatrix} \\ &= \begin{bmatrix} 1 & 0 \\ Z_{b_1} & 1 \end{bmatrix} \begin{bmatrix} A_{R_1} & B_{R_1} \\ C_{R_1} & D_{R_1} \end{bmatrix} \begin{bmatrix} 1 & 0 \\ \frac{1}{Z_{R_2D}} & 1 \end{bmatrix} \begin{bmatrix} A_1 & B_1 \\ C_1 & D_1 \end{bmatrix}. \end{aligned}$$

Therefore, the CTF for R_1 - S path can be expressed as

$$\tilde{H}^{(2)}_{R_1S} = \frac{Z_S}{A^{(2)}_{R_1S} Z_S + B^{(2)}_{R_1S} + C^{(2)}_{R_1S} Z_S Z_{SR_1} + D^{(2)}_{R_1S} Z_{SR_1}}. \tag{5.30}$$

Finally, the composite path gain of the entire D - R_1 - S link is given by

$$\tilde{H}^{(R_1)}_{DS} = (\tilde{H}^{(1)}_{DR_1} A) + \tilde{H}^{(2)}_{R_1S}. \tag{5.31}$$

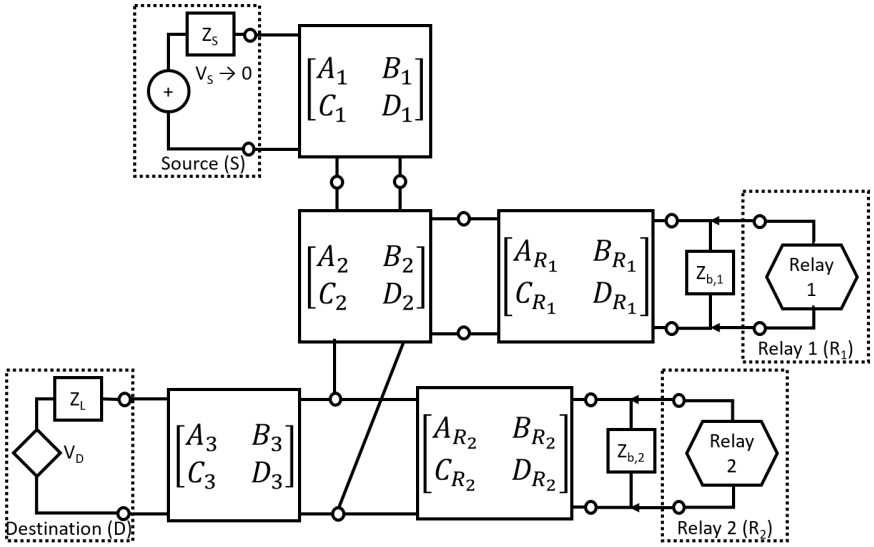

Figure 5.12: Network layout of the path D - R_2

(g) Transfer function of the path D to S through R_2 Using similar method, the link D to S through R_2 consists of 2 paths, i.e. D - R_2 path and R_2 - S path.

- Fig. 5.12 shows the first path where S and R_1 are considered as branches. The path matrix from D to R_2 is

$$\begin{aligned}\Phi^{(1)}_{DR_2} &= \begin{bmatrix} A^{(1)}_{DR_2} & B^{(1)}_{DR_2} \\ C^{(1)}_{DR_2} & D^{(1)}_{DR_2} \end{bmatrix} \\ &= \begin{bmatrix} A_3 & B_3 \\ C_3 & D_3 \end{bmatrix} \begin{bmatrix} 1 & 0 \\ \frac{1}{Z_{SR_1}} & 1 \end{bmatrix} \begin{bmatrix} A_{R_2} & B_{R_2} \\ C_{R_2} & D_{R_2} \end{bmatrix}. \end{aligned} \tag{5.32}$$

Therefore, the CTF for D - R_2 path is

$$\tilde{H}^{(1)}_{DR_2} = \frac{Z'_{LR_2}}{A^{(1)}_{DR_2} Z'_{LR_2} + B^{(1)}_{DR_2} + C^{(1)}_{DR_2} Z'_{LR_2} Z_L + D^{(1)}_{DR_2} Z_L}. \tag{5.33}$$

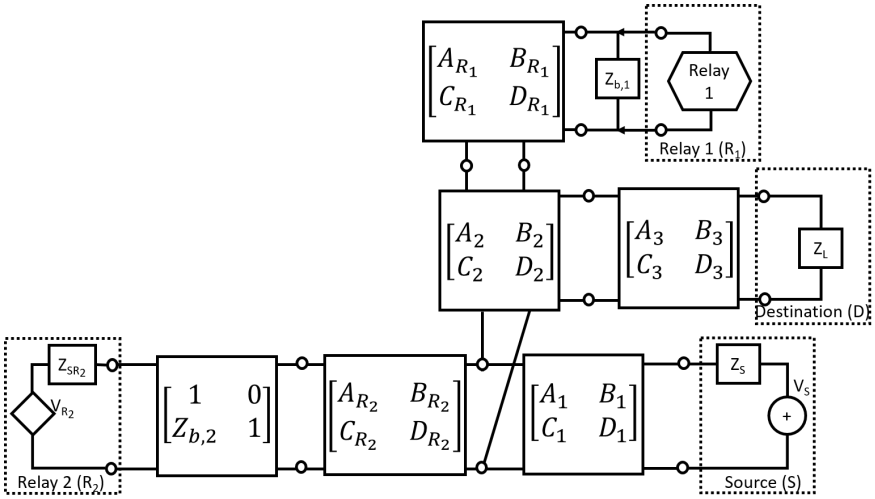

Figure 5.13: Network layout of the path R_2 - S

- In the second path as shown in Fig. 5.13, R_1 and D become the branches. The matrix for R_2 - S path is given by

$$\begin{aligned} \Phi^{(2)}_{R_2S} &= \begin{bmatrix} A^{(2)}_{R_2S} & B^{(2)}_{R_2S} \\ C^{(2)}_{R_2S} & D^{(2)}_{R_2S} \end{bmatrix} \\ &= \begin{bmatrix} 1 & 0 \\ Z_{b_2} & 1 \end{bmatrix} \begin{bmatrix} A_{R_2} & B_{R_2} \\ C_{R_2} & D_{R_2} \end{bmatrix} \begin{bmatrix} 1 & 0 \\ \frac{1}{Z_{Deq}} & 1 \end{bmatrix} \\ &\times \begin{bmatrix} A_2 & B_2 \\ C_2 & D_2 \end{bmatrix} \begin{bmatrix} 1 & 0 \\ \frac{1}{Z_{eqb,1}} & 1 \end{bmatrix} \begin{bmatrix} A_1 & B_1 \\ C_1 & D_1 \end{bmatrix} \end{aligned} \tag{5.34}$$

Therefore, the CTF for R_2 - S path is

$$\tilde{H}^{(2)}_{R_2S} = \frac{Z_S}{A^{(2)}_{R_2S} Z_S + B^{(2)}_{R_2S} + C^{(2)}_{R_2S} Z_S Z_{SR_2} + D^{(2)}_{R_2S} Z_{SR_2}}. \tag{5.35}$$

As usual, the path gain of the entire D - R_2 - S link is given by

$$\tilde{H}^{(R_2)}_{DS} = (\tilde{H}^{(1)}_{DR_2} A) + \tilde{H}^{(2)}_{R_2S}. \tag{5.36}$$

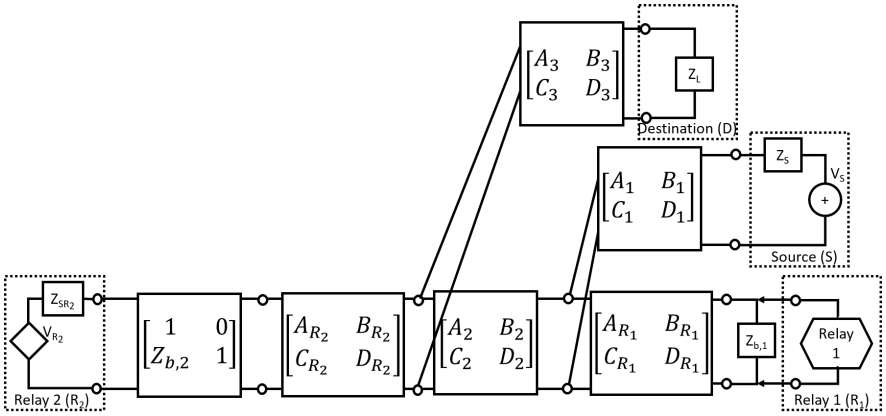

Figure 5.14: Network layout of the path R_2 - R_1

(h) Transfer function of the path from D to S through R_1 - R_2 The link consists of three paths, i.e. D to R_2, R_2 to R_1, and R_1 to S. The matrices for D to R_2 and R_1 to S has been derived earlier. From Fig. 5.14, the matrix for R_2 - R_1 path is

$$\begin{aligned} \Phi^{(2)}_{R_2R_1} &= \begin{bmatrix} A^{(2)}_{R_2R_1} & B^{(2)}_{R_2R_1} \\ C^{(2)}_{R_2R_1} & D^{(2)}_{R_2R_1} \end{bmatrix} \\ &= \begin{bmatrix} 1 & 0 \\ Z_{b_2} & 1 \end{bmatrix} \begin{bmatrix} A_{R_2} & B_{R_2} \\ C_{R_2} & D_{R_2} \end{bmatrix} \begin{bmatrix} 1 & 0 \\ \frac{1}{Z_{Deq}} & 1 \end{bmatrix} \\ &\times \begin{bmatrix} A_2 & B_2 \\ C_2 & D_2 \end{bmatrix} \begin{bmatrix} 1 & 0 \\ \frac{1}{Z_{Seq}} & 1 \end{bmatrix} \begin{bmatrix} A_{R_1} & B_{R_1} \\ C_{R_1} & D_{R_1} \end{bmatrix}. \end{aligned} \tag{5.37}$$

As a result, the CTF for R_2 - R_1 path is

$$\tilde{H}^{(2)}_{R_2R_1} = \frac{Z'_{LR_1}}{A^{(2)}_{R_2R_1} Z'_{LR_1} + B^{(2)}_{R_2R_1} + C^{(2)}_{R_2R_1} Z_{SR_1} Z'_{LR_2} + D^{(2)}_{R_2S} Z_{SR_2}}. \tag{5.38}$$

The composite path gain of the entire D - R_2 - R_1 - S link is expressed as

$$\tilde{H}^{(R_2R_1)}_{DS} = (\tilde{H}^{(1)}_{DR_2} A) + (\tilde{H}^{(2)}_{R_2R_1} A) + \tilde{H}^{(2)}_{R_1S}. \tag{5.39}$$

Table 5.1: Channel realisation parameters

Line section	Length	Cable type	Terminated load
Backbone 1	$d_1 = 46.1m$	$n_{d_1} = 4$	N/A
Branch-tap 1	$d_{b,1} = 11.7m$	$n_{d_{b,1}} = 1$	$Z_1(f,T)$
Backbone 2	$d_2 = 39.6m$	$n_{d_2} = 3$	N/A
Branch-tap 2	$d_{b,2} = 23.5m$	$n_{d_{b,2}} = 2$	$Z_2(f,T)$
Backbone 3	$d_3 = 44.6m$	$n_{d_3} = 5$	N/A
Branch-tap 3	$d_{d,3} = 0$	N/A	$Z_{b,3} = \infty$
Backbone 4	$d_4 = 0$	N/A	N/A

5.4 Numerical Examples

For simulations, the source is assumed to have an inner impedance of 50Ω, and each terminated load (of R_1, R_2, and D) has the impedance of 150Ω. Note that the load impedance is commonly larger than the source impedance. Z_b is the frequency-dependent load impedance at the relay which has the uniform distribution of $R' = \{200, 1800\}\Omega$, $\omega_0/2\pi = \{2, 28\}MHz$, and $Q_f = \{5, 25\}$ [46]. The amplification factor, A, is assumed to be 1. In this section, there will be two different types of simulations.

In Simulation 1, the segment and link CTFs of the two-relay two-way PLC can be simulated using the derivation discussed earlier. The PLC channel realisation parameters for Simulation 1 are given in Table 5.1. Each signalling path in the relay-assisted channel is treated as an equivalent P2P channel. Using Canete's PLC channel simulator, the transfer function can be obtained as shown in Fig. 5.15. The summation of the respective CTFs of the segment can get the desired composite CTF as shown in Fig. 5.16. It can be seen that attenuation is higher in high frequencies.

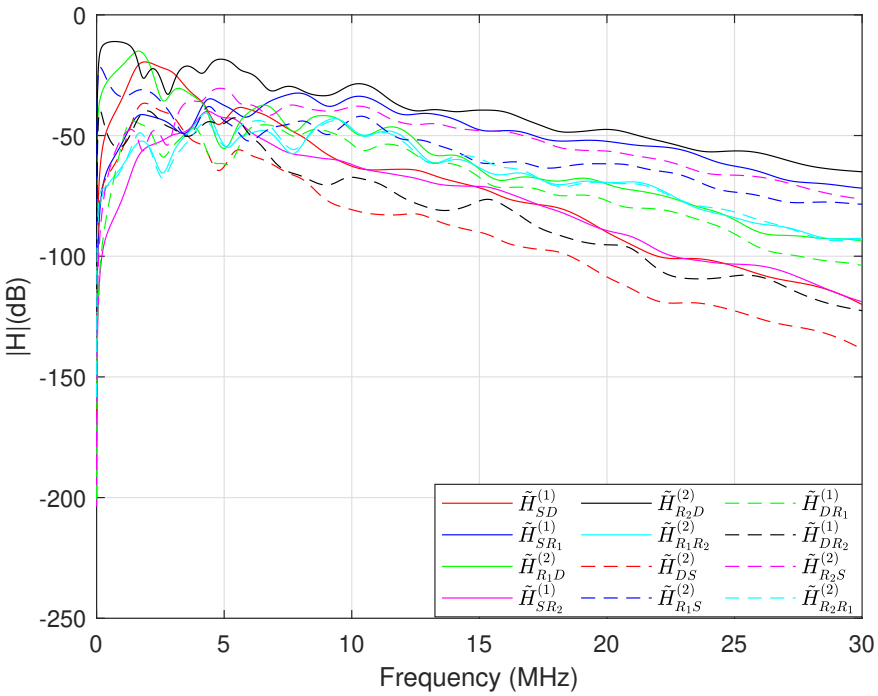

Figure 5.15: Simulation Example 1 - CTFs of a two-relay two-way PLC system

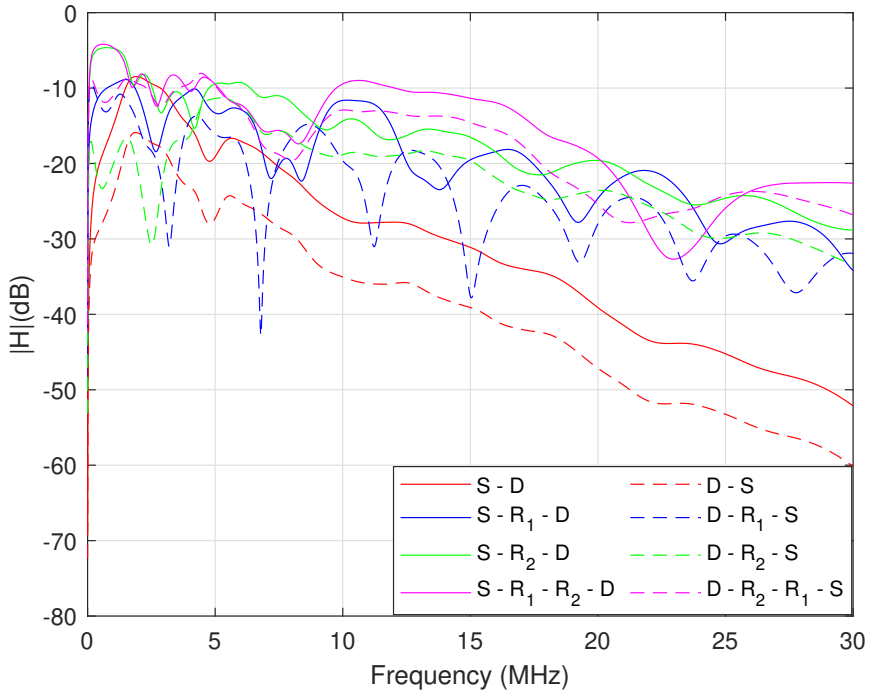

Figure 5.16: Simulation Example 1 - The composite CTFs for two-relay PLC forward and backward channels

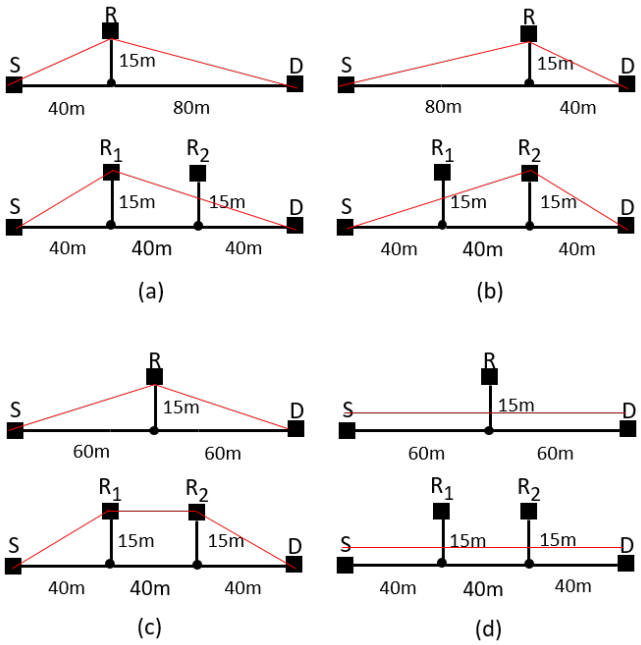

Figure 5.17: Simulation Example 2 - Topologies for comparing two-way PLC systems with single-relay and two-relay: (a) scenario 1, (b) scenario 2, (c) scenario 3, and (d) scenario 4.

In Simulation 2, the link CTFs of single-relay two-way PLC system (SYS A) is compared with two-relay two-way PLC system (SYS B). For the sake of fair comparison, four topologies and scenarios are designed, as in Fig. 5.17 to observe the channel characteristics for both systems. Note that the same cable type 4 is used for all segments. When there is only one relay used, the link CTF is compared. In the first and second scenarios, the CTFs of the S - R - D and D - R - S links of the two systems are compared. SYS B uses only one of its relays, either R_1 or R_2. The relay in SYS A is placed according to the respective SYS B relay position to see the effect of the idle relay in SYS B. In scenario 3, the CTF of the S - R_1 - R_2 - D and D - R_2 - R_1 - S links are observed in SYS B. To make the comparison as fair as possible, the relay in SYS A is placed at the midpoint of R_1 - R_2 distance. Lastly, scenario 4 compares the CTFs of SYS A and SYS B for their direct S - D and D - S links. The simulation results of the four topologies are compared and depicted in Fig. 5.18.

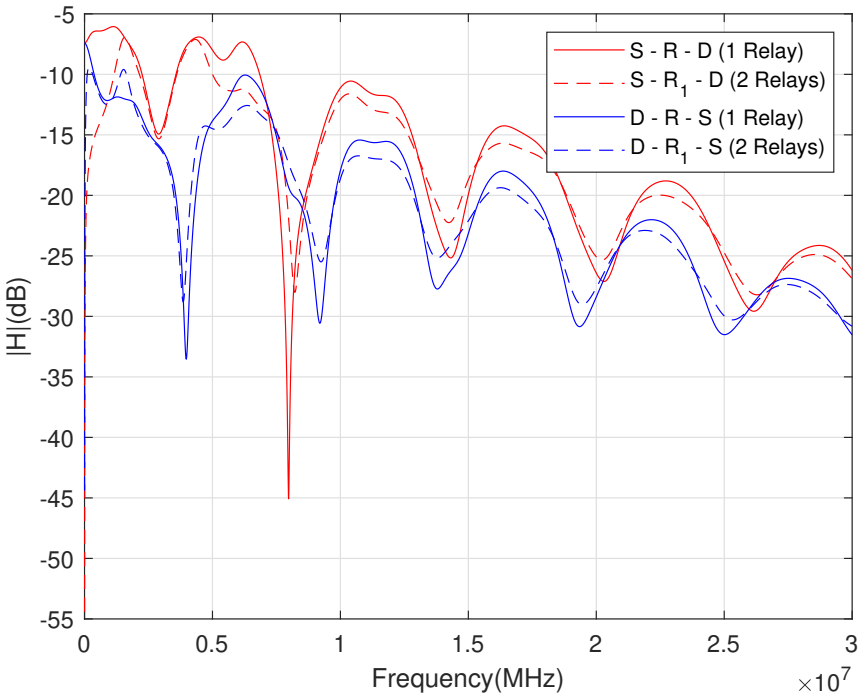

(a) Scenario 1

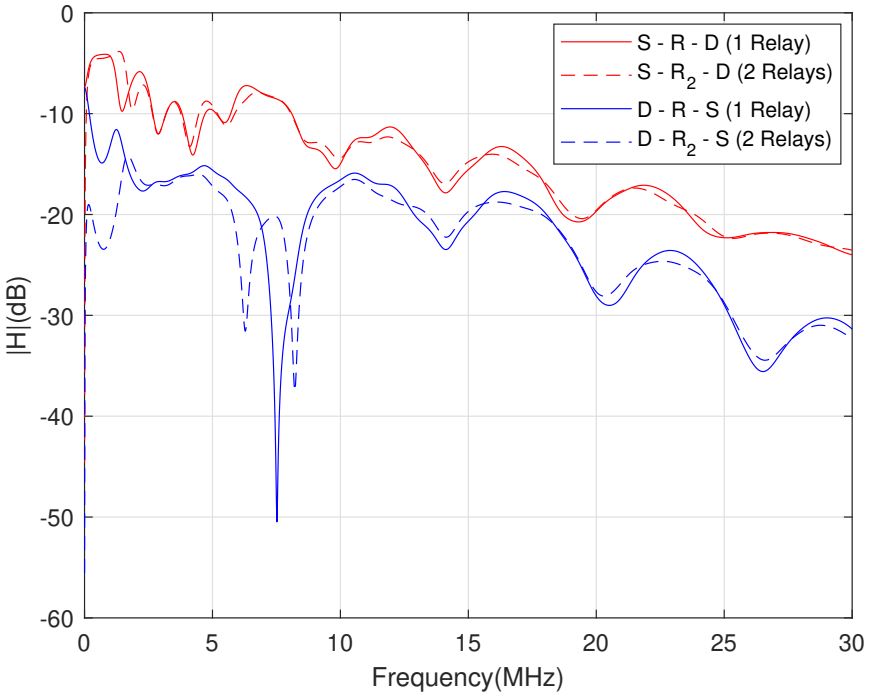

(b) Scenario 2

Figure 5.18: Simulation Example 2 - Part 1 of the comparison between single-relay and two-relay two-way PLC system

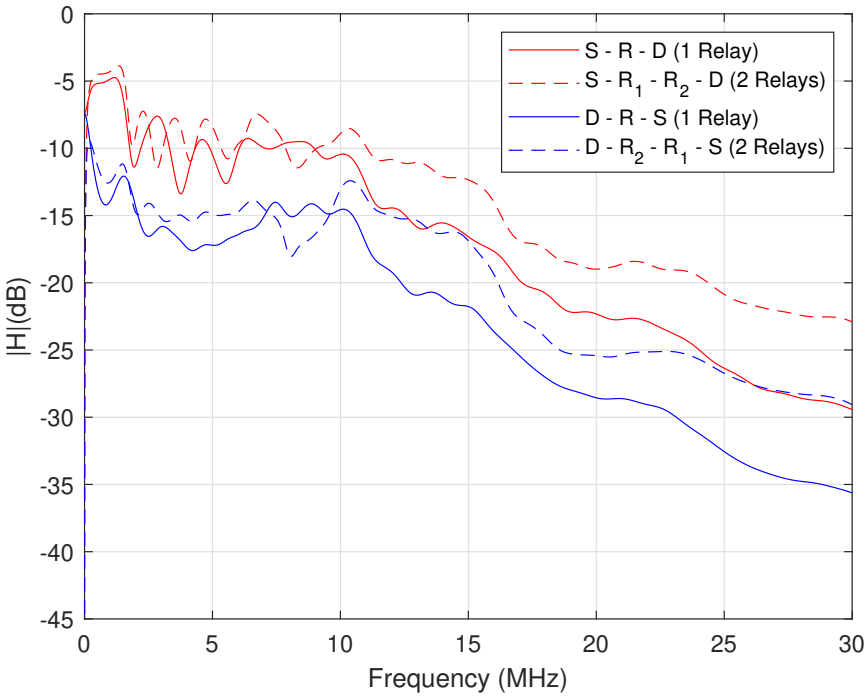

(c) Scenario 3

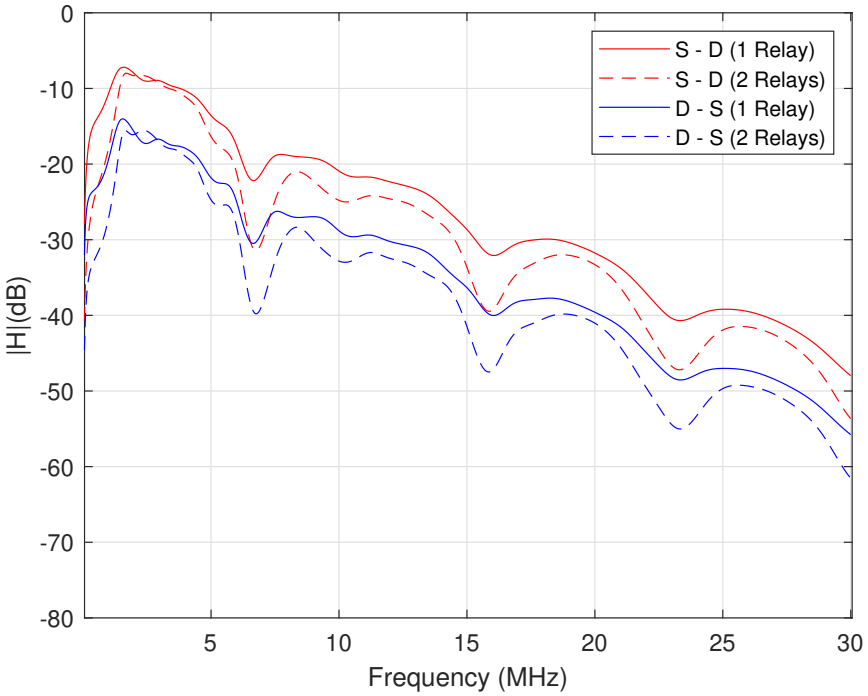

(d) Scenario 4

Figure 5.18: Simulation Example 2 - Part 2 of the comparison between single-relay and two-relay two-way PLC system

It can be seen that all forward channels give relatively better CTFs compared to the backward channels as the load impedance is larger than the source impedance. For the first scenario, it can be seen that SYS A and SYS B have relatively the same forward CTFs, except that at certain frequencies, SYS B gives deeper attenuation. However, the backward CTFs of the two systems are relatively indifferentiable. Similar to scenario 1, scenario 2 shows indistinguishable characteristics for SYS A and SYS B. It can also be seen that backward CTFs gives deeper attenuation at certain frequencies.

On the other hand, there are noticeable differences, especially in high frequencies, between SYS A and SYS B in scenario 3. It can be seen that SYS B has better forward and backward CTFs at high frequencies. For the direct links, it can be observed that SYS A provides better performance than SYS B. It can be understood by looking at the addition of branches, which adds the channel attenuation.

5.5 Chapter Summary

The CTFs of two-relay two-way PLC system have been investigated in this chapter. The ABCD method has been applied to get the CTFs for both forward and backward channels where each signalling path in the relay-assisted channel is treated as an equivalent P2P channel. The composite CTFs for a certain link can be found by summing the respective CTFs of the constructive segments. Simulation results show that attenuation is higher in high frequencies. Furthermore, the CTFs between single-relay and two-relay two-way PLC systems have been compared. It has been shown that two-relay systems can be used when taking the advantages of the number of relays as the CTFs for non-direct links are relatively similar or better than the single-relay PLC systems. On the other hand, a single-relay PLC system is preferred if considering the direct channel for data transmission.

Chapter 6

Channel models of Two-way PLC Systems

This chapter discusses the model of a bottom-up multipath channel for single-relay two-way PLC channel based on transmission and reflection coefficients. This model is compared with the two most popular methods of bottom-up approach, which are the ABCD method and VRA methods. An introduction of PLC channel models is presented in Section 6.1. In Section 6.2, the CTF expressions of a three PLC channel models are shown and derived. The numerical examples are given in Section 6.3 to verify the result. Finally the chapter is briefly summarised in Section 6.4.

6.1 Introduction

Relay-based PLC systems can be well designed through the understanding of PLC channel characteristics, which can be obtained through channel modelling. In the literature, PLC channel models are grouped into a top-down approach and a bottom-up approach.

The top-down approach uses a set of parameters to describe the channel and behaviour characteristics of PLC networks [117]. The parameter values are derived from statistical analysis based on measurement data. This approach can work in either the time-domain or frequency-domain. However, it is hard to connect to the physical topology due to the difficulties in setting up large test loops with physical characteristics and configurations [118]. A well-known top-down PLC model was proposed by Zimmermann and Dostert in [119]. The Zimmermann-Dostert PLC channel model is represented by the sum of multipath components where each multipath component consists of a weighting factor, an attenuation factor, and a delay coefficient. The weighting and attenuation factors are obtained from measurement data. Another top-down method was proposed by Tonello in [118].

On the other hand, the bottom-up approach is performed by implementing the TL theory to obtain the CTF using the network information [41]–[43]. The bottom-up approach is more preferred as it represents the topology of the power-line network. PLC channel modelling task can be difficult because of the different topology of power networks and its harsh nature. Yet, many researchers were able to model the PLC channel. In this approach, the PLC transfer function was derived by using several means, such as the ABCD matrix [109], the S-parameter [120], the multiconductor transmission line (MTL) approach [115], [121], IIR-Filter [122], and the VRA in [123]. A comparison between the ABCD and VRA models has been discussed in [124].

A single-relay PLC channel model with the ABCD method has been proposed in [107]. An extension of this model to two-way single-relay PLC was discussed in Chapter 4. The derivation of composite CTF of the single-relay and two-relay two-way PLC systems has been discussed in Chapter 5. In this chapter, a bottom-up multipath channel model for single-relay two-way PLC channel is proposed. This method is derived from the top-down Zimmermann-Dostert model with modification of the parameters to be a bottom-up model. The parameters

are obtained from the transmission and reflection coefficients, as given in [125]. The proposed model is then compared with the ABCD and VRA models.

6.2 Single-relay PLC Channel Modelling

This chapter focuses on three types of channel models, i.e., the newly proposed multipath model, the ABCD method, and the VRA method. For simplicity, a single-relay PLC system model consisting of the source (S), relay (R), and destination (D) is used. The two-way PLC channel has two modes: forward mode and reverse mode. The forward mode refers to the mode when the signal is transmitted from S to D, and the reverse mode refers to the mode when the signal is transmitted from D (which acts as a transmitter) to S (which acts as a receiver). Each channel model is formulated below. The length of each link is assumed to be long enough so that there is no reflection from the far end. Each channel model is formulated below.

Besides, the source, relay, and destination nodes can act as either a transmitter or a receiver. Therefore, their inner impedance value during the transmitting mode will be different from the one in the receiving mode.

6.2.1 Proposed Multipath Model

The bottom-up multipath model proposed in [125] is shown in Fig. 6.1. Note that Z_S, Z_b, Z_{LR}, and Z_L are the load impedances at the source, branch, relay, and destination, respectively. It is assumed that Z_b is the frequency-dependent impedance given by [46]

$$Z_b = \frac{R'}{1 + jQ_f(\frac{\omega}{\omega_0} - \frac{\omega_0}{\omega})}, \tag{6.1}$$

where R', ω_0 and Q_f are the resistance at resonance, resonance angular frequency, and quality factor respectively [46].

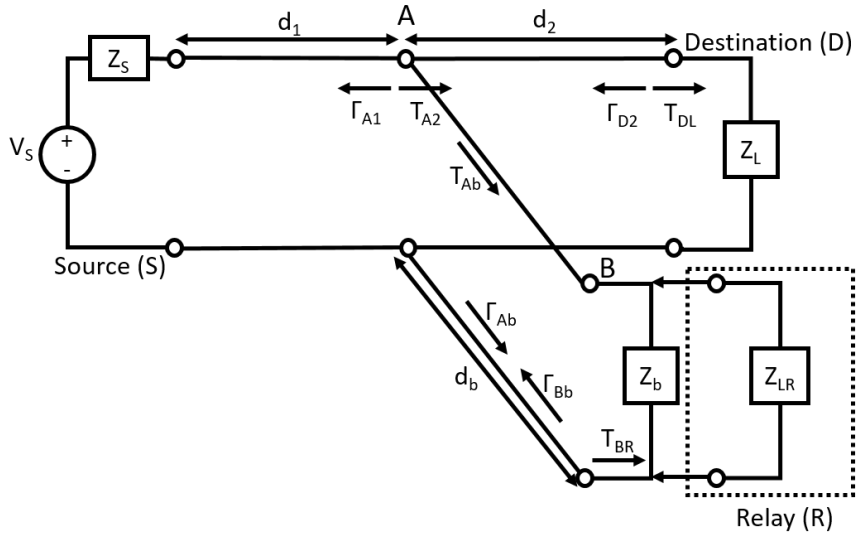

Figure 6.1: Detailed topology of a PLC system for multipath model. The transmission and reflection factors shown here are only for the forward mode.

The overall CTF of a relay-based PLC network in each mode is given by

$$\tilde{H}(f) = \sum_{i=1}^{N} g_i \alpha_i e^{-j2\pi f \tau_i}, \tag{6.2}$$

where g_i is the gain factor of the i-th path derived from the transmission (T) and reflection coefficients (Γ), $\alpha_i = e^{-\gamma d_i}$ is the attenuation factor for the i-th path, γ is given by Eqn. (2.4), d_i is the length of the i-th path, $\tau_i = d_i\sqrt{\epsilon_r}/c_0$ is the delay of the i-th path, ϵ_r is the relative permeability of the cable material, c_0 is the speed of light, and N is the number of relay links. This chapter considers two-relay links for each mode, i.e. S-D and S-R-D for forward mode and D-S and D-R-S for reverse mode. The CTF for each link is derived except the overall CTF. Note that, without loss of generality, the reflected paths for each relay link are not considered.

(a) CTF of S-D Path. The signal travels from S to the branch point A and then to D. As a result, the CTF is given by

$$\tilde{H}_{SD}(f) = g_{SD}\alpha_{SD}e^{-j2\pi f \tau_{SD}}, \tag{6.3}$$

where $\tau_{SD} = d_{SD}\sqrt{\epsilon_r}/c_0$, $d_{SD} = d_1 + d_2$, $\alpha_{SD} = e^{-\gamma d_{SD}}$, and $g_{SD} = T_{A2}T_{DL}$. Here, $T_{A2} = 1 + \Gamma_{A1}$ is the transmission coefficient from node A to line 2 and $T_{DL} = 1 + \Gamma_{D2}$ is the transmission coefficient from node D to the load. Note that T_{DL} is included, as the load does not match the characteristic impedance of the power-line. The reflection coefficients are expressed as $\Gamma_{A1} = (Z_0/2 - Z_0)/(Z_0/2 + Z_0)$ and $\Gamma_{D2} = (Z_L - Z_0)/(Z_L + Z_0)$.

(b) CTF of S-R-D Path. The CTF function for this path is given by

$$\tilde{H}_{SRD}(f) = g_{SRD}\alpha_{SRD}e^{-j2\pi f\tau_{SRD}} + g_{RD}\alpha_{RD}e^{-j2\pi f\tau_{RD}}, \tag{6.4}$$

where $\tau_{SRD} = d_{SRD}\sqrt{\epsilon_r}/c_0$, $\tau_{RD} = d_{RD}\sqrt{\epsilon_r}/c_0$, $d_{SRD} = d_1 + 2d_b + d_2$, $d_{RD} = d_b + d_2$, $\alpha_{SRD} = e^{-\gamma d_{SRD}}$, $\alpha_{RD} = e^{-\gamma d_{RD}}$, $g_{SRD} = T_{Ab}\Gamma_{Bb}T_{A2}T_{DL}$, $g_{RD} = T_{A2}T_{DL}$, $\Gamma_{Ab} = \Gamma_{A2}$, $\Gamma_{Bb} = (Z'_{LR} - Z_0)/(Z'_{LR} + Z_0)$ and Z'_{LR} is the equivalent impedance of branch Z_b parallel to load impedance of the receiving relay node Z_{LR} which can be written as

$$Z'_{LR} = Z_b \parallel Z_{LR}. \tag{6.5}$$

The first term of (6.4) shows that the signal travels from S to the branch point A then to the relay point B. However, upon acceptance of the relay, part of the signal is reflected to the branch and goes to point D. In addition, the second part of (6.4) shows that the relay transmits the signal to point D.

(c) CTF of D-R-S Path. Similar to the S-R-D path, the CTF of the D-R-S path can be written as

$$\tilde{H}_{DRS}(f) = g_{DRS}\alpha_{DRS}e^{-j2\pi f\tau_{DRS}} + g_{RS}\alpha_{RS}e^{-j2\pi f\tau_{RS}}, \tag{6.6}$$

where $d_{DRS} = d_{SRD}$, $d_{RS} = d_{SR}$, $\tau_{DRS} = \tau_{SRD}$, $\tau_{RS} = \tau_{SR}$, $\alpha_{DRS} = \alpha_{SRD}$, $\alpha_{RS} = \alpha_{SR}$, $g_{DRS} = T_{Ab}\Gamma_{Bb}T_{A1}T_S$, and $g_{RS} = T_{A1}T_S$.

(d) CTF of D-S Path. Using the same concept as the S-D path, the CTF can be formulated as

$$\tilde{H}_{DS}(f) = g_{DS}\alpha_{DS}e^{-j2\pi f\tau_{DS}}, \tag{6.7}$$

where $g_{DS} = T_{A1}T_S$, $T_{A1} = 1 + \Gamma_{A2}$, $\Gamma_{A2} = \Gamma_{A1}$, $T_S = 1 + \Gamma_S$, $\Gamma_S = (Z_S - Z_0)/(Z_S + Z_0)$, $\tau_{DS} = d_{DS}\sqrt{\epsilon_r}/c_0$, $d_{DS} = d_{SD}$, and $\alpha_{DS} = e^{-\gamma d_{DS}}$.

6.2.2 ABCD Method

In order to get the ABCD matrix, Canate's hybrid point-to-point (P2P) channel model is used, which consists of two segments and one branch terminated by a load impedance. The CTFs has been discussed and formulated as in 4.3. The amplification factor is assume that $A_F = 1$.

(a) CTF of the direct path S to D. The CTF of the direct path S to D is given in (4.18).

(b) CTF of the path S to D through R. This part describes the connection between two paths, i.e., S to R and R to D. The CTF of the path from S to R and from R to D are (4.21) and (4.24) respectively. The composite path gain of the entire S-R-D link is given by

$$\tilde{H}_{SRD} = \tilde{H}^{(1)}_{SR}A_F + \tilde{H}^{(2)}_{RD}. \tag{6.8}$$

(c) CTF of the path D to S through R. Using a similar method, link D to S through R consists of two paths, i.e., D to R path and R to S path. The CTF of the path from D to R and from R to S are (4.32) and (4.36) respectively. Finally, the composite path gain of the entire D-R-S link can be expressed as

$$\tilde{H}_{DRS} = \tilde{H}^{(1)}_{DR}A_F + \tilde{H}^{(2)}_{RS}. \tag{6.9}$$

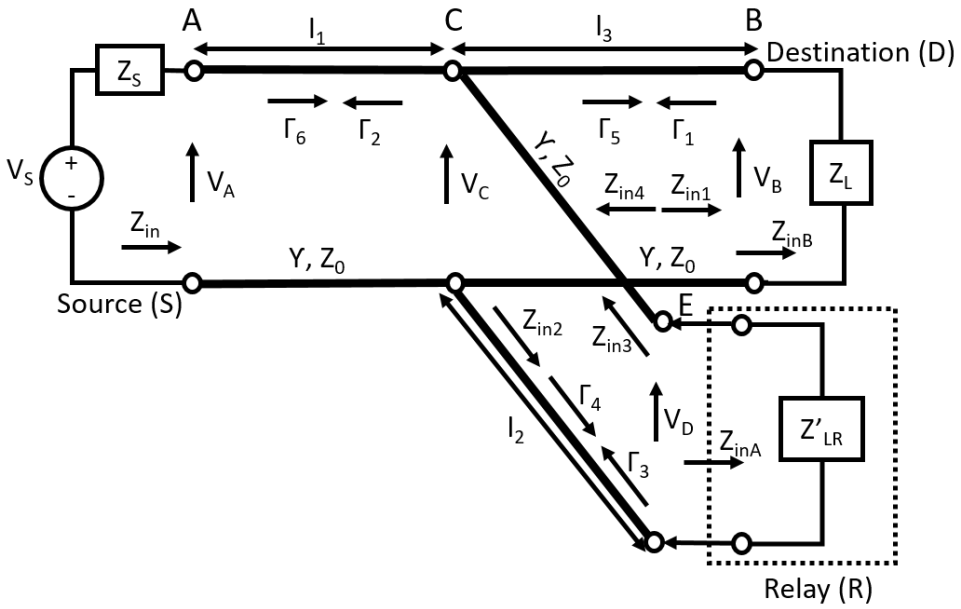

Figure 6.2: Detailed topology of a PLC system for the VRA method.

(d) CTF of the direct path D to S. The CTF of the direct path D to S is given in (4.34).

6.2.3 VRA Method

Using VRA for the PLC network shown in Fig. 6.2, the CTFs of a PLC channel can be calculated as follows [120], [123], [124], [126].

(a) CTF of the direct path S to D. The reflection coefficient of the end path, Γ_1 and reflection coefficient of Γ_2 from the tap point are

$$\Gamma_1 = \frac{Z_L - Z_0}{Z_L + Z_0}, \tag{6.10}$$

$$\Gamma_2 = \frac{Z_0/2 - Z_0}{Z_0/2 + Z_0}, \tag{6.11}$$

The length of each link is assumed to be long enough. Thus, the input impedances can be approximated by $Z_{in} \approx Z_0$, $Z_{in1} \approx Z_0$, and $Z_{in2} \approx Z_0$.

By applying shifting in reference planes [127],

$$\frac{V_B}{V_C} = \frac{(1+\Gamma_1)\, e^{-\gamma l_3}}{1+\Gamma_1 e^{-\gamma l_3}}, \tag{6.12}$$

$$\frac{V_C}{V_A} = \frac{(1+\Gamma_2)\, e^{-\gamma l_1}}{1+\Gamma_2 e^{-\gamma l_1}}, \tag{6.13}$$

$$\frac{V_A}{V_S} = \frac{Z_{in}}{Z_{in}+Z_S}. \tag{6.14}$$

Thus, the CTF of of the direct path S to D using the VRA method can be obtained as follows

$$\tilde{H}_{SD}(f) = \frac{V_A}{V_S} \times \frac{V_C}{V_A} \times \frac{V_B}{V_C}. \tag{6.15}$$

(b) CTF of the path S to D through R. This session describes the connection between two paths, i.e. S to R and R to D. Looking at the first path, the CTF of the path S to R is given by

$$\tilde{H}_{SR}(f) = \frac{V_A}{V_S} \times \frac{V_C}{V_A} \times \frac{V_E}{V_C}, \tag{6.16}$$

where

$$\frac{V_E}{V_C} = \frac{(1+\Gamma_3)\, e^{-\gamma l_2}}{1+\Gamma_3 e^{-\gamma l_2}}. \tag{6.17}$$

The reflective coefficient of the end path, Γ_3 is

$$\Gamma_3 = \frac{Z'_{LR} - Z_0}{Z'_{LR} + Z_0}. \tag{6.18}$$

Therefore, the CTF of the path R to D is given by

$$\tilde{H}_{RD}(f) = \frac{V_{B'}}{V_{A'}} \times \frac{V_{A'}}{V_C} \times \frac{V_C}{V_R} \tag{6.19}$$

where

$$\frac{V_E}{V_R} = \frac{Z_{inA}}{Z_{inA} + Z'_{LR}}, \tag{6.20}$$

$$\frac{V_C}{V_E} = \frac{(1+\Gamma_4)\, e^{-\gamma l_2}}{1+\Gamma_4 e^{-\gamma l_2}}. \tag{6.21}$$

Note that V_R is the source voltage when the relay acts as a transmitter and $Z_{inA} \approx Z_0$. The reflection coefficient of Γ_4 from the tap point is

$$\Gamma_4 = \frac{Z_0/2 - Z_0}{Z_0/2 + Z_0}, \tag{6.22}$$

Finally, the composite path gain of the entire S-R-D link is given by

$$\tilde{H}_{SRD} = \tilde{H}_{SR} + \tilde{H}_{RD}. \tag{6.23}$$

(c) CTF of the path D to S through R. Using similar method, link D to S through R consists of two paths, i.e. D-R path and R-S path. For the first path, the CTF of path D to R is

$$\tilde{H}_{DR}(f) = \frac{V_B}{V_L} \times \frac{V_C}{V_B} \times \frac{V_E}{V_C}, \tag{6.24}$$

where

$$\frac{V_B}{V_L} = \frac{Z_{inB}}{Z_{inB} + Z_L}, \tag{6.25}$$

$$\frac{V_C}{V_B} = \frac{(1+\Gamma_5)\, e^{-\gamma l_3}}{1+\Gamma_5 e^{-\gamma l_3}}. \tag{6.26}$$

Similarly, V_L is the source voltage when the destination acts as the transmitter and thus, having $Z_{inB} \approx Z_0$.The reflection coefficient of Γ_5 is

$$\Gamma_5 = \frac{Z_0/2 - Z_0}{Z_0/2 + Z_0}. \tag{6.27}$$

For the second path, the CTF of path R to S is given by

$$\tilde{H}_{RS}(f) = \frac{V_E}{V_R} \times \frac{V_C}{V_E} \times \frac{V_A}{V_C}, \tag{6.28}$$

where

$$\frac{V_A}{V_C} = \frac{(1+\Gamma_6)\, e^{-\gamma l_1}}{1+\Gamma_6 e^{-\gamma l_1}}. \tag{6.29}$$

The reflection coefficient of Γ_6 is

$$\Gamma_6 = \frac{Z_S - Z_0}{Z_S + Z_0}. \tag{6.30}$$

Lastly, the composite path gain of the entire D-R-S link is given by

$$\tilde{H}_{DRS} = \tilde{H}_{DR} + \tilde{H}_{RS}. \tag{6.31}$$

(d) CTF of the direct path D to S. The CTF of direct path D to S is given by

$$\tilde{H}_{DS}(f) = \frac{V_B}{V_L} \times \frac{V_C}{V_B} \times \frac{V_A}{V_C}. \tag{6.32}$$

6.3 Numerical Examples

A simple three-node two-way topology used for simulations is shown in Fig. 6.3. As mentioned previously, the cable type 4 is used in each segment of the network. The cable parameters are as follows [46]: $R_0 = 6.25 \times 10^{-5}\Omega/m$, $L = 0.78 \times 10^{-6} H/m$, $C = 25 \times 10^{-12} F/m$, $G_0 = 42.5 \times 10^{-14} S/m$, $\ell = 5$, and $\epsilon_r = 1.73$. Moreover, R', $\omega_0/2\pi$, and Q_f of Z_b are drawn from uniform distributions on $\{200, 1800\}\Omega$, $\{2, 28\} MHz$, and $\{5, 25\}$, respectively [46]. A realisation of the frequency response of Z_b is depicted in Fig. 6.4. The inner impedance in transmitting and receiving modes are set to 50Ω and 150Ω, respectively.

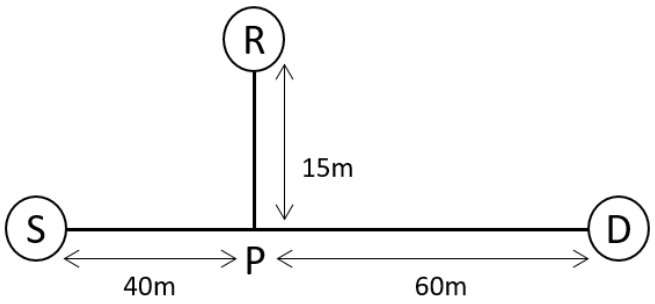

Figure 6.3: Topology of a PLC channel

Three different channel models are compared under four scenarios, i.e., S-D link, S-R-D link, D-R-S link, and D-S link. The simulation results of the four scenarios are compared and depicted in Figs. 6.5 to 6.8. It can be seen from the four figures that the proposed model does not fluctuate much, especially in the high frequency. In other words, it does not show much deep fades. This is because the reflected paths in the relay links are not included. The reflection results in more fluctuations; interested readers may include the reflected paths. For example (refer to Fig. 6.3), reflected paths S-P-S-P-D path could be used for S-D link and S-R-P-R-P-D path (first term) and R-P-R-P-D path (second term) could be used for S-R-D link. However, these additional terms may have little effect on the CTF and can be neglected.

From Fig. 6.5, the CTFs of the ABCD model and the VRA model do not differ much, and the multipath model gives the smallest attenuation. It can be seen from Fig. 6.6 that the three models are relatively equivalent, but the VRA model has high attenuation at high frequencies. On the other hand, it can be seen from Fig. 6.7 that the VRA model gives the lowest attenuation at high frequencies. From Fig. 6.8, it can be seen that the ABCD and VRA models give similar CTFs. In terms of attenuation at high frequencies, the VRA model provides the largest attenuation for the SDR path and the smallest attenuation for the DRS path. For the SD and DS paths, the three models are relatively comparable.

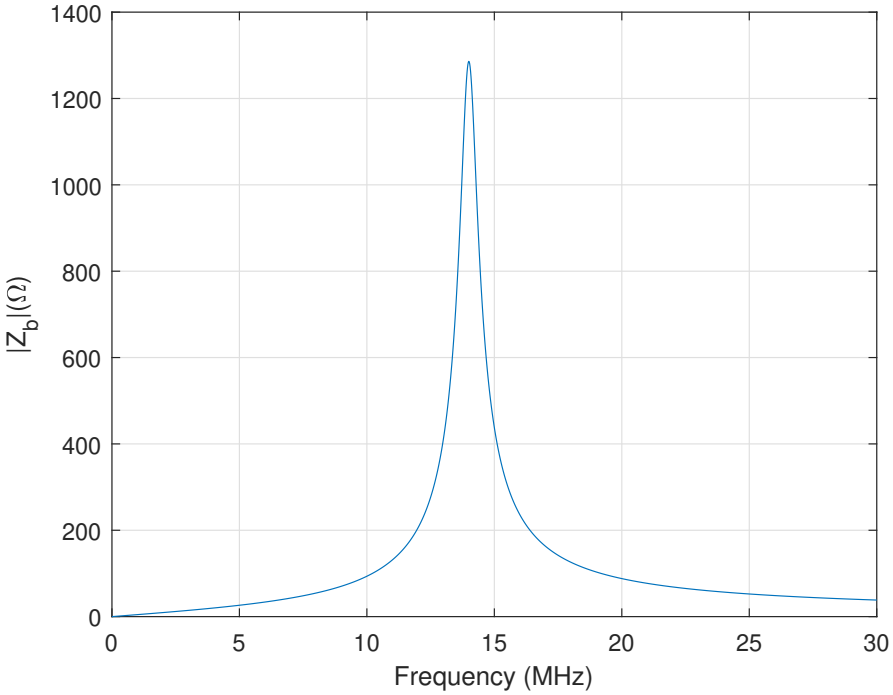

Figure 6.4: Frequency response of Z_b

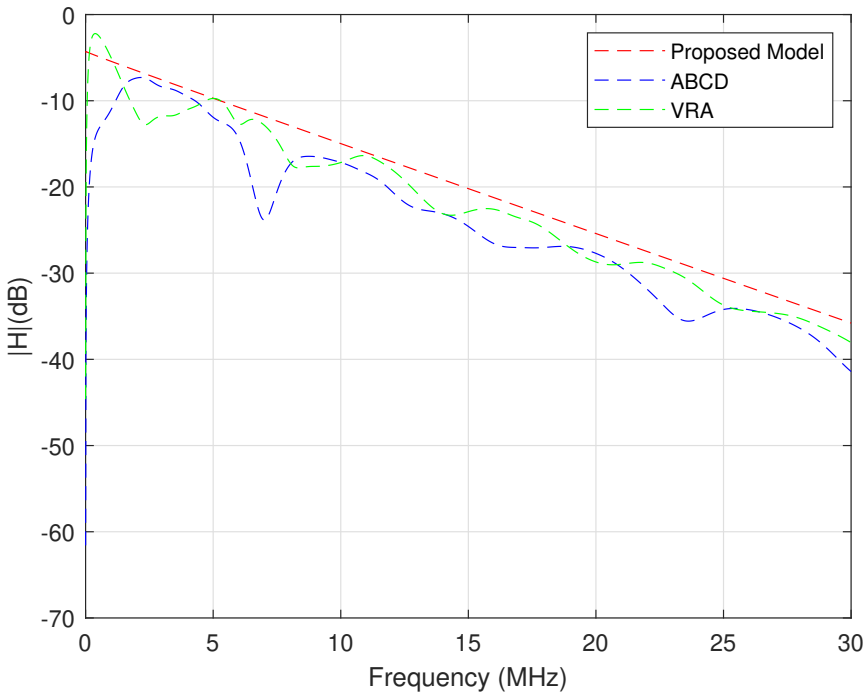

Figure 6.5: Comparison of CTFs of the direct path S to D

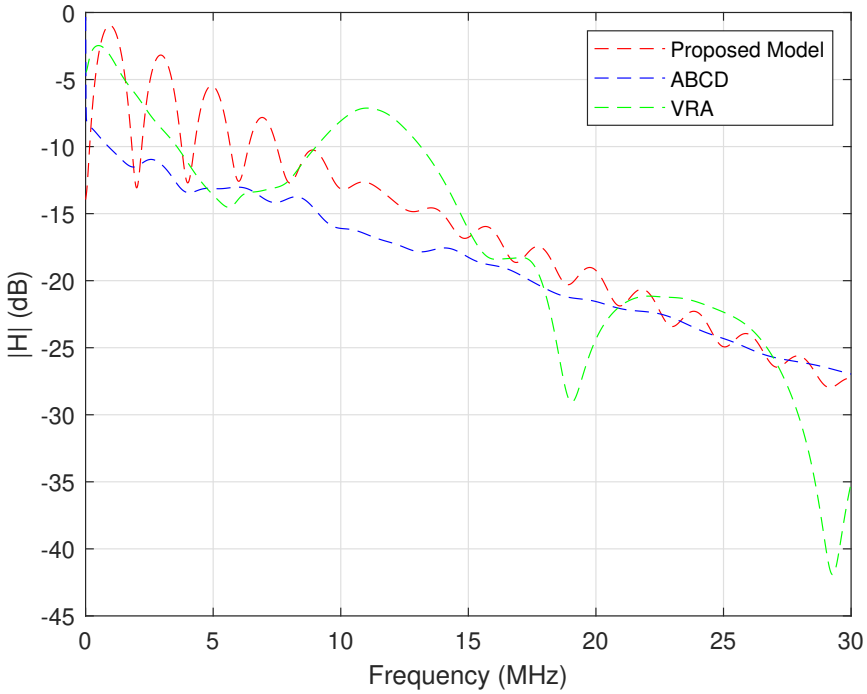

Figure 6.6: Comparison of CTFs of the path S to D through R

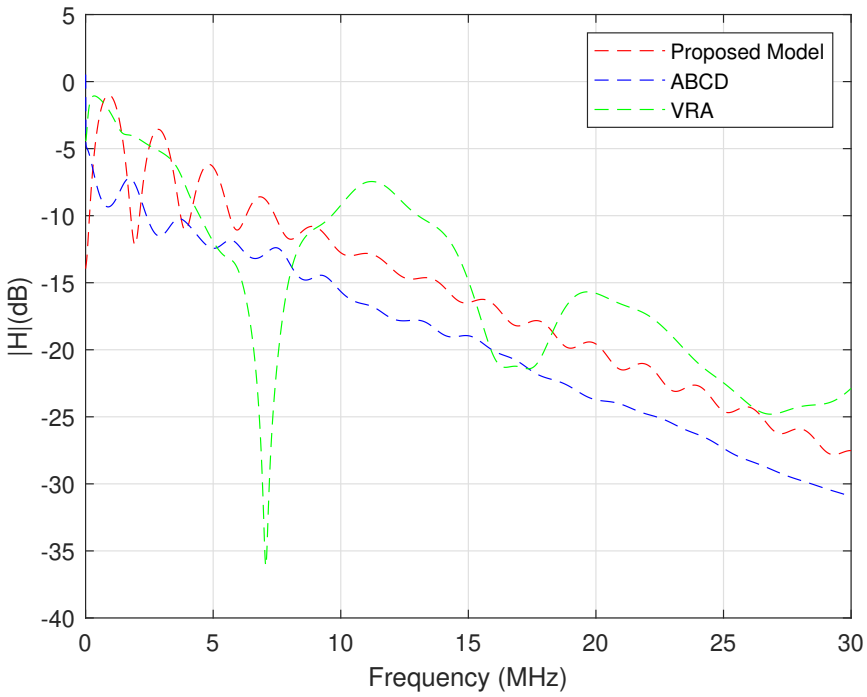

Figure 6.7: Comparison of CTFs of the path D to S through R

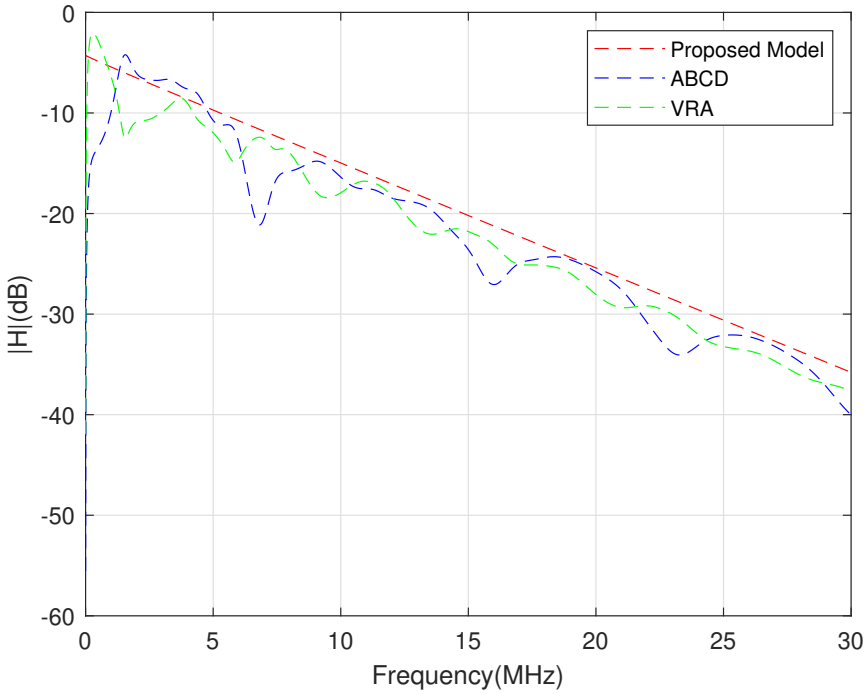

Figure 6.8: Comparison of CTFs of the direct path D to S

6.4 Chapter Summary

The bottom-up multipath channel model for a single-relay two-way PLC channel has been proposed in the chapter. This model has been derived on the modification of parameters of the top-down Zimmermann-Dostert model. The proposed model of a single-relay two-way PLC system has also been compared with the ABCD and VRA models. The three channel models are discussed and formulated with the assumption that there is no reflection from the far end. It has been shown by simulations that the proposed model does not have many fluctuations/deep fades. It can also be seen that, for the direct paths, the three models show a similar profile. On the other hand, for the SRD path at high frequencies, it has been observed that the proposed model has similar attenuation to the ABCD model. Finally, for the DRS path, the proposed model has better attenuation than the ABCD model at high frequencies.

Chapter 7

Optimal Power Allocation

In Chapter 4, the channel model of a three-node two-way relay-assisted PLC systems has been discussed. With the knowledge of channel modelling, the system model of a three-node two-way relay-assisted BMA multicarrier scheme for an indoor PLC networks is proposed in this chapter. In the proposed design, the optimal powers are derived with the consideration of QoS constraint. In practical environment, PLC systems emit lower electromagnetic interference (EMI) at smaller transmission power. Thus, the QoS criteria have to be set to the lower bound of the data traffic capacity. Since the QoS constrained power allocation problem is highly non-convex, the AO algorithm may be used to decomposed the optimisation problem to sub-problems. An introduction of relay-assisted PLC systems is described in Section 7.1. Section 7.2 represents the system model of the proposed system and introduces the protocol of the forward and reverse network operations. Next, mathematical problems are derived and solved in Section 7.3 by using the KKT conditions and AO algorithm. The numerical examples will be shown in Section 7.4 through simulations. Finally, the chapter summary is highlighted in Section 7.5.

7.1 Introduction

Researches in relay-assisted PLC have been actively conducted in the past years. In a non-regenerative scheme, or so-called AF relaying, the received signal is amplified and then forwarded to the destination. This makes AF relay scheme having shorter processing delays and easy to implement as it is less complex. It has been shown in [128] that SNR can be cooperatively achieved by placing a relay device in-between the transmitter and receiver of a PLC system. Moreover, in [129], it has been studied that the PLC achievable data exchange rate can be increased by employing a two-way AF relay system.

As relays can be considered as transceiver nodes, relay-assisted PLC systems need more power consumption than the conventional PLC systems. It is necessary to optimise power usage to meet the system requirement and establish a green communications infrastructure. In [130], two-way AF relay system for indoor PLC network was optimised with QoS consideration. The system model discussed in [130] consisted of two terminals with a relay between them. In other words, the direct link between the source and destination nodes was not available in this system. In contrast, a direct link in the relay-assisted PLC system was presented in [106]. The system was optimised for the source and relay power allocation in a general BMA multicarrier relay transmission system to minimise the total power consumption. In [106], a TDD mode was assumed and no reverse channels were discussed. Furthermore, the authors used AF relay-involved PLC system to achieve both time and spatial diversity [131]. Note that in a BMA mode, the signal is broadcasted by the source node to the other two nodes in the first phase transmission. In the second phase, the source node continues to broadcast while the relay node forwards its received signal to the destination node. It has also been shown that the two-way relay systems can effectively support data exchange within the two phases in BMA [132], [133].

As mentioned previously, smart grid systems need two-way communication links. To the best of knowledge, two-way power-optimised relay-assisted PLC systems with a direct link between the source and destination terminal nodes have not been discussed in the existing research works. It is worth mentioning that it is beneficial to include a direct link in a communication system under harsh channels to provide spatial diversity, thereby improving the system performance [134]. To fill this gap, a power optimisation of a three-node two-way relay-assisted BMA multicarrier scheme is proposed for an indoor PLC network with consideration of QoS constraints. In practical environment, PLC systems emit lower EMI at smaller transmission power. Thus, the QoS criteria have to be set to the lower-bound of the data traffic capacity. Since the QoS-constrainted power allocation problem is highly non-convex, the AO algorithm may be used to decomposed the optimisation problem to sub-problems. In particular, the system model of the proposed system is build and then introduce the protocol of the forward and reverse network operations. Next, mathematical problems are derived and solved by using the KKT conditions and AO algorithm. The numerical examples will be shown through simulations.

7.2 System Model

A multicarrier three-node two-way PLC system with a source node (T_1), a relay node (R) and a destination node (T_2) is depicted in Fig. 7.1. It is assumed that OFDM is employed as the modulation technique [135]. The available system bandwidth, B is divided uniformly into K subcarriers so that the channel fading can be considered as flat at each subcarrier. The discrete channel frequency response (CFR) at the k-th ($k = 1, 2, .., K$) subcarrier from node L_1 to node L_2 is denoted by $h_{L_1L_2}^{[k],(n)}$, where $L_1, L_2 \in \{T_1, T_2, R\}$.

Furthermore, the source and relay node is assumed to operate in a half-duplex mode where the nodes can either transmit or receive signal at one particular time. On the contrary, the destination node is assumed to employ an ideal circulator.

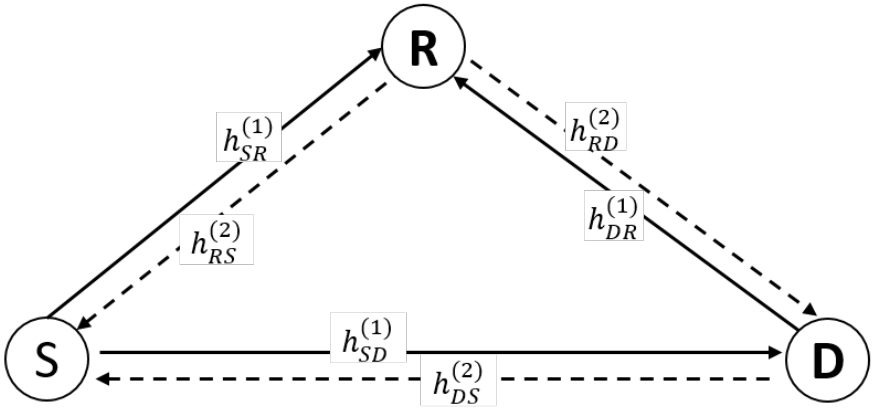

Figure 7.1: A three-way relay system model where the solid-lines indicate first phase and the dash-line indicate the second phase.

As a result, it can operate in in-band full-duplex mode, i.e., it can transmit and receive simultaneously and over the same frequency, with negligible self-interference [136]–[138].

The proposed protocol can be explained as follows. In the first phase, the source node T_1 broadcasts X_1 signal to R and T_2 while the destination node T_2 transmits X_2 signal to R. In the second phase, the node R amplify and broadcast the sum of the received signals to T_1 and T_2. At the same time, T_2 transmits X_2 to T_1. To avoid confusion, the 'source node' and 'destination node' terms are no longer used. The data flow $T_1 \rightarrow (R) \rightarrow T_2$ is referred as *forward mode* while the flow $T_1 \leftarrow (R) \leftarrow T_2$ is referred as *reverse mode*.

K is assumed to be large enough so that $X_1^{[k]}$ and $X_2^{[k]}$ follow Gaussian distribution with zero mean and unit variance. Let the transmission power at the k-th subcarrier from T_1 be $P_{T_1}^{[k]}$, from T_2 be $P_{T_2}^{[k]}$, and from R be $P_R^{[k]}$. In the forward mode, node T_1 broadcasts the signal $X_1^{[k]}$ with power $P_{T_1}^{[k]}$. On the other hand, in the reverse mode, node T_2 broadcasts $X_2^{[k]}$ with power $P_{T_{2,1}}^{[k]}$ and $P_{T_{2,2}}^{[k]}$ in the first and second phase, respectively. The total transmit power of node T_2 is given by

$$P_{T_2}^{[k]} = P_{T_{2,1}}^{[k]} + P_{T_{2,2}}^{[k]}. \tag{7.1}$$

Therefore, the total network power is given by

$$P_\sigma = \sum_{k=1}^{K} P_{T_1}^{[k]} + \sum_{k=1}^{K} P_{T_2}^{[k]} + \sum_{k=1}^{K} P_R^{[k]}. \tag{7.2}$$

As the broadcasting nature of the power line makes the received signal in relay node and destination node have different channel gain and noise disturbances, the received signals in the first phase can be mathematically modeled as

$$Y_{R,1}^{[k]} = h_{T_1R}^{[k],(1)} \sqrt{P_{T_1}^{[k]}} X_1^{[k]} + h_{T_2R}^{[k],(1)} \sqrt{P_{T_{2,1}}^{[k]}} X_2^{[k]} + N_R^{[k]}, \tag{7.3}$$

$$Y_{T_{2,1}}^{[k]} = h_{T_1T_2}^{[k],(1)} \sqrt{P_{T_1}^{[k]}} X_1^{[k]} + N_{T_2}^{[k]}, \tag{7.4}$$

where $Y_{L,1}^{[k]}$ and $N_L^{[k]}$ represent the received signal in the first phase at node L and in the first phase noise at node L where $L \in \{R, T_2\}$. Following [130], the PSD of noise is assumed to be same for each node between two successive phases.

In the second phase, the relay node amplifies the received signal with amplitude gain g, then it broadcasts the amplified signal to the node T_1 and to node T_2 with power $P_R^{[k]}$. The received signals in the second phase can be mathematically modeled by

$$Y_{T_{1,2}}^{[k]} = h_{RT_1}^{[k],(2)} g^{[k]} Y_{R,1}^{[k]} + h_{T_2T_1}^{[k],(2)} \sqrt{P_{T_{2,2}}^{[k]}} X_2^{[k]} + N_{T_1}^{[k]}, \tag{7.5}$$

$$Y_{T_{2,2}}^{[k]} = h_{RT_2}^{[k],(2)} g^{[k]} Y_{R,1}^{[k]} + N_{T_2}^{[k]}, \tag{7.6}$$

where $Y_{L,2}^{[k]}$ represents the received signal in the second phase at node L where $L \in \{T_1, T_2\}$. The gain $g^{[k]}$ can be expressed as

$$g^{[k]} = \sqrt{\frac{P_R^{[k]}}{P_{T_1}^{[k]} \left| h_{T_1R}^{[k],(1)} \right|^2 + P_{T_{2,1}}^{[k]} \left| h_{T_2R}^{[k],(1)} \right|^2 + W^{[k]}}}, \tag{7.7}$$

where $W^{[k]}$ is the noise power.

Substituting (7.3) and (7.4) into (7.5) and (7.6) gives

$$\begin{aligned} Y_{T_{1,2}}^{[k]} &= \left(h_{T_1R}^{[k],(1)} h_{RT_1}^{[k],(2)} g^{[k]} \sqrt{P_{T_1}^{[k]}}\right) X_1^{[k]} \\ &+ \left(h_{T_2R}^{[k],(1)} h_{RT_1}^{[k],(2)} g^{[k]} \sqrt{P_{T_{2,1}}^{[k]}} + h_{T_2T_1}^{[k],(2)} \sqrt{P_{T_{2,2}}^{[k]}}\right) X_2^{[k]} \\ &+ h_{RT_1}^{[k],(2)} g^{[k]} N_R^{[k]} + N_{T_1}^{[k]}, \end{aligned} \tag{7.8}$$

and

$$\begin{aligned} Y_{T_{2,2}}^{[k]} &= \left(h_{T_1R}^{[k],(1)} h_{RT_2}^{[k],(2)} g^{[k]} \sqrt{P_{T_1}^{[k]}}\right) X_1^{[k]} + \left(h_{T_2R}^{[k],(1)} h_{RT_2}^{[k],(2)} g^{[k]} \sqrt{P_{T_{2,1}}^{[k]}}\right) X_2^{[k]} \\ &+ h_{RT_2}^{[k],(2)} g^{[k]} N_R^{[k]} + N_{T_2}^{[k]}. \end{aligned} \tag{7.9}$$

It is assumed that the channel state information (CSI) is available to the nodes. Since T_1 has full knowledge of $X_1^{[k]}$, the first term in Eqn. (7.8) can be readily eliminated and the remaining term is used to decode the information of signal $X_2^{[k]}$. Similarly, the second term in Eqn. (7.9) is eliminated and the remaining term is used to decode the information of signal $X_1^{[k]}$. As a result, the SNRs at T_1, $T_{2,1}$ and $T_{2,2}$ can be calculated in Appendix.

$$SNR_{T_1} = \frac{\left(\sqrt{\sigma\upsilon} + \sqrt{\phi(1+\rho+\upsilon)}\right)^2}{1+\rho+\upsilon+\sigma}, \tag{7.10}$$

$$SNR_{T_{2,1}} = \varrho, \tag{7.11}$$

$$SNR_{T_{2,2}} = \frac{\tau\rho}{1+\rho+\upsilon+\tau}, \tag{7.12}$$

where

$$\rho = P_{T_1}^{[k]} \lambda_{T_1 R}^{[k],(1)}, \tag{7.13}$$

$$\varrho = P_{T_1}^{[k]} \lambda_{T_1 T_2}^{[k],(1)}, \tag{7.14}$$

$$\sigma = P_{R}^{[k]} \lambda_{R T_1}^{[k],(2)}, \tag{7.15}$$

$$\tau = P_{R}^{[k]} \lambda_{R T_2}^{[k],(2)}, \tag{7.16}$$

$$\upsilon = P_{T_{2,1}}^{[k]} \lambda_{T_2 R}^{[k],(1)}, \tag{7.17}$$

$$\phi = P_{T_{2,2}}^{[k]} \lambda_{T_2 T_1}^{[k],(2)}, \tag{7.18}$$

and the normalised path gain from node L_1 to L_2 in the n-th ($n = 1, 2$) phase is given by

$$\lambda_{L_1 L_2}^{[k],(n)} = \frac{\left| h_{L_1 L_2}^{[k],(n)} \right|^2}{W^{[k]}}. \tag{7.19}$$

The average sub-channel capacities (ASC) (in bits/s/Hz/subcarrier) of the data traffic from T_2 to T_1 and from T_1 to T_2 are respectively given by

$$\overline{C}_1 = \frac{1}{2K} \sum_{k=1}^{K} \log_2 \left(1 + SNR_{T_1}\right), \tag{7.20}$$

$$\overline{C}_2 = \frac{1}{2K} \sum_{k=1}^{K} \log_2 \left(1 + SNR_{T_{2,1}} + SNR_{T_{2,2}}\right). \tag{7.21}$$

Note that the factor $\frac{1}{2}$ appears due to the two-phase system.

By applying QoS criteria as the lower-bound of the system capacity, an optimisation problem is developed to make the most efficient utilisation of the system total power as follows

$$\min_{P_{T_1}^{[k]}, P_{T_2}^{[k]}, P_R^{[k]}} P_\Sigma \tag{7.22}$$

subject to

$$\overline{C}_1 \geq \overline{q}_1, \tag{7.23}$$

$$\overline{C}_2 \geq \overline{q}_2, \tag{7.24}$$

$$P_{T_1}^{[k]}, P_{T_2}^{[k]}, P_R^{[k]} \geq 0, \qquad \forall k, \tag{7.25}$$

where (7.22) is the objective function of the total network transmitting power, and both $\overline{q}_1$ and $\overline{q}_2$ show the minimal link capacity required to support the smart grid applications.

As the optimisation problem is non-convex, the exact solution to the optimisation problem is hard to obtain. Thus, an alternating optimisation is proposed by firstly optimising the $P_R^{[k]}$ given the $P_{T_1}^{[k]}$, $P_{T_{2,1}}^{[k]}$ and $P_{T_{2,2}}^{[k]}$ values. With the given $P_{T_{2,1}}^{[k]}$ and $P_{T_{2,2}}^{[k]}$ as well as previously optimised $P_R^{[k]}$, $P_{T_1}^{[k]}$ is optimised. Next, optimise $P_{T_{2,1}}^{[k]}$ given the $P_{T_{2,2}}^{[k]}$ and previously optimised $P_{T_1}^{[k]}$ and $P_R^{[k]}$. The last step is to optimise $P_{T_{2,2}}^{[k]}$ given the previously optimised $P_R^{[k]}$, $P_{T_1}^{[k]}$ and $P_{T_{2,1}}^{[k]}$. The process is repeated until convergent, i.e., the difference between the total power obtained in two successive iteration is less than a certain threshold. The resulting sub-problems are convex for any two groups of fixed power allocation parameters. Thus, the overall algorithm is developed to solve the initial problem (7.22) - (7.25) which will be discussed in the following subsections.

7.3 Optimal Power Allocation

This section discusses the optimisation problem (7.22) - (7.25) are breakdown into sub-problems. The optimal power allocation using the KKT and AO algorithm are derived and discussed.

7.3.1 Optimal Relay Power Allocation Given First and Second Terminal Power Allocations

Using the given initial values of $P_{T_1}^{[k]}$, $P_{T_{2,1}}^{[k]}$ and $P_{T_{2,2}}^{[k]}$, the problem (7.22) - (7.25) become

$$\min_{P_R^{[k]}} \sum_{k=1}^{K} P_R^{[k]}, \tag{7.26}$$

subject to

$$2K\overline{q}_1 - \sum_{k=1}^{K} \log_2 \left(A_k + \frac{B_k + C_k \sqrt{P_R^{[k]}}}{D_k P_R^{[k]} + E_k} \right) \leq 0, \tag{7.27}$$

$$2K\overline{q}_2 - \sum_{k=1}^{K} \log_2 \left(F_k - \frac{G_k}{H_k P_R^{[k]} + E_k} \right) \leq 0, \tag{7.28}$$

$$P_R^{[k]} \geq 0, \forall k, \tag{7.29}$$

where

$$A_k = 1 + P_{T_{2,1}}^{[k]} \lambda_{T_2R}^{[k],(1)}, \tag{7.30}$$

$$B_k = \left(P_{T_{2,2}}^{[k]} \lambda_{T_2T_1}^{[k],(2)} - P_{T_{2,1}}^{[k]} \lambda_{T_2R}^{[k],(1)} \right) \left(1 + P_{T_1}^{[k]} \lambda_{T_1R}^{[k],(1)} + P_{T_{2,1}}^{[k]} \lambda_{T_2R}^{[k],(1)} \right), \tag{7.31}$$

$$C_k = 2\sqrt{P_{T_{2,1}}^{[k]} \lambda_{T_2R}^{[k],(1)} P_{T_{2,2}}^{[k]} \lambda_{T_2T_1}^{[k],(2)} \lambda_{RT_1}^{[k],(2)} \left(1 + P_{T_1}^{[k]} \lambda_{T_1R}^{[k],(1)} + P_{T_{2,1}}^{[k]} \lambda_{T_2R}^{[k],(1)} \right)}, \tag{7.32}$$

$$D_k = \lambda_{RT_1}^{[k],(2)}, \tag{7.33}$$

$$E_k = 1 + P_{T_1}^{[k]} \lambda_{T_1R}^{[k],(1)} + P_{T_{2,1}}^{[k]} \lambda_{T_2R}^{[k],(1)}, \tag{7.34}$$

$$F_k = 1 + P_{T_1}^{[k]} \lambda_{T_1R}^{[k],(1)}, \tag{7.35}$$

$$G_k = P_{T_1}^{[k]} \lambda_{T_1R}^{[k],(1)} \left(1 + P_{T_1}^{[k]} \lambda_{T_1R}^{[k],(1)} + P_{T_{2,1}}^{[k]} \lambda_{T_2R}^{[k],(1)} \right), \tag{7.36}$$

$$H_k = \lambda_{RT_2}^{[k],(2)}. \tag{7.37}$$

Applying Karush-Kuhn-Tucker (KKT) conditions to the problems (7.26) - (7.29) results in the expressions (7.38) - (7.42)

$$1+\alpha_1 \frac{C_k D_k P_R^{[k]} + 2B_k D_k \sqrt{P_R^{[k]}} - C_k E_k}{2\ln(2)\left(A_k D_k P_R^{[k]} + A_k E_k + C_k \sqrt{P_R^{[k]}} + B_k\right)\sqrt{P_R^{[k]}}\left(D_k P_R^{[k]} + E_k\right)} - \alpha_2 \frac{G_k H_k}{\ln(2)\left(F_k - \frac{G_k}{H_k P_R^{[k]} + E_k}\right)\left(H_k P_R^{[k]} + E_k\right)^2} = 0 \quad (7.38)$$

$$\alpha_1 \left[2K\overline{q}_1 - \sum_{k=1}^{K} \log_2\left(A_k + \frac{B_k + C_k\sqrt{P_R^{[k]}}}{D_k P_R^{[k]} + E_k}\right)\right] = 0 \quad (7.39)$$

$$\alpha_2 \left[2K\overline{q}_2 - \sum_{k=1}^{K} \log_2\left(F_k - \frac{G_k}{H_k P_R^{[k]} + E_k}\right)\right] = 0 \quad (7.40)$$

$$\alpha_1, \alpha_2 \geq 0 \quad (7.41)$$

$$P_R^{[k]} \geq 0 \quad (7.42)$$

Proposition 1. The problem (7.26) - (7.29) becomes convex with the condition of $\{P_R^{[k]} | P_R^{[k]} \geq 0\}$. When $\alpha_1, \alpha_2 > 0$, the LHS of (7.38) - (7.41) are monotone function of $P_R^{[k]}$. Thus, a bi-section search algorithm may be used to solve (7.38) - (7.42), which is also the solution of problem (7.26) - (7.29).

7.3.2 Optimal First Terminal Power Allocation Given Second Terminal and Relay Power Allocations

Using the newly optimised value $P_R^{[k]}$ and the given initial value $P_{T_{2,1}}^{[k]}$ and $P_{T_{2,2}}^{[k]}$, the problem (7.22) - (7.25) becomes

$$\min_{P_{T_1}^{[k]}} \sum_{k=1}^{K} P_{T_1}^{[k]}, \quad (7.43)$$

subject to

$$2K\overline{q}_1 - \sum_{k=1}^{K} \log_2\left(I_k + \frac{J_k + K_k\sqrt{L_k + M_k P_{T_1}^{[k]}}}{M_k P_{T_1}^{[k]} + N_k}\right) \leq 0, \quad (7.44)$$

$$2K\overline{q}_2 - \sum_{k=1}^{K} \log_2\left(O_k + Q_k P_{T_1}^{[k]} - \frac{R_k}{M_k P_{T_1}^{[k]} + S_k}\right) \leq 0, \quad (7.45)$$

$$P_{T_1}^{[k]} \geq 0, \qquad \forall k, \quad (7.46)$$

where

$$I_k = 1 + P_{T_{2,2}}^{[k]} \lambda_{T_2T_1}^{[k],(2)}, \tag{7.47}$$

$$J_k = P_R^{[k]} \lambda_{RT_1}^{[k],(2)} \left(P_{T_{2,1}}^{[k]} \lambda_{T_2R}^{[k],(1)} - P_{T_{2,2}}^{[k]} \lambda_{T_2T_1}^{[k],(2)} \right), \tag{7.48}$$

$$K_k = 2\sqrt{P_R^{[k]} \lambda_{RT_1}^{[k],(2)} P_{T_{2,1}}^{[k]} \lambda_{T_2R}^{[k],(1)} P_{T_{2,2}}^{[k]} \lambda_{T_2T_1}^{[k],(2)}}, \tag{7.49}$$

$$L_k = 1 + P_{T_{2,1}}^{[k]} \lambda_{T_2R}^{[k],(1)}, \tag{7.50}$$

$$M_k = \lambda_{T_1R}^{[k],(1)}, \tag{7.51}$$

$$N_k = 1 + P_R \lambda_{RT_1}^{[k],(2)} + P_{T_{2,1}}^{[k]} \lambda_{T_2R}^{[k],(1)}, \tag{7.52}$$

$$O_k = 1 + P_R \lambda_{RT_2}^{[k],(2)}, \tag{7.53}$$

$$Q_k = \lambda_{T_1T_2}^{[k],(2)}, \tag{7.54}$$

$$R_k = P_R \lambda_{RT_2}^{[k],(2)} \left(1 + P_R \lambda_{RT_2}^{[k],(2)} + P_{T_{2,1}}^{[k]} \lambda_{T_2R}^{[k],(1)} \right), \tag{7.55}$$

$$S_k = 1 + P_R \lambda_{RT_2}^{[k],(2)} + P_{T_{2,1}}^{[k]} \lambda_{T_2R}^{[k],(1)}. \tag{7.56}$$

Similar to the previous problems, KKT conditions is applied to the problem (7.43) - (7.46) to have the expressions (7.57) - (7.61).

$$1 + \beta_1 \frac{M_k \left(K_k M_k P_{T_1}^{[k]} + 2J_k \sqrt{M_k P_{T_1}^{[k]} + L_k} + 2K_k L_k - K_k N_k \right)}{2\ln(2) \left(I_k M_k P_{T_1}^{[k]} + K_k \sqrt{M_k P_{T_1}^{[k]} + L_k} + I_k N_k + J_k \right) \sqrt{M_k P_{T_1}^{[k]} + L_k} \left(M_k P_{T_1}^{[k]} + N_k \right)}$$
$$- \beta_2 \frac{Q_k + \frac{R_k M_k}{\left(M_k P_{T_1}^{[k]} + S_k \right)^2}}{\ln(2) \left(O_k + Q_k P_{T_1}^{[k]} - \frac{R_k}{M_k P_{T_1}^{[k]} + S_k} \right)^2} = 0 \tag{7.57}$$

$$\beta_1 \left[2K\overline{q}_1 - \sum_{k=1}^{K} \log_2 \left(I_k + \frac{J_k + K_k \sqrt{L_k + M_k P_{T_1}^{[k]}}}{M_k P_{T_1}^{[k]} + N_k} \right) \right] = 0 \tag{7.58}$$

$$\beta_2 \left[2K\overline{q}_2 - \sum_{k=1}^{K} \log_2 \left(O_k + Q_k P_{T_1}^{[k]} - \frac{R_k}{M_k P_{T_1}^{[k]} + S_k} \right) \right] = 0 \tag{7.59}$$

$$\beta_1, \beta_2 \geq 0 \tag{7.60}$$

$$P_{T_1}^{[k]} \geq 0 \tag{7.61}$$

Proposition 2. The problem (7.43) - (7.46) becomes convex with the condition of $\{P_{T_1}^{[k]} | P_{T_1}^{[k]} \geq 0\}$. When $\beta_1, \beta_2 > 0$, the LHS of (7.57) - (7.59) are monotonic functions of $P_{T_1}^{[k]}$. A bi-section search algorithm may be used to solve (7.57) - (7.61), which is also the solution of problems (7.43) - (7.46).

7.3.3 Optimal Second Terminal Power Allocation of First Phase Given First Terminal and Relay Power Allocations

Using the newly optimised value $P_R^{[k]}$ and $P_{T_1}^{[k]}$ obtained from the previous steps and the given initial value $P_{T_{2,2}}^{[k]}$, the problem (7.22) - (7.25) becomes

$$\min_{P_{T_{2,1}}^{[k]}} \sum_{k=1}^{K} P_{T_{2,1}}^{[k]}, \tag{7.62}$$

subject to

$$2K\overline{q}_1 - \sum_{k=1}^{K} \log_2 \left(T_k + \frac{U_k + V_k \sqrt{P_{T_{2,1}}^{[k]} (X_k + Y_k P_{T_{2,1}}^{[k]})}}{Y_k P_{T_{2,1}}^{[k]} + Z_k} \right) \leq 0, \tag{7.63}$$

$$2K\overline{q}_2 - \sum_{k=1}^{K} \log_2 \left(a_k + \frac{b_k}{Y_k P_{T_{2,1}}^{[k]} + C_k} \right) \leq 0, \tag{7.64}$$

$$P_{T_{2,1}}^{[k]} \geq 0, \qquad \forall k, \tag{7.65}$$

where

$$T_k = 1 + P_R^{[k]} \lambda_{RT_1}^{[k],(2)} + P_{T_{2,2}}^{[k]} \lambda_{T_2T_1}^{[k],(2)}, \tag{7.66}$$

$$U_k = -P_R^{[k]} \lambda_{RT_1}^{[k],(2)} (1 + P_{T_1}^{[k]} \lambda_{T_1R}^{[k],(1)} + P_R^{[k]} \lambda_{RT_1}^{[k],(2)} + P_{T_{2,2}}^{[k]} \lambda_{T_2T_1}^{[k],(2)}), \tag{7.67}$$

$$V_k = 2\sqrt{P_R^{[k]} \lambda_{RT_1}^{[k],(2)} \lambda_{T_2R}^{[k],(1)} P_{T_{2,2}}^{[k]} \lambda_{T_2T_1}^{[k],(2)}}, \tag{7.68}$$

$$X_k = 1 + P_{T_1} \lambda_{T_1R}^{[k],(1)}, \tag{7.69}$$

$$Y_k = \lambda_{T_2R}^{[k],(1)}, \tag{7.70}$$

$$Z_k = 1 + P_{T_1} \lambda_{T_1R}^{[k],(1)} + P_R^{[k]} \lambda_{RT_1}^{[k],(2)}, \tag{7.71}$$

$$a_k = 1 + P_{T_1} \lambda_{T_1T_2}^{[k],(1)}, \tag{7.72}$$

$$b_k = P_R^{[k]} \lambda_{RT_2}^{[k],(2)} P_{T_1} \lambda_{T_1R}^{[k],(1)}, \tag{7.73}$$

$$c_k = 1 + P_R^{[k]} \lambda_{RT_2}^{[k],(2)} + P_{T_1}^{[k]} \lambda_{T_1R}^{[k],(1)}. \tag{7.74}$$

After applying KKT conditions to the problems (7.62) - (7.65), (7.75) - (7.79) are as shown

$$1+\gamma_1\frac{V_kX_kY_kP_{T_{2,1}}^{[k]}-2V_kY_kZ_kP_{T_{2,1}}^{[k]}-V_kX_kZ_k+2U_kY_k\sqrt{P_{T_{2,1}}^{[k]}\left(Y_kP_{T_{2,1}}^{[k]}+X_k\right)}}{2\ln(2)\left(T_kY_kP_{T_{2,1}}^{[k]}+V_k\sqrt{P_{T_{2,1}}^{[k]}\left(Y_kP_{T_{2,1}}^{[k]}+X_k\right)}+T_kZ_k+U_k\right)\sqrt{P_{T_{2,1}}^{[k]}\left(Y_kP_{T_{2,1}}^{[k]}+X_k\right)}\left(Y_kP_{T_{2,1}}^{[k]}+Z_k\right)}$$
$$+\gamma_2\frac{b_kY_k}{\ln(2)\left(a_k+\frac{b_k}{Y_kP_{T_{2,1}}^{[k]}+c_k}\right)\left(Y_kP_{T_{2,1}}^{[k]}+c_k\right)^2} = 0 \quad (7.75)$$

$$\gamma_1\left[2K\overline{q}_1-\sum_{k=1}^{K}log_2\left(T_k+\frac{U_k+V_k\sqrt{P_{T_{2,1}}^{[k]}(X_k+Y_kP_{T_{2,1}}^{[k]})}}{Y_kP_{T_{2,1}}^{[k]}+Z_k}\right)\right] = 0 \quad (7.76)$$

$$\gamma_2\left[2K\overline{q}_2-\sum_{k=1}^{K}log_2\left(a_k+\frac{b_k}{Y_kP_{T_{2,1}}^{[k]}+c_k}\right)\right] = 0 \quad (7.77)$$

$$\gamma_1,\gamma_2 \geq 0 \quad (7.78)$$

$$P_{T_{2,1}}^{[k]} \geq 0 \quad (7.79)$$

Proposition 3. The problem (7.62) - (7.65) becomes convex with the condition of $\{P_{T_{2,1}}^{[k]}|P_{T_{2,1}}^{[k]}\geq 0\}$. When $\gamma_1,\gamma_2>0$, the LHS of (7.75) - (7.77) are monotone function of $P_{T_{2,1}}^{[k]}$. Once again, a bi-section search algorithm may be used to solve (7.75) - (7.79), which is also the solution of problem (7.62) - (7.65).

7.3.4 Optimal Second Terminal Power Allocation of Second Phase Given First Terminal and Relay Power Allocations

Using the newly optimised value $P_R^{[k]}$, $P_{T_1}^{[k]}$ and $P_{T_{2,1}}^{[k]}$ obtained from the previous steps, the problem (7.22) - (7.25) becomes

$$\min_{P_{T_{2,2}}^{[k]}}\sum_{k=1}^{K}P_{T_{2,2}}^{[k]}, \quad (7.80)$$

subject to

$$2K\overline{q}_1-\sum_{k=1}^{K}\log_2\left(1+d_k+e_kP_{T_{2,2}}^{[k]}+f_k\sqrt{P_{T_{2,2}}^{[k]}}\right)\leq 0, \quad (7.81)$$

$$P_{T_{2,2}}^{[k]}\geq 0, \qquad \forall k, \quad (7.82)$$

where

$$d_k = \frac{P_R^{[k]}\lambda_{RT_1}^{[k],(2)}P_{T_{2,1}}^{[k]}\lambda_{T_2R}^{[k],(1)}}{1+P_{T_1}^{[k]}\lambda_{T_1R}^{[k],(1)}+P_{T_{2,1}}^{[k],(1)}\lambda_{T_2R}^{[k],(1)}+P_R^{[k]}\lambda_{RT_1}^{[k],(2)}}, \tag{7.83}$$

$$e_k = \frac{\lambda_{T_2T_1}^{[k],(2)}\left(1+P_{T_1}^{[k]}\lambda_{T_1R}^{[k],(1)}+P_{T_{2,1}}^{[k],(1)}\lambda_{T_2R}^{[k],(1)}\right)}{1+P_{T_1}^{[k]}\lambda_{T_1R}^{[k],(1)}+P_{T_{2,1}}^{[k],(1)}\lambda_{T_2R}^{[k],(1)}+P_R^{[k]}\lambda_{RT_1}^{[k],(2)}}, \tag{7.84}$$

$$f_k = \frac{2\sqrt{P_R^{[k]}\lambda_{RT_1}^{[k],(2)}P_{T_{2,1}}^{[k],(1)}\lambda_{T_2R}^{[k],(1)}\lambda_{T_2T_1}^{[k],(2)}}}{1+P_{T_1}^{[k]}\lambda_{T_1R}^{[k],(1)}+P_{T_{2,1}}^{[k],(1)}\lambda_{T_2R}^{[k],(1)}+P_R^{[k]}\lambda_{RT_1}^{[k],(2)}} \times \sqrt{\left(1+P_{T_1}^{[k]}\lambda_{T_1R}^{[k],(1)}+P_{T_{2,1}}^{[k],(1)}\lambda_{T_2R}^{[k],(1)}\right)}. \tag{7.85}$$

Applying KKT conditions to the problems (7.80) - (7.82) results in the expressions (7.86) - (7.89).

$$1-\delta_1\frac{2e_k\sqrt{P_{T_{2,2}}^{[k]}}+f_k}{2\ln(2)\sqrt{P_{T_{2,2}}^{[k]}}\left(1+d_k+e_kP_{T_{2,2}}^{[k]}+f_k\sqrt{P_{T_{2,2}}^{[k]}}\right)}=0 \tag{7.86}$$

$$\delta_1\left[2K\overline{q}_1-\sum_{k=1}^{K}log_2\left(1+d_k+e_kP_{T_{2,2}}^{[k]}+f_k\sqrt{P_{T_{2,2}}^{[k]}}\right)\right]=0 \tag{7.87}$$

$$\delta_1 \geq 0 \tag{7.88}$$

$$P_{T_{2,2}}^{[k]} \geq 0 \tag{7.89}$$

Proposition 4. The problem (7.80) - (7.82) becomes convex with the condition of $\{P_{T_{2,2}}^{[k]}|P_{T_{2,2}}^{[k]} \geq 0\}$. When $\delta_1 > 0$, the LHS of (7.86) - (7.87) are monotone function of $P_{T_{2,2}}^{[k]}$. Once again, a bi-section search algorithm may be used to solve (7.86) - (7.89), which is also the solution of problem (7.80) - (7.82).

Based on the discussion in Section 7.3.1 to 7.3.4, the proposed AO algorithm is summarised in Table 7.1 for solving the problem (7.22) - (7.25). For each sub-problem, the global optimum obtained proved the proposed AO algorithm converges to a stationary point of the objective function (7.22).

Table 7.1: AO algorithm to solve the optimisation problem

1) Initialise $P_{R,1}^{[1]} = p_{R,1}$ when $P_{R,1}^{[k]} = 0$ for $k = 2, 3, ..., K$, $P_{T_1,1}^{[1]} = p_{T_1,1}$ when $P_{T_1,1}^{[k]} = 0$ for $k = 2, 3, ..., K$; $P_{T_{2,1},1}^{[1]} = p_{T_{2,1},1}$ when $P_{T_{2,1},1}^{[k]} = 0$ for $k = 2, 3, ..., K$ and $P_{T_{2,2},1}^{[1]} = p_{T_{2,2},1}$ when $P_{T_{2,2},1}^{[k]} = 0$ for $k = 2, 3, ..., K$. The scalars $p_{R,1}, p_{T_1,1}$, $p_{T_{2,1},1}$ and $p_{T_{2,2},1}$ satisfy the constraints (7.23) - (7.25).
2) The new set of $P_R^{[k]}$ is found using the initial given $P_{T_1}^{[k]}$, $P_{T_{2,1}}^{[k]}$ and $P_{T_{2,2}}^{[k]}$.
3) The new set of $P_{T_1}^{[k]}$ is found using the newly obtained $P_R^{[k]}$ and the initial given $P_{T_{2,1}}^{[k]}$ and $P_{T_{2,2}}^{[k]}$.
4) The new set of $P_{T_{2,1}}^{[k]}$ is found using the newly obtained $P_R^{[k]}$ and $P_{T_1}^{[k]}$ and initial given $P_{T_{2,2}}^{[k]}$.
5) The new set of $P_{T_{2,2}}^{[k]}$ is found using newly obtained $P_R^{[k]}$, $P_{T_1}^{[k]}$ and $P_{T_{2,1}}^{[k]}$.
6) Calculate the total power value using (7.2) with the obtained power allocation values.
7) Repeat Step 2 to Step 5 until it is convergence, i.e., the difference between the total power obtained in two successive iterations is less than a present threshold.

7.4 Numerical Examples

A simple three-node two-way relay-assisted PLC channel model is given in Fig. 7.2 where different segments of the network used different type of cables. The characteristics of each type of the commonly used cables are given in Table 2.1 [46]. The simulation parameters are set according to the physical layer specification of HomePlug AV protocol [139]–[141].

The noise of PLC system is modelled as filtered white Gausssian noise as discussed in Section 2.3.1. The noise on different nodes of the network are assumed to be independent and identically distributed (i.i.d) and share the common PSD as shown in Fig. 7.3.

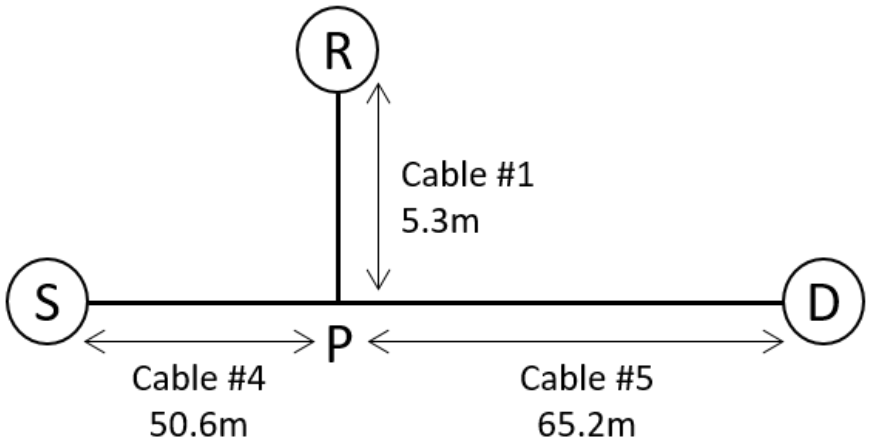

Figure 7.2: Topology of a three-node two-way channel

The source node has an inner impedance $Z_S = 50\Omega$ in transmit mode and load impedance $Z_l = 150\Omega$ in receive mode. Whereas, the relay node has an inner impedance $Z_{SR} = 50\Omega$ in transmit mode and load impedance $Z_{LR} = 150\Omega$ in receive mode.

The relay is attached to the branch where its preexisting load Z_b has the characteristics shown in Fig. 7.4.

The channel transfer functions of the relay-assisted PLC channel are found by dividing them into group of an equivalent P2P PLC channels which adapt the Canate's channel model [46]. The details of this approach can be found in Chapter 4. By configuring the parameters used for this P2P channel, a group of correlated path gains can be generated in Fig. 7.5.

The normalised path gains on each sub-carrier are calculated using (7.19) and the results are shown in Fig. 7.6.

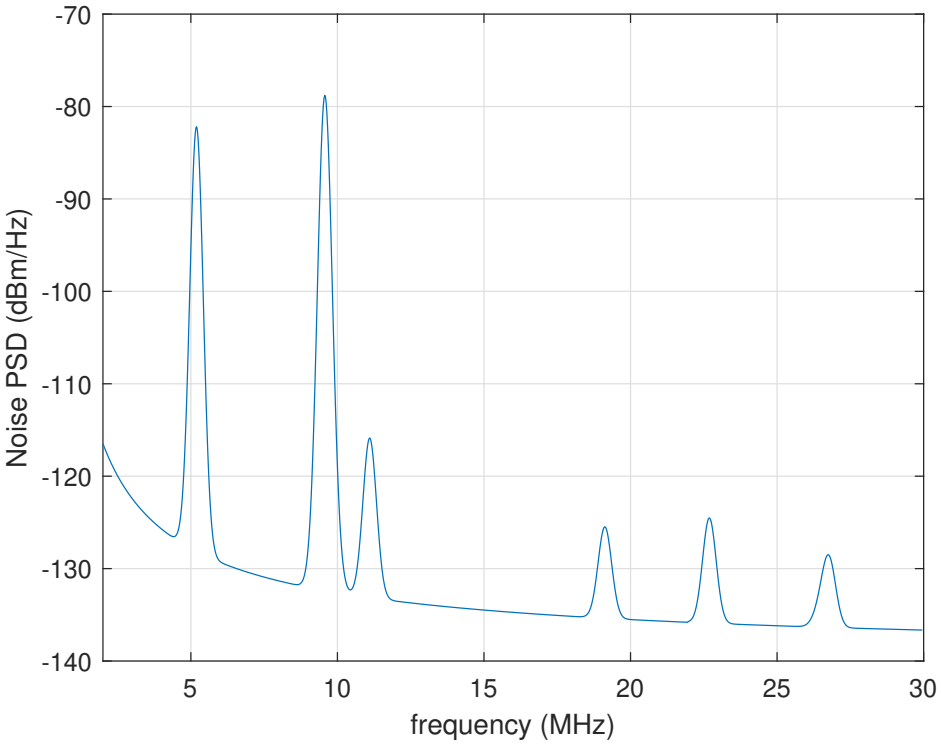

Figure 7.3: PSD of the noise in a PLC system

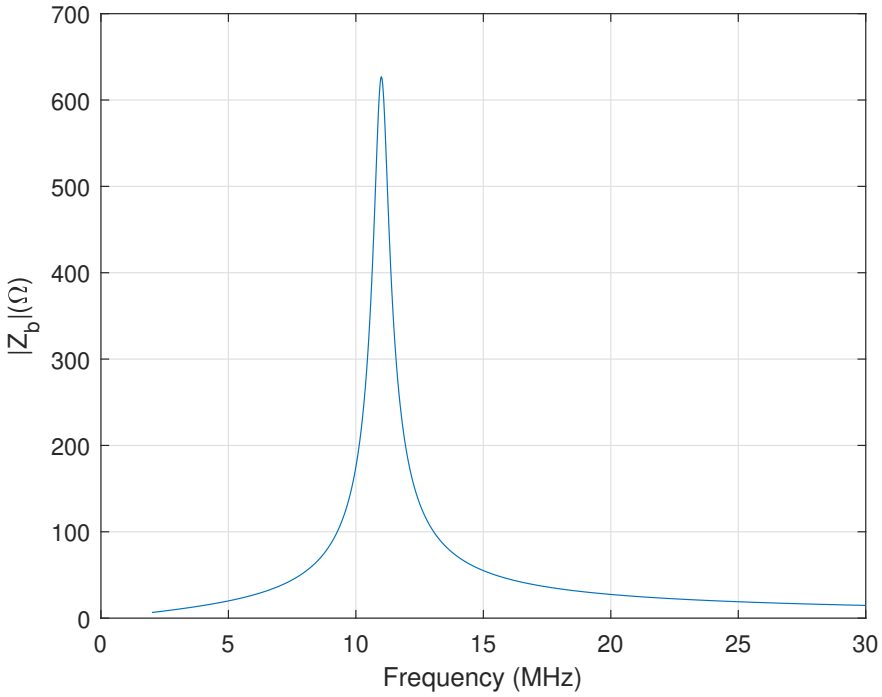

Figure 7.4: Frequency response of preexisting load Z_b

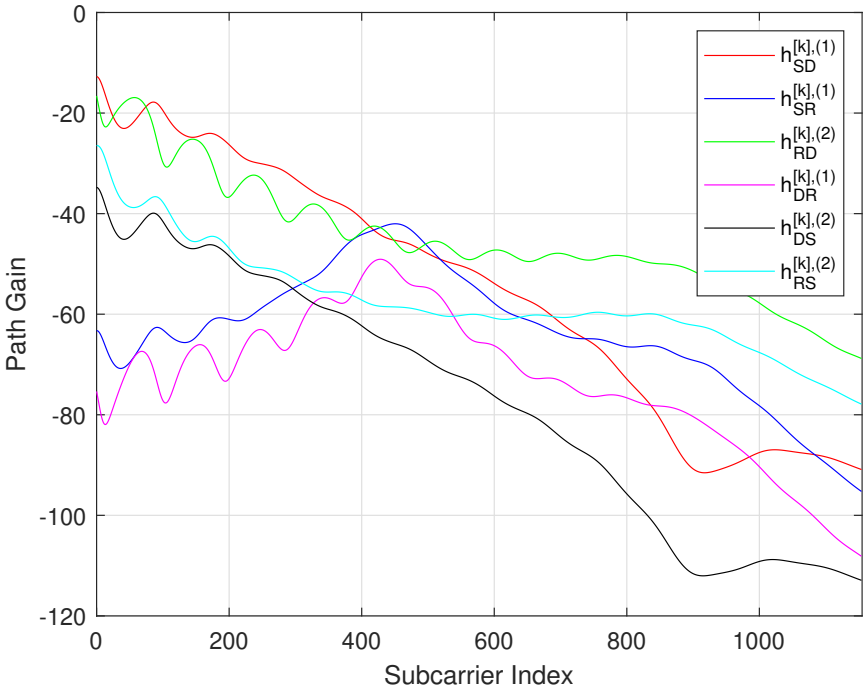

Figure 7.5: Path gain of a three-node two-way relay system

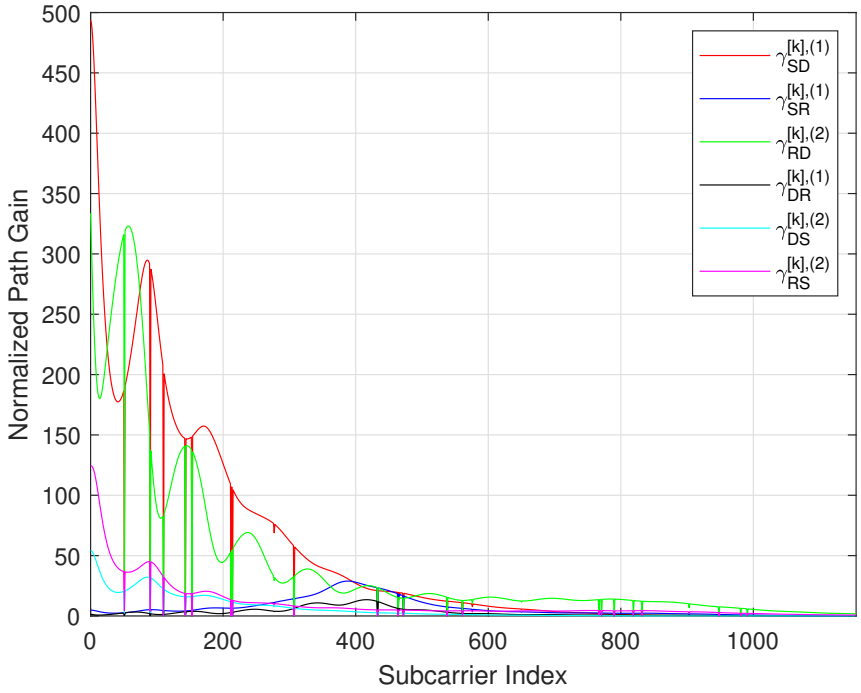

Figure 7.6: Normalised path gain of a three-node two-way relay system

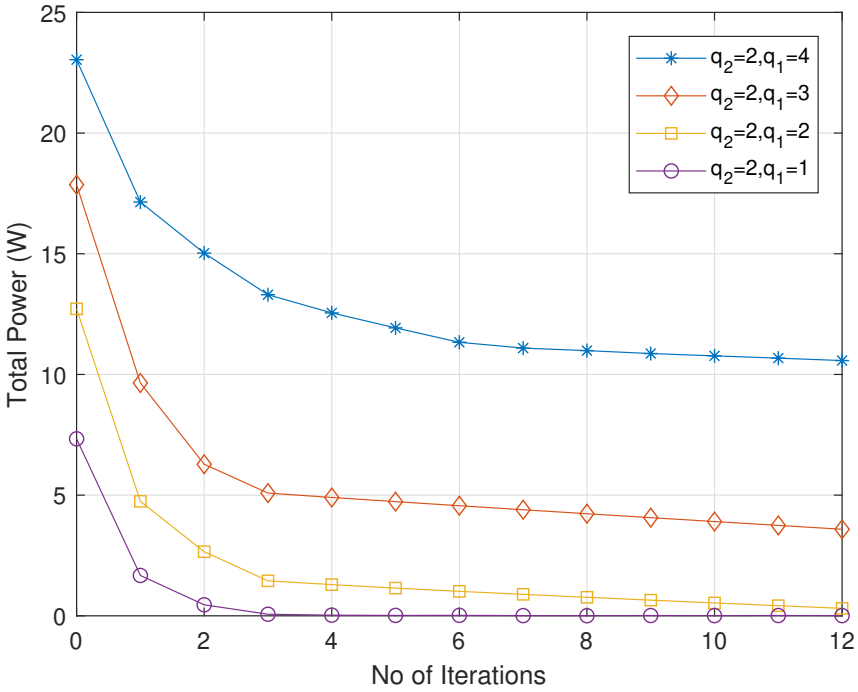

Figure 7.7: Total power versus number of iterations

Table 7.2 shows the summary of simulation parameters used. The simulation results are then used in the proposed iterative algorithm where the convergence condition is specified as the difference between the total power obtained in two successive iterations is less than 10^{-5}.

The minimal total power is obtained while satisfying the minimal ASC requirement. In the simulations, $\overline{q}_2$ is set to 2 bits/s/Hz/subcarrier and $\overline{q}_1$ is varied from 1.0 to 4.0 bits/s/Hz/subcarrier, respectively. Fig. 7.7 shows the total power

Table 7.2: System parameters used for simulation

Frequency band	2MHz to 30MHz
Total OFDM subcarriers number	K=1155
Signalling path gain $h^{[k],(n)}$	Fig 7.5
General Background noise $N^{[k],(n)}$	Fig 7.3
Normalised path gains $\gamma^{[k],(n)}$	Fig 7.6

versus the number of iterations. It can be seen that the AO algorithm converges within six iterations. Since the decreasing of the total power is very small after six iterations, the good performance of the AO algorithm can be achieved with only a few iterations. This also shows that the AO algorithm has a short processing delay, which can fulfil the requirement of a practical relay PLC systems. It is obvious that increasing the minimal ASC requirement needs more transmission power to meet the QoS constraint.

Furthermore, the proposed scheme is compared with the conventional bidirectional direct transmission (BDT) and R2WX systems under the same configuration of PLC system. The conventional BDT system is configured such that in the first phase, the source node T_1 sends $X_1^{[k]}(k = 1, 2, ..., K)$ signal with power $P_{T_1}^{[k]}$ to destination node subjecting to the QoS constraints. Whereas, in the second phase, the destination node T_2 replies $X_2^{[k]}(k = 1, 2, ..., K)$ signal with power $P_{T_2}^{[k]}$ to source node subjecting to the QoS requirement on the traffic direction. To meet the ASC constraint on the traffic direction, the power allocations at T_1 and T_2 use the water-filling algorithm [142]. Meanwhile, the R2WX system in [130] is configured such that in the first phase, the source node T_1 sends $X_1^{[k]}(k = 1, 2, ..., K)$ signal with power $P_{T_1}^{[k]}$ to the relay node and at the same time, the destination node T_2 sends $X_2^{[k]}(k = 1, 2, ..., K)$ signal with power $P_{T_2}^{[k]}$ to the relay node. In the second phase, the relay node amplifies the received signal with amplitude gain and then broadcasts the amplified signal to the node T_1 and T_2.

The total power versus the QoS constraints plots for the conventional BDT, R2WX and proposed systems are shown in Fig. 7.8. The simulation results show that the proposed system consumed about 40% less total power than the conventional BDT system to meet the same QoS requirements. Moreover, the R2WX system needs more total power than the proposed system as the direct link between the source and destination terminal nodes is not considered. In short, the proposed system consumes less power compared to the conventional BDT and R2WX systems.

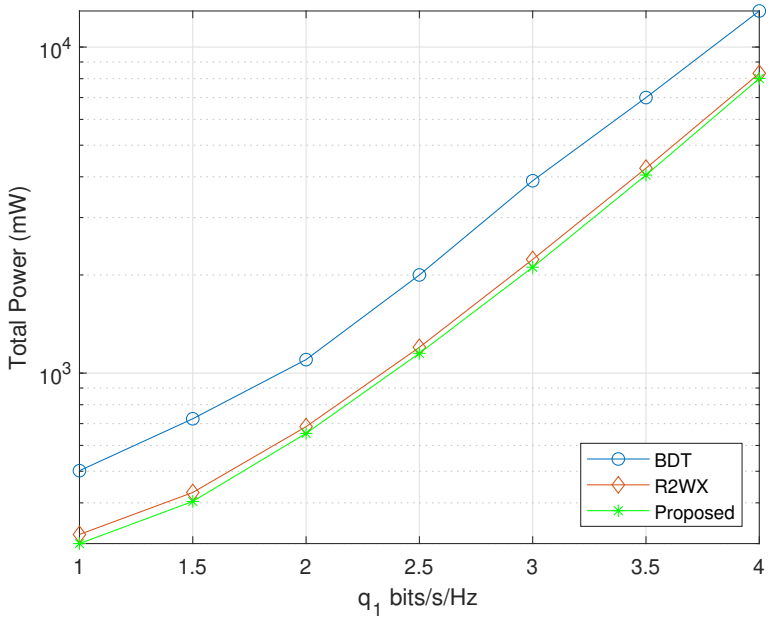

Figure 7.8: Total power versus one directional ASC, $\overline{q}_1$

7.5 Chapter Summary

In this chapter, the system model of a three-node two-way relay assisted BMA multicarrier scheme for a PLC system is proposed. The mathematical expressions of the proposed system is derived to obtain the optimal power allocation. The AO algorithm has been employed to solve the optimization problems. The minimal channel capacity requirement has been applied to the PLC applications to examine the total transmission power minimization. The simulation results show that the AO algorithm converges within six iterations, which indicates that AO algorithm has a short processing delay to meet the requirements of a relay-assisted PLC system. The minimal ASC requirement increases with transmission power as more transmission power is needed to meet the QoS constraint. Next, the proposed scheme has been compared with the conventional BDT and R2WX systems. It has been shown that the proposed method is able to make the system attain the same QoS requirement with less total power compared to the conventional BDT and R2WX systems.

Chapter 8

Conclusions and Future Work

The research on power-lines as the means for information delivery started in the late 1990s. Ever since then, power-line communication (PLC) technology has been popular for data transmission for indoor and outdoor data communication as power-line infrastructure is available widely. With the high power demand and the introduction of successful deployment toward achieving the smart grid system can meet the the demand of the the higher data-transmission rate. In this thesis, a blanking preprocessor bank has been designed to blindly mitigate the impulse noise into PLC system. Due to the performance of the PLC system degrades, a two-way relay-assisted PLC system has been proposed, which is also the main contribution in this thesis. A channel model of two-way relay-assisted PLC system has been proposed and analysed. With the results, the two-way two-relay PLC has been designed and compared with the single-relay PLC system. The three different bottom-up two-way single-relay PLC channel models have been discussed and compared. Using a two-way relay-assisted PLC system, power optimisation has been analysed with the consideration of QoS constraints.

8.1 Concluding Remarks

In Chapter 2, the basic fundamental knowledge of the OFDM-based PLC system has been reviewed. The OFDM based model used in PLC system has been discussed. Different types of channel and noise have been modelled. It has been seen that the top-down approach has been preferred to be used when there is no relay in PLC system, whereas the bottom-up approach is preferred to be used in a relay-assisted PLC system. In a relay-assisted PLC system, the existing Canete's P2P PLC channel model has been used to get the transfer function. The relay nodes have worked in two modes and hereby, assumed AF relay has been used in this thesis.

In Chapter 3, a blanking preprocessor bank consisting of multiple blanking preprocessors with different thresholds has been proposed. The proposed method has used the existing top-down channel and noise model, as there is no relay implemented. The threshold selection has been carefully considered by not setting the lower and higher thresholds too large and too small. Simulation results have demonstrated that the proposed method has outperformed the optimal blanking in terms of BER, PAPR, outage probability and also the effect of thresholds selection.

In Chapter 4, the two-way communication links have been fulfilled for all PLC application. The CTF of the two-way relay-assisted PLC channel has been modelled by dividing into group of an equivalent P2P PLC channels. Simulation results have demonstrated the proposed two-way PLC channel has a better correlation than one-way.

Then, in Chapter 5, the two-way relay-assisted PLC channel has been extended to the two-relay system. The CTFs of the two-way two-relay PLC system have been derived. The composite CTF of the certain link has been found by summing the respective CTFs of the segments which constitute the link. Both composite CTFs of single-relay and two-relay PLC systems have been compared

and have proven that two-relay system performed better when dealing with the non-direct link. In contrast, a single-relay system is preferred for direct channel data transmission.

In Chapter 6, a bottom-up multipath channel for two-way single-relay PLC has been proposed. This model has been derived based on the parameter of the modified top-down Zimmermann-Dostert model. The proposed multipath, ABCD, and VRA models have been discussed and formulated to get the composite path gains. Simulation results have shown that the proposed model does not have much fluctuation. In the direct path, the three models show a similar profile. In the SRD path, the proposed model and the ABCD model have similar attenuation at high frequencies. Meanwhile, in the DRS path, the proposed multipath model has better attenuation than ABCD at high frequencies.

Finally, in Chapter 7, the optimal power allocation problem has been proposed for the two-way single-relay/ relay-assisted PLC system based on QoS constraints. The proposed design scheme has been assumed to operate in in-band full-duplex mode, and CSI is available to the nodes. The optimisation problem has been developed by applying QoS constraints. Since the optimisation problem is non-convex, AO algorithm and KKT have been used to breakdown into sub-problem and optimise the transmission power. Simulation results have shown that the AO algorithm converges after a few iterations and has a short processing delay. The increasing of the minimal ASC requirement has made more transmission power needed to meet the strict QoS constraint in PLC system. The AO algorithm is able to make the system attain the same QoS requirement with less total power compared with the BDT system and with insignificant additional power compared with the R2WX system.

To conclude this thesis, here are the list of contributions made.

- A blanking preprocessor bank consisting of multiple blanking preprocessors with different thresholds has been proposed to mitigate the impulse noise blindly without knowing the noise parameters in PLC systems.

- The channel model of the two-way relay-assisted PLC system has been proposed with the consideration of the direct link between the source and the destination terminal nodes.
- The channel model of the two-way two-relay PLC system has been proposed.
- A bottom-up multipath channel for two-way single-relay PLC system has been proposed based on the modification of top-down Zimmermann-Dostert model.
- A power optimisation of a two-way single-relay BMA multicarrier scheme in PLC system has been proposed with the consideration of QoS constraints.

8.2 Future Works

In this thesis, few channel modelling and impulse noise mitigations have been developed for relay-assisted PLC systems with the assumption that AF relay is used in a broadband PLC systems. However, there are still many possibilities for extending this work.

In Chapter 3, a blanking preprocessor bank has been proposed to mitigate the impulse noise in PLC system, assuming there is no relay in PLC system. Hence, in future work, the relay can be incorporated to obtain better performance of the thresholds.

It will also be interesting to investigate the performance of the two-way channel model in Chapter 4, assuming that the system has load impedance at the source, relay, and destination, respectively. In the proposed PLC systems, it has been assumed that the load impedance at source and relay are considered. In future works, it can be assumed that there is a load impedance of destination.

The extended work of Chapter 4 has been investigated in Chapter 5. In Chapter 5, the channel modelling of a two-way two-relay PLC system has been proposed as the system's performance improved with the increase of relays. It has been assumed that the load impedance at the source and relay is considered

and is a half-duplex system. In future works, the system can run in full-duplex with the consideration of load impedance at the destination.

In Chapter 6, the performance of the proposed multipath channel model has been investigated with the ABCD and VRA models in a PLC system assuming that it is an ideal multipath model with an amplification factor of 1. In future work, the proposed model in Chapter 6 can be extended with load impedance at the destination node and a higher amplification factor. For getting better performance, the two-relay can be implemented here too.

The performance of power allocation of the two-way relay-assisted system has been investigated in Chapter 7, assuming that the CSI and QoS are considered. Future work can be analysed with the two-way two-relay PLC system assuming the noise modelling includes impulse noise mitigation on it. The power allocation can be extended to a full-duplex instead of a half-duplex system.

Appendix A

Derivation of SNR in Chapter 7

A.1 Derivation of $\mathbf{SNR_{T_1}}$

The received signal at T_1 in the second phase is given in (7.8). Since T_1 has full knowledge of $X_1^{[k]}$ and the channels, the first term of (7.8) can be eliminated. After elimination it becomes

$$Y'^{[k]}_{T_{1,2}} = (\xi + \varsigma)X_2^{[k]} + H^{[k],(2)}_{RT_1} g^{[k]} N_R^{[k]} + N^{[k]}_{T_1}, \tag{A.1}$$

where

$$\xi = H^{[k],(1)}_{T_2R} H^{[k],(2)}_{RT_1} g^{[k]} \sqrt{P^{[k]}_{T_{2,1}}}, \tag{A.2}$$

$$\varsigma = H^{[k],(2)}_{T_2T_1} \sqrt{P^{[k]}_{T_{2,2}}}, \tag{A.3}$$

and $g^{[k]}$ is given in (7.7).

The power of signal at T_1 is given by

$$\begin{aligned} P_{T_1} &= E\{\left|(\xi + \varsigma)X_2^{[k]}\right|^2\} \\ &= |(\xi + \varsigma)|^2 \, E\{\left|X_2^{[k]}\right|^2\} \\ &= \left(|\xi|^2 + |\varsigma|^2 + 2\sqrt{|\xi|^2 \, |\varsigma|^2}\right) E\{\left|X_2^{[k]}\right|^2\} \end{aligned} \tag{A.4}$$

where

$$|\xi|^2 = \frac{P_R^{[k]} P_{T_{2,1}}^{[k]} \left|H_{T_2R}^{[k],(1)}\right|^2 \left|H_{RT_1}^{[k],(2)}\right|^2}{P_{T_1}^{[k]} \left|H_{T_1R}^{[k],(1)}\right|^2 + P_{T_{2,1}}^{[k]} \left|H_{T_2R}^{[k],(1)}\right|^2 + W^{[k]}}, \tag{A.5}$$

$$|\varsigma|^2 = P_{T_{2,2}}^{[k]} \left|H_{T_2T_1}^{[k],(2)}\right|^2. \tag{A.6}$$

Note that $E\{|X_2^{[k]}|^2\} = 1$. For the sake of simplicity, we normalise the channel power to the noise power $W^{[k]}$. Therefore, we have the following:

$$\tilde{P}_{T_1} = |\xi|_N^2 + |\varsigma|_N^2 + 2\sqrt{|\xi|_N^2 |\varsigma|_N^2}, \tag{A.7}$$

where

$$|\xi|_N^2 = \frac{P_R^{[k]} P_{T_{2,1}}^{[k]} \lambda_{T_2R}^{[k],(1)} \lambda_{RT_1}^{[k],(2)} W^{[k]}}{1 + P_{T_1}^{[k]} \lambda_{T_1R}^{[k],(1)} + P_{T_{2,1}}^{[k]} \lambda_{T_2R}^{[k],(1)}}, \tag{A.8}$$

$$|\varsigma|_N^2 = P_{T_{2,2}}^{[k]} \lambda_{T_2T_1}^{[k],(2)} W^{[k]}, \tag{A.9}$$

and

$$\lambda_{L_1L_2}^{[k],(n)} = \frac{\left|H_{L_1L_2}^{[k],(n)}\right|^2}{W^{[k]}} \tag{A.10}$$

is the normalised path gain from node L_1 to L_2 in the n-th ($n = 1, 2$) phase.

The power of noise at T_1 is given by

$$\begin{aligned} P_{N_{T_1}} &= E\{\left|H_{RT_1}^{[k],(2)} g^{[k]} N_R^{[k]}\right|^2\} + E\{\left|N_{T_1}^{[k]}\right|^2\} \\ &= \left|H_{RT_1}^{[k],(2)}\right|^2 \left|g^{[k]}\right|^2 E\{\left|N_R^{[k]}\right|^2\} + E\{\left|N_{T_1}^{[k]}\right|^2\} \end{aligned} \tag{A.11}$$

Keep in mind that we assume that the power of noise is the same at each node for two successive phases. Thus, $E\{\left|N_R^{[k]}\right|^2\} = E\{\left|N_{T_1}^{[k]}\right|^2\} = W^{[k]}$. Similar to the signal power, after using (7.7) and normalizing the channel power, it becomes

$$\tilde{P}_{N_{T_1}} = \frac{P_R^{[k]} \lambda_{RT_1}^{[k],(2)} W^{[k]}}{1 + P_{T_1}^{[k]} \lambda_{T_1R}^{[k],(1)} + P_{T_{2,1}}^{[k]} \lambda_{T_2R}^{[k],(1)}} + W^{[k]} \tag{A.12}$$

Finally, the SNR at T_1 source node can be calculated as given in (A.1).

$$
\begin{aligned}
SNR_{T_1} &= \frac{\tilde{P}_{T_1}}{\tilde{P}_{N_{T_1}}} \\
&= \frac{\frac{P_R^{[k]} P_{T_{2,1}}^{[k]} \lambda_{T_2R}^{[k],(1)} \lambda_{RT_1}^{[k],(2)} W^{[k]}}{1+P_{T_1}^{[k]} \lambda_{T_1R}^{[k],(1)} + P_{T_{2,1}}^{[k]} \lambda_{T_2R}^{[k],(1)}} + P_{T_{2,2}}^{[k]} \lambda_{T_2T_1}^{[k],(2)} W^{[k]} + 2\sqrt{\left(\frac{P_R^{[k]} P_{T_{2,1}}^{[k]} \lambda_{T_2R}^{[k],(1)} \lambda_{RT_1}^{[k],(2)} W^{[k]}}{1+P_{T_1}^{[k]} \lambda_{T_1R}^{[k],(1)} + P_{T_{2,1}}^{[k]} \lambda_{T_2R}^{[k],(1)}}\right)\left(P_{T_{2,2}}^{[k]} \lambda_{T_2T_1}^{[k],(2)} W^{[k]}\right)}}{\frac{P_R^{[k]} \lambda_{RT_1}^{[k],(2)} W^{[k]}}{1+P_{T_1}^{[k]} \lambda_{T_1R}^{[k],(1)} + P_{T_{2,1}}^{[k]} \lambda_{T_2R}^{[k],(1)}} + W^{[k]}} \\
&= \frac{\left(\sqrt{\frac{P_R^{[k]} P_{T_{2,1}}^{[k]} \lambda_{T_2R}^{[k],(1)} \lambda_{RT_1}^{[k],(2)} W^{[k]}}{1+P_{T_1}^{[k]} \lambda_{T_1R}^{[k],(1)} + P_{T_{2,1}}^{[k]} \lambda_{T_2R}^{[k],(1)}}} + \sqrt{P_{T_{2,2}}^{[k]} \lambda_{T_2T_1}^{[k],(2)} W^{[k]}}\right)^2}{\frac{W^{[k]}\left(P_R^{[k]} \lambda_{RT_1}^{[k],(2)} + 1 + P_{T_1}^{[k]} \lambda_{T_1R}^{[k],(1)} + P_{T_{2,1}}^{[k]} \lambda_{T_2R}^{[k],(1)}\right)}{1+P_{T_1}^{[k]} \lambda_{T_1R}^{[k],(1)} + P_{T_{2,1}}^{[k]} \lambda_{T_2R}^{[k],(1)}}} \\
&= \frac{\frac{W^{[k]}\left(\sqrt{P_R^{[k]} P_{T_{2,1}}^{[k]} \lambda_{T_2R}^{[k],(1)} \lambda_{RT_1}^{[k],(2)}} + \sqrt{P_{T_{2,2}}^{[k]} \lambda_{T_2T_1}^{[k],(2)}\left(1+P_{T_1}^{[k]} \lambda_{T_1R}^{[k],(1)} + P_{T_{2,1}}^{[k]} \lambda_{T_2R}^{[k],(1)}\right)}\right)^2}{1+P_{T_1}^{[k]} \lambda_{T_1R}^{[k],(1)} + P_{T_{2,1}}^{[k]} \lambda_{T_2R}^{[k],(1)}}}{\frac{W^{[k]}\left(P_R^{[k]} \lambda_{RT_1}^{[k],(2)} + 1 + P_{T_1}^{[k]} \lambda_{T_1R}^{[k],(1)} + P_{T_{2,1}}^{[k]} \lambda_{T_2R}^{[k],(1)}\right)}{1+P_{T_1}^{[k]} \lambda_{T_1R}^{[k],(1)} + P_{T_{2,1}}^{[k]} \lambda_{T_2R}^{[k],(1)}}} \\
&= \frac{\left(\sqrt{P_R^{[k]} \lambda_{RT_1}^{[k],(2)} P_{T_{2,1}}^{[k]} \lambda_{T_2R}^{[k],(1)}} + \sqrt{P_{T_{2,2}}^{[k]} \lambda_{T_2T_1}^{[k],(2)}\left(1 + P_{T_1}^{[k]} \lambda_{T_1R}^{[k],(1)} + P_{T_{2,1}}^{[k]} \lambda_{T_2R}^{[k],(1)}\right)}\right)^2}{1 + P_{T_1}^{[k]} \lambda_{T_1R}^{[k],(1)} + P_{T_{2,1}}^{[k]} \lambda_{T_2R}^{[k],(1)} + P_R^{[k]} \lambda_{RT_1}^{[k],(2)}}
\end{aligned}
\tag{A.13}
$$

A.2 Derivation of $\mathbf{SNR_{T_{2,1}}}$

Similarly to Appendix A.1 approach, the received signal at $T_{2,1}$ in the first phase becomes

$$Y'_{T_{2,1}}{}^{[k]} = \psi X_1^{[k]} + N_{T_{2,1}}^{[k]} \tag{A.14}$$

where

$$\psi = H_{T_1T_2}^{[k],(1)} \sqrt{P_{T_1}^{[k]}} \tag{A.15}$$

and $g^{[k]}$ is given in (7.7). The power of signal is given by

$$\begin{aligned} P_{T_{2,1}} &= E\{\left|X_1^{[k]}\right|^2\} \\ &= |\psi|^2 \, E\{\left|X_1^{[k]}\right|^2\} \end{aligned} \tag{A.16}$$

where

$$|\psi|^2 = P_{T_1}^{[k]} \left|H_{T_1T_2}^{[k],(1)}\right|^2 \tag{A.17}$$

After normalizing the signal power, we have the following:

$$\tilde{P}_{T_{2,1}} = P_{T_1}^{[k]} \lambda_{T_1T_2}^{[k],(1)} W^{[k]} \tag{A.18}$$

The power of noise at $T_{2,1}$ is given by

$$P_{N_{T_{2,1}}} = E\{\left|N_{T_{2,1}}^{[k]}\right|^2\} \tag{A.19}$$

With the same assumption in Appendix A.1, the normalised noise power at $T_{2,1}$ is given by

$$\tilde{P}_{N_{T_{2,1}}} = W^{[k]} \tag{A.20}$$

The SNR at $T_{2,1}$ destination node can be calculated as given in (A.21).

$$\begin{aligned} SNR_{T_{2,1}} &= \frac{\tilde{P}_{T_{2,1}}}{\tilde{P}_{N_{T_{2,1}}}} \\ &= \frac{P_{T_1}^{[k]} \lambda_{T_1T_2}^{[k],(1)} W^{[k]}}{W^{[k]}} \\ &= P_{T_1}^{[k]} \lambda_{T_1T_2}^{[k],(1)} \end{aligned} \tag{A.21}$$

A.3 Derivation of $\mathbf{SNR_{T_{2,2}}}$

The received signal at $T_{2,2}$ in the second phase becomes

$$Y'^{[k]}_{T_{2,2}} = \iota X^{[k]}_1 + H^{[k],(2)}_{RT_2} g^{[k]} N^{[k]}_R + N^{[k]}_{T_2} \tag{A.22}$$

where

$$\iota = H^{[k],(1)}_{T_1R} H^{[k],(2)}_{RT_2} g^{[k]} \sqrt{P^{[k]}_{T_1}} \tag{A.23}$$

and $g^{[k]}$ is given in (7.7). The power of signal is given by

$$\begin{aligned} P_{T_{2,2}} &= E\{\left|\iota X^{[k]}_1\right|^2\} \\ &= |\iota|^2 E\{\left|X^{[k]}_1\right|^2\} \end{aligned} \tag{A.24}$$

where

$$|\iota|^2 = \frac{P^{[k]}_R P^{[k]}_{T_1} \left|H^{[k],(1)}_{T_1R}\right|^2 \left|H^{[k],(2)}_{RT_2}\right|^2}{P^{[k]}_{T_1} \left|H^{[k],(1)}_{T_1R}\right|^2 + P^{[k]}_{T_{2,1}} \left|H^{[k],(1)}_{T_2R}\right|^2 + W^{[k]}} \tag{A.25}$$

After normalizing the signal power

$$\tilde{P}_{T_{2,2}} = \frac{P^{[k]}_R P^{[k]}_{T_1} \lambda^{[k],(1)}_{T_1R} \lambda^{[k],(2)}_{RT_2} W^{[k]}}{P^{[k]}_{T_1} \lambda^{[k],(1)}_{T_1R} + P^{[k]}_{T_{2,1}} \lambda^{[k],(1)}_{T_2R} + 1} \tag{A.26}$$

The power of noise at $T_{2,2}$ is given by

$$\begin{aligned} P_{N_{T_{2,2}}} &= E\{\left|H^{[k],(2)}_{RT_2} g^{[k]} N^{[k]}_R\right|^2\} + E\{\left|N^{[k]}_{T_2}\right|^2\} \\ &= \left|H^{[k],(2)}_{RT_2}\right|^2 \left|g^{[k]}\right|^2 E\{\left|N^{[k]}_R\right|^2\} + E\{\left|N^{[k]}_{T_2}\right|^2\} \end{aligned} \tag{A.27}$$

With the same assumption in Appendix A.1, the normalised noise power at $T_{2,2}$ is given by

$$\tilde{P}_{N_{T_{2,2}}} = \frac{P^{[k]}_R \lambda^{[k],(2)}_{RT_2} W^{[k]}}{P^{[k]}_{T_1} \lambda^{[k],(1)}_{T_1R} + P^{[k]}_{T_{2,1}} \lambda^{[k],(1)}_{T_2R} + 1} + W^{[k]} \tag{A.28}$$

The SNR at $T_{2,2}$ destination node can be calculated as given in (A.29).

$$\begin{aligned} SNR_{T_{2,2}} &= \frac{\tilde{P}_{T_{2,2}}}{\tilde{P}_{N_{T_{2,2}}}} \\ &= \frac{\frac{P_R^{[k]} P_{T_1}^{[k]} \lambda_{T_1R}^{[k],(1)} \lambda_{RT_2}^{[k],(2)} W^{[k]}}{P_{T_1}^{[k]} \lambda_{T_1R}^{[k],(1)} + P_{T_{2,1}}^{[k]} \lambda_{T_2R}^{[k],(1)} + 1}}{\frac{P_R^{[k]} \lambda_{RT_2}^{[k],(2)} W^{[k]}}{P_{T_1}^{[k]} \lambda_{T_1R}^{[k],(1)} + P_{T_{2,1}}^{[k]} \lambda_{T_2R}^{[k],(1)} + 1} + W^{[k]}} \\ &= \frac{P_R^{[k]} P_{T_1}^{[k]} \lambda_{T_1R}^{[k],(1)} \lambda_{RT_2}^{[k],(2)} W^{[k]}}{W^{[k]} \left(P_R^{[k]} \lambda_{RT_2}^{[k],(2)} + 1 + P_{T_1}^{[k]} \lambda_{T_1R}^{[k],(1)} + P_{T_{2,1}}^{[k]} \lambda_{T_2R}^{[k],(1)} \right)} \\ &= \frac{P_R^{[k]} \lambda_{RT_2}^{[k],(2)} P_{T_1}^{[k]} \lambda_{T_1R}^{[k],(1)}}{1 + P_{T_1}^{[k]} \lambda_{T_1R}^{[k],(1)} + P_{T_{2,1}}^{[k]} \lambda_{T_2R}^{[k],(1)} + P_R^{[k]} \lambda_{RT_2}^{[k],(2)}} \end{aligned} \tag{A.29}$$

References

[1] J. A. Corchado, J. A. Cortés, F. J. Cañete, and L. Díez, "An MTL-based channel model for indoor broadband MIMO power line communications," *IEEE J. Sel. Areas Commun.*, vol. 34, no. 7, pp. 2045–2055, July 2016.

[2] J. Ying, Y. Chen, W. Ji, M. Liu, Y. you, and M. Zhang, "Topology modeling method for distribution network via power line communication," in *Proc. IEEE Innovative Smart Grid Technol. - Asia (ISGT Asia)*, Chengdu, China, May 2019, pp. 323–327.

[3] T. A. Papadopoulos, C. G. Kaloudas, A. I. Chrysochos, and G. K. Papagiannis, "Application of narrowband power-line communication in medium-voltage smart distribution grids," *IEEE Trans. Power Del.*, vol. 28, no. 2, pp. 981–988, April 2013.

[4] L. T. Berger, A. Schwager, and J. J. Escudero-Garzas, "Power line communications for smart grid applications," *IEEE J. Comput. Electr. Eng.*, Jun. 2013.

[5] F. Chiti, R. Fantacci, D. Marabissi, and A. Tani, "Performance evaluation of an efficient and reliable multicast power line communication system," *IEEE J. Sel. Areas Commun.*, vol. 34, no. 7, pp. 1953–1964, Jul. 2016.

[6] A. M. Tonello and A. Pittolo, "Considerations on narrowband and broadband power line communication for smart grids," in *2015 IEEE Int. Conf.*

Smart Grid Commun. (SmartGridComm), Miami, FL, USA, 2015, pp. 13–18.

[7] D. B. Unsal and T. Yalcinoz, "Application of new power line communication model for smart grids," *IEEE J. Comput. Electr. Eng.*, vol. 7, no. 3, pp. 168–178, Jun. 2015.

[8] P. Mlynek, J. Misurec, Z. Kolka, J. Slacik, and R. Fujdiak, "Narrowband power line communication for smart metering and street lighting control," vol. 48, no. 4, Jun. 2015, pp. 215–219.

[9] K. Rabie, A. M. Tonello, N. Al-Dhahir, J. Song, and A. Sendin, "IEEE Access special section editorial: advances in power line communication and its applications," *IEEE Access*, vol. 7, pp. 133 371–133 374, 2019.

[10] Y. P. Zhong, P. W. Huang, B. Wang, and J. Liao, "An efficient security scheme and its application in intelligent home system based on power-line," in *Proc. IEEE Int. Symp. on Power Line Commun. and Its Appl. (ISPLC)*, Pisa, Italy, 2007, pp. 83–86.

[11] M. Korki, N. Hosseinzadeh, and T. Moazzeni, "Performance evaluation of a narrowband power line communications for smart grid with noise reduction technique," *IEEE Trans. Consum. Electron.*, vol. 57, pp. 1598–1606, Nov. 2011.

[12] A. Mannan, D. K. Saxena, and M. Banday, "A study of power line communication," *IEEE J. Scientific and Research Publications*, vol. 4, no. 7, Jul. 2014.

[13] P. Oksa, M. Soini, L. Sydanheimo, and M. Kivikoski, "Considerations of using power line communication in the amr system," in *Proc. IEEE Int. Symp. on Power Line Commun. and Its Appl. (ISPLC)*, Orlando, FL, USA, 2006, pp. 208–211.

[14] L. d. M. B. A. Dib, V. Fernandes, M. de L. Filomeno, and M. V. Ribeiro, "Hybrid PLC/wireless communication for smart grids and internet of things applications," *IEEE Internet Things J.*, vol. 5, no. 2, pp. 655–667, Apr. 2018.

[15] G. Artale, A. Cataliotti, V. Cosentino, D. D. Cara, R. Fiorelli, S. Guaiana, and G. Tiné, "A new low cost coupling system for power line communication on medium voltage smart grids," *IEEE Trans. Smart Grid*, vol. 9, no. 4, pp. 3321–3329, Jul. 2018.

[16] F. H. Juwono, Q. Guo, D. D. Huang, Y. Chen, L. Xu, and K. P. Wong, "On the performance of blanking nonlinearity in real–valued OFDM-based PLC," *IEEE Trans. Smart Grid*, vol. 9, no. 1, pp. 449–457, Jan. 2018.

[17] T. Gupta and R. Bhatia, "Communication technologies in smart grid at different network layers: an overview," in *Proc. IEEE Int. Conf. Intell. Eng. Manag. (ICIEM)*, London, United Kingdom, Jun. 2020, pp. 177–182.

[18] Z. Fan, P. Kulkarni, S. Gormus, C. Efthymiou, G. Kalogridis, M. Sooriyabandara, Z. Zhu, S. Lambotharan, and W. H. Chin, "Smart grid communications: Overview of research challenges, solutions, and standardization activities," *IEEE Commun. Surveys Tuts.*, vol. 15, no. 1, pp. 21–38, Jan. 2013.

[19] M. S. Yousuf and M. El-Shafei, "Power line communications: An overview - part I," in *Proc. IEEE Int. Conf. Innov. Inf. Technol. (IIT)*, Dubai, Dubai, 2007, pp. 218–222.

[20] M. S. Yousuf, S. Z. Rizvi, and M. El-Shafei, "Power line communications: An overview - part II," in *Proc. IEEE Int. Conf. Inf. Commun. Technol. : From Theory to Applications*, Damascus, Syria, 2008, pp. 1–6.

[21] M. d. L. Filomeno, M. L. R. de Campos, H. V. Poor, and M. V. Ribeiro, "Hybrid power line/wireless systems: an optimal power allocation perspective," *IEEE Trans. Wireless Commun.*, vol. 19, no. 10, pp. 6289–6300, 2020.

[22] S. Galli, A. Scaglione, and Z. Wang, "For the grid and through the grid: The role of power line communications in the smart grid," *Proc. IEEE*, vol. 99, no. 6, pp. 998–1027, 2011.

[23] K. H. Aftkhamie, S. Katarand L. Yonge, and R. Newman, "An overview of the upcoming HomePlug AV standard," May 2005, pp. 400 – 404.

[24] A. G. Merkulov and V. P. Shuvalov, "The perspectives and practice of PLC HomePlug AV modems application in the network devices and industrial tools," in *Proc. Global Power Energy Commun. Conf. (GPECOM)*, Nevsehir, Turkey, Jun. 2019, pp. 46–49.

[25] T. Liu, "Channel estimation for power line communication," in *Proc. IEEE Int. Conf. on Commun. Tech. (ICCT)*, Oct 2017, pp. 272–276.

[26] B. Praho, M. Tlich, P. Pagani, A. Zeddam, and F. Nouvel, "Cognitive detection method of radio frequencies on power line networks," in *Proc. IEEE Int. Symp. on Power Line Commun. and Its Appl. (ISPLC)*, Rio de Janeiro, Brazil, Mar. 2010, pp. 225–230.

[27] L. T. Berger, A. Schwager, P. Pagani, and D. M. Schneider, "MIMO power line communications," *IEEE Commun. Surveys Tuts.*, vol. 17, no. 1, pp. 106–124, 2015.

[28] G. Bumiller, "Single frequency network technology for medium access and network management," in *Proc. IEEE Int. Symp. on Power Line Commun. and Its Appl. (ISPLC)*, Athens, Greece, Mar. 2002.

[29] G. Bumiller, L. Lampe, and H. Hrasnica, "Power line communication networks for large-scale control and automation systems," *IEEE Commun. Mag.*, vol. 48, no. 4, pp. 106–113, 2010.

[30] L. Lampe, R. Schober, and Simon Yiu, "Distributed space-time coding for multihop transmission in power line communication networks," *IEEE J. Sel. Areas Commun.*, vol. 24, no. 7, pp. 1389–1400, 2006.

[31] A. M. Tonello, F. Versolatto, and S. D'Alessandro, "Opportunistic relaying in in-home plc networks," in *IEEE Global Commun. Conf. (GLOBECOM)*, Miami, FL, USA, 2010, pp. 1–5.

[32] L. Lampe and A. J. H. Vinck, "Cooperative multihop power line communications," in *Proc. IEEE Int. Symp. on Power Line Commun. and Its Appl. (ISPLC)*, Beijing, China, 2012, pp. 1–6.

[33] A. W. Kabore, V. Meghdadi, and J. Cances, "Cooperative relaying in narrow-band plc networks using fountain codes," in *Proc. IEEE Int. Symp. on Power Line Commun. and Its Appl. (ISPLC)*, Glasgow, UK, 2014, pp. 306–310.

[34] V. B. Balakirsky and A. J. Han Vinck, "Potential performance of plc systems composed of several communication links," in *Proc. IEEE Int. Symp. on Power Line Commun. and Its Appl. (ISPLC)*, Vancouver, BC, Canada, Canada, 2005, pp. 12–16.

[35] N. K. N. A. Ikpehai, P. O. Aiyelabowo and B. Adebisi, "Cooperative relaying in power line environment: A survey and tutorial," vol. 3, no. 5, pp. 4224–4247, may 2015.

[36] H. A. Garcia-Baleon and V. Alarcon-Aquino, "A power-line communication modem based on OFDM," in *Proc. Int. Conf. Electr. Commun. Comp.*, Cholula, Puebla, Mexico, 2009, pp. 208–213.

[37] M. Al-Ansi, I. Elshafiey, A. Al-Sanie, S. Alghuwainem, and H. Al-Sharari, "MC-OFDMA for multi-user detection schemes in powerline communication," *J. Circuits Syst. Comp.*, vol. 22, 09 2013.

[38] J. J. Sánchez-Martínez, J. A. Cortés, L. Díez, F. J. Cañete, and L. M. Torres, "Performance analysis of OFDM modulation on indoor PLC channels in the frequency band up to 210 MHz," *Proc. IEEE Int. Symp. on Power Line Commun. and Its Appl. (ISPLC)*, pp. 38–43, 2010.

[39] R. Rashmi and S. M. Sarala, "OFDM: Modulation technique for wireless communication," *Int. J. Innov. Research in Advanced Eng. (IJIRAE)*, vol. 1, 03 2014.

[40] M. Colombo, Hernández, and J. Ureña, "Low-complexity joint time synchronization and channel estimation for OFDM-based PLC systems," *IEEE Access*, vol. 7, pp. 121 446–121 456, 2019.

[41] J. Anatory, N. Theethayi, R. Thottappillil, M. M. Kissaka, and N. H. Mvungi, "An experimental validation for broadband power-line communication (bplc) model," *IEEE Trans. Power Del.*, vol. 23, no. 3, pp. 1380–1383, 2008.

[42] J. Anatory, N. Theethayi, and R. Thottappillil, "Power-line communication channel model for interconnected networks—part I: Two-conductor system," *IEEE Trans. Power Del.*, vol. 24, no. 1, pp. 118–123, 2009.

[43] A. M. Tonello and F. Versolatto, "Bottom-up statistical PLC channel modeling—part I: Random topology model and efficient transfer function computation," *IEEE Trans. Power Del.*, vol. 26, no. 2, pp. 891–898, 2011.

[44] B. Nikfar and A. J. Han Vinck, "Relay selection in cooperative power line communication: A multi-armed bandit approach," *J. Commun. Netw.*, vol. 19, no. 1, pp. 1–9, 2017.

[45] F. Versolatto and A. M. Tonello, "Analysis of the plc channel statistics using a bottom-up random simulator," in *Proc. IEEE Int. Symp. on Power Line Commun. and Its Appl. (ISPLC)*, Rio de Janeiro, Brazil, 2010, pp. 236–241.

[46] F. J. Canete, J. A. Cortes, L. Diez, and J. T. Entrambasaguas, "A channel model proposal for indoor power line communications," *IEEE Commun. Mag.*, vol. 49, no. 12, pp. 166–174, 2011.

[47] F. J. Cañete, L. Díez, J. A. Cortés, and J. T. Entrambasaguas, "Cyclic signals and systems in power line communications," *IEEE Access*, vol. 7, pp. 96 799–96 817, 2019.

[48] M. Gebhardt, F. Weinmann, and K. Dostert, "Physical and regulatory constraints for communication over the power supply grid," *IEEE Commun. Mag.*, vol. 41, no. 5, pp. 84–90, 2003.

[49] L. Lampe, A. Tonello, and T. Swart, *Power line communications: Principles, standards and applications from multimedia to smart grid: Second edition.* Hoboken, NJ: Wiley, 04 2016.

[50] D. Shrestha, X. Mestre, and M. Payaro, "On channel estimation for power line communication systems in the presence of impulsive noise," *Comput. Electr. Eng.*, vol. 72, pp. 406–419, 2018.

[51] L. Bai, M. Tucci, and M. Raugi, "Impulsive noise mitigation with interleaving based on music in power line communication," *IEEE Trans. Smart Grid*, vol. 10, no. 4, pp. 3575–3584, Jul. 2019.

[52] M. Yong-tao, L. Kai-hua, Q. Zhi-jun, Y. Jie-xiao, and G. Xiao-lin, "Modeling the colored background noise of power line communication channel based on artificial neural network," in *Proc. IEEE Int. Conf. Wireless Optical Commun.*, Shanghai, China, 2010, pp. 1–4.

[53] D. Benyoucef, "A new statistical model of the noise power density spectrum for powerline communication," in *Proc. IEEE Int. Symp. on Power Line Commun. and Its Appl. (ISPLC)*, Kyoto, Japan, 2003, pp. 136–141.

[54] P. Mlynek, J. Misurec, and M. Koutny, "Noise modeling for power line communication model," in *Proc. Int. Conf. Telecom. Signal Process. (TSP)*, Prague, Czech Republic, 2012, pp. 282–286.

[55] T. Zhouwen, L. Ziji, and C. Yun, "Noise modeling and analysis for indoor broadband power line communication," in *Int. Conf. Cloud Comp. Security*, 2018, pp. 517–527.

[56] N. Andreadou and F.-N. Pavlidou, "Modelling the noise on the OFDM power-line communications systems," *IEEE Trans. Power Del.*, vol. 25, no. 1, pp. 150–157, 2010.

[57] S. M. ÇÜRÜK, "Impulsive noise models used in power line communication," *Balkan J. Elect. Comput. Eng.*, vol. 7, pp. 115–122, 4 2019.

[58] J. A. Cortés, A. Sanz, P. Estopiñan, and J. I. García, "On the suitability of the middleton class a noise model for narrowband PLC," in *Proc. IEEE Int. Symp. on Power Line Commun. and Its Appl. (ISPLC)*, Bottrop, Germany, April 2016, pp. 58–63.

[59] M. Ghosh, "Analysis of the effect of impulse noise on multicarrier and single carrier QAM systems," *IEEE Transactions on Communications*, vol. 44, no. 2, pp. 145–147, 1996.

[60] K. Khalil, P. Corlay, F. Coudoux, M. G. Gazalet, and M. Gharbi, "Analysis of the impact of impulsive noise parameters on BER performance of OFDM power-line communication," in *Proc. IEEE Int. Symp. on Signal, Image, Video and Commun. (ISIVC)*, Marrakech, Morocco, Nov. 2014.

[61] S. V. Zhidkov, "Impulsive noise suppression in OFDM-based communcation systems," *IEEE Trans. Consum. Electr.*, vol. 49, no. 4, pp. 944–948, 2003.

[62] B. Han, V. Stoica, C. Kaiser, N. Otterbach, and K. Dostert, "Noise characterization and emulation for low-voltage power line channels across narrowband and broadband," *Digital signal process.*, vol. 69, pp. 259–274, 2017.

[63] F. Rouissi, J. H. Vinck, H. Gassara, and A. Ghazel, "Statistical characterization and modelling of impulse noise on indoor narrowband PLC environment," in *Proc. IEEE Int. Symp. on Power Line Commun. and Its Appl. (ISPLC)*, Madrid, Spain, April 2017, pp. 1–6.

[64] L. Di Bert, P. Caldera, D. Schwingshackl, and A. M. Tonello, "On noise modeling for power line communications," in *Proc. IEEE Int. Symp. on Power Line Commun. and Its Appl. (ISPLC)*, Udine, Italy, 2011, pp. 283–288.

[65] G. Laguna-Sanchex and M. Lopez-Guerrero, "On the use of alpha–stable distribution in noise modeling for PLC," *IEEE Trans. Power Del.*, vol. 30, no. 4, pp. 1863–1870, 2015.

[66] P. G. Georgiou, P. Tsakalides, and C. Kyriakakis, "Alpha-stable modeling of noise and robust time-delay estimation in the presence of impulsive noise," *IEEE Trans. Multimedia*, vol. 1, no. 3, pp. 291–301, 1999.

[67] A. Rajan and C. Tepedelenlioglu, "Diversity combining over rayleigh fading channels with symmetric alpha–stable noise," *IEEE Trans. Wireless Commun.*, vol. 9, no. 9, pp. 2968–2976, 2010.

[68] E. E. Kuruoglu, W. J. Fitzgerald, and P. J. W. Raymer, "Near optimal detection of signals in impulsive noise modeled with a symmetric/spl alpha/-stable distribution," *IEEE Commun. Lett.*, vol. 2, no. 10, pp. 282–284, 1998.

[69] S. D'Alessandro, A. M. Tonello, and F. Versolatto, "Power savings with opportunistic decode and forward over in-home plc networks," in *Proc. IEEE Int. Symp. on Power Line Commun. and Its Appl. (ISPLC)*, Udine, Italy, 2011, pp. 176–181.

[70] K. M. Rabie, B. Adebisi, A. M. Tonello, and G. Nauryzbayev, "More robust decode-and-forward relaying over impulsive noise power line channels," in *Proc. IEEE Int. Symp. on Power Line Commun. and Its Appl. (ISPLC)*, Madrid, Spain, 2017, pp. 1–5.

[71] A. Dubey and R. K. Mallik, "PLC system performance with AF relaying," *IEEE Trans. Commun.*, vol. 63, no. 6, pp. 2337–2345, 2015.

[72] F. Passerini and A. M. Tonello, "Analog full-duplex amplify-and-forward relay for power line communication networks," *IEEE Commun. Lett.*, vol. 23, no. 4, pp. 676–679, 2019.

[73] K. M. Rabie and B. Adebisi, "Enhanced amplify-and-forward relaying in non-gaussian plc networks," *IEEE Access*, vol. 5, pp. 4087–4094, 2017.

[74] H. Meng, Y. L. Guan, and S. Chen, "Modeling and analysis of noise effects on broadband power-line communications," *IEEE Trans. Power Del.*, vol. 20, no. 2, pp. 630–637, 2005.

[75] G. Ndo, P. Siohan, and M.-H. Hamon, "Adaptive noise mitigation in impulsive environtment: Application to power-line communications," *IEEE Trans. Power Del.*, vol. 25, no. 2, pp. 647–656, 2010.

[76] J. Lin, M. Nassar, and B. L. Evans, "Impulsive noise mitigation in power-line communications using sparse bayesian learning," *IEEE J. Select. Areas Commun.*, vol. 31, no. 7, pp. 1972–1183, 2013.

[77] N. Andreadou and G. Fulli, "NB-PLC channel: Estimation of periodic impulsive noise parameters and mitigation techniques," *Int. J. Elec. Power Energy Syst.*, vol. 103, pp. 146–158, 2018.

[78] F. H. Juwono, Q. Guo, D. Huang, and K. P. Wong, "Joint peak amplitude and impulsive noise clippings in OFDM-based power line communications," in *Proc. Asia Pacific Conf. Commun.*, Denpasar, Indonesia, 2013, pp. 567–571.

[79] F. H. Juwono, Q. Guo, D. Huang, and K. P. Wong, "Deep clipping for impulsive noise mitigation in OFDM-based power-line communications," *IEEE Trans. Power Del.*, vol. 29, no. 3, pp. 1335–1343, 2014.

[80] Y. Chien and H. Yu, "Mitigating impulsive noise for wavelet-OFDM powerline communication," *Energies*, vol. 12, no. 8, pp. 1–13, Apr. 2019.

[81] H. Yu, Y. Chien, and H. Tsao, "A study of impulsive noise immunity for wavelet-OFDM-based power line communications," in *Proc. Int. Conf. Commun. Problem-Solving*, Taipei, Taiwan, 2016, pp. 1–2.

[82] P. D. Mariyam, F. H. Juwono, P. D. Pamungkasari, and D. Gunawan, "How to deal with impulsive noise in OFDM-based PLC: A survey," in *Proc. Int. Conf. Elect. Eng. Inform. (ICELTICs)*, Banda Aceh, Indonesia, 2017, pp. 163–168.

[83] K. M. Rabie and E. Alsusa, "Performance analysis of adaptive hybrid nonlinear preprocessors for impulsive noise mitigation over power-line channels," in *Proc. IEEE Int. Conf. Commun. (ICC)*, London, UK, 2015, pp. 728–733.

[84] Y. Chien, "Iterative channel estimation and impulsive noise mitigation algorithm for OFDM-based receivers with application to power-line communications," *IEEE Transactions on Power Delivery*, vol. 30, no. 6, pp. 2435–2442, 2015.

[85] M. Mao, G. Xie, J. Gao, G. Wu, and K. Liu, "Adaptive IN mitigation in OFDM-based power-line communication system with jointed blanking and robust channel estimation," in *Proc. IEEE Int. Conf. Comput. Commun.*, Chengdu, China, 2016, pp. 2573–2576.

[86] Y. Chien, J. Chen, and S. S. Xu, "A multilayer perceptron-based impulsive noise detector with application to power-line-based sensor networks," *IEEE Trans. Power Del.*, no. 6, pp. 21 778–21 787, 2018.

[87] F. H. Juwono, Q. Guo, D. Huang, K. Wong, and L. Xu, "Impulse noise detection in PLC with smoothed L0-norm," in *Proc. IEEE Int. Acoust. Speech Signal Process.*, Brisbane, Australia, 2015, pp. 3232–3236.

[88] G. Ren, S. Qiao, and Y. Hei, "Asynchronous impulsive noise mitigation in OFDM using adaptive threshold compressive sensing," in *Proc. Wireless Microwave Technol. Conf.*, Tampa, FL, USA, 2014, pp. 1–5.

[89] B. Adebisi, K. Anoh, K. M. Rabie, A. Ikpehai, M. Fernando, and A. Wells, "A new approach to peak threshold estimation for impulsive noise reduction over power line fading channels," *IEEE Systems J.*, vol. 13, no. 2, pp. 1682–1693, Jun. 2019.

[90] F. H. Juwono, R. Reine, L. Liu, J. Liu, and D. Huang, "Performance of impulsive noise blanking in precoded OFDM-based PLC systems," in *Proc. Int. Conf. Commun. Syst.*, Shenzhen, China, 2016, pp. 1–6.

[91] F. Fang and Z. Yang, "Improved blanking nonlinearity scheme for powerline communication system in impulsive noise scenarios," in *Proc. IEEE Int. Conf. Comput. Commun. and the Internet*, Wuhan, China, 2016, pp. 70–75.

[92] E. Alsusa and K. M. Rabie, "Dynamic peak-based threshold estimation method for mitigating impulsive noise in power-line communication systems," *IEEE Trans. Power Del.*, vol. 28, no. 4, pp. 2201–2208, Oct. 2013.

[93] K. M. Rabie and E. Alsusa, "Improving blanking/clipping based impulsive noise mitigation over powerline channels," in *Proc. IEEE Int. Symp. Pers. Indoor Mobile Radio Commun. (PIMRC)*, London, UK, 2013, pp. 3413–3417.

[94] K. M. Rabie and E. Alsusa, "Effective noise cancellation using single-carrier FDMA transmission in power-line channels," *IEEE Trans. Power Del.*, vol. 29, no. 5, pp. 2110–2117, 2014.

[95] T. Kageyama, O. Muta, and H. Gacanin, "Enhanced selected mapping for impulsive noise blanking in multi-carrier power-line communication systems," *IEICE Trans. Commun.*, vol. E102B, no. 11, pp. 2174–2182, May 2019.

[96] F. H. Juwono, R. Reine, J. Liu, and P. D. Pamungkasari, "BITFCM-OFDM scheme for power-line communication systems," *AEU - Int. J. Electron Commun.*, vol. 105, pp. 116–123, 2019.

[97] D. Huang, K. B. Letaief, and J. Lu, "Bit-interleaved time-frequency coded modulation for OFDM systems over time-varying channels," *IEEE Trans. Commun.*, vol. 53, no. 7, pp. 1191–1199, Jul. 2005.

[98] M. Zimmermann and K. Dostert, "A multi-path signal propagation model for the power line channel in the high frequency range," in *Proc. IEEE Int. Symp. on Power Line Commun. and Its Appl. (ISPLC)*, 1999, pp. 45–51.

[99] U. Epple, K. Shibli, and M. Schnell, "Investigation of blanking nonlinearity in OFDM systems," in *Proc. Int. Conf. Commun.*, Kyoto, Japan, 2011, pp. 1–5.

[100] F. H. Juwono, Q.Guo, Y. Chen, D. Huang, and K. P. Wong, "Linear combining of nonlinear preprocessors for OFDM-based power-line communications," *IEEE Trans. Smart Grid*, vol. 7, no. 1, pp. 253–260, 2016.

[101] H. Mohimani, M. Babaie-Zadeh, and C. Jutten, "A fast approach for overcomplete sparse decomposition based on ℓ^0 norm," *IEEE Trans. Signal Process.*, vol. 57, no. 1, pp. 289–301, Jan. 2009.

[102] A. Mathur, Y. Ai, M. Cheffena, and M. R. Bhatnagar, "Performance of hybrid ARQ over power line communications channels," in *Proc. IEEE Vehi. Technol. Conf.*, Antwerp, Belgium, 2020, pp. 1–6.

[103] A. Chelli, A. Hadjtaieb, and M.-S. Alouini, "Performance analysis of hybrid ARQ with incremental redundancy over amplify-and-froward dual-hop relay channels," *arXiv*, 2014.

[104] S. K. Mohanty and R. K. Giri, "Measurement of channel characteristic by bottom–up approach for indoor PLC channel," in *Proc. IEEE Region 10 Conf.*, Bangkok, Thailand, Oct. 2014, pp. 1–6.

[105] H. Zhang, X. Zhao, S. Geng, W. Lu, and Y. Ma, "Selection of indoor relay node positions for a three-hop low-voltage broadband power line communication system," *IET Commun.*, vol. 14, no. 5, pp. 746–751, 2020.

[106] X. Wu and Y. Rong, "Optimal power allocation for non-regenerative multicarrier relay-assisted PLC systems with QoS constraints," in *Proc. IEEE Int. Symp. on Power Line Commun. and Its Appl. (ISPLC)*, Austin, TX, USA, Mar. 2015, pp. 142–147.

[107] X. Wu, B. Zhu, and Y. Rong, "Channel model proposal for indoor relay–assisted power line communications," *IET Communications*, vol. 12, no. 10, pp. 1236–1244, Jun. 2018.

[108] D. M. Pozar, *Microwave engineering*. Hoboken, NJ: Wiley, 2012, vol. 4.

[109] T. Esmailian, F. R. Kschischang, and P. G. Gulak, "In-building power lines as high-speed communication channels: channel characterization and a test channel ensemble," *Int. J. of Commun. Systems*, pp. 381–400, 2003.

[110] G. Xie, S. Li, Y. Zeng, and Y. Wang, "Research on multi-node broadband power line channel modeling," in *Proc. IEEE Int. Conf. Comput. Netw. Electron. Autom. (ICCNEA)*, Xi'an, China, Sept. 2020, pp. 342–346.

[111] R. K. Ahiadormey, P. Anokye, H. Jo, and K. Lee, "Performance analysis of two-way relaying in cooperative power line communications," *IEEE Access*, vol. 7, pp. 97 264–97 280, 2019.

[112] M. Rozman, A. Ikpehai, B. Adebisi, and K. M. Rabie, "Channel characterisation of cooperative relaying power line communication systems," in *Proc. IEEE Int. Symp. Commun. Syst. Netw. Digit. Signal Process. (CSNDSP)*, Prague, Czech Republic, July 2016, pp. 1–5.

[113] K. M. Rabie, B. Adebisi, H. Gacanin, G. Nauryzbayev, and A. Ikpehai, "Performance evaluation of multi-hop relaying over non-gaussian PLC channels," *J. Commun. Netw.*, vol. 19, no. 5, pp. 531–538, 2017.

[114] K. Kale and S. K. Patra, "Characterization of broadband power line channel," in *Proc. of Conf. Commun. Technol. (GCCT)*, Thuckalay, India, 2015, pp. 673–677.

[115] S. Galli and T. Banwell, "A novel approach to the modeling of the indoor power line channel-part II: Transfer function and its properties," *IEEE Trans. Power Del.*, vol. 20, no. 3, pp. 1869–1878, 2005.

[116] S. Liu, B. Gou, H. Li, and R. Kavasseri, "Power-line communication channel characteristics under transient model," *IEEE Trans. Power Del.*, vol. 29, no. 4, pp. 1701–1708, 2014.

[117] X. Zhao, H. Zhang, W. Lu, and L. Li, "Approach for modelling of broadband low-voltage PLC channels using graph theory," *IET Commun.*, vol. 12, no. 13, pp. 1524–1530, 2018.

[118] A. M. Tonello, F. Versolatto, B. Bejar, and S. Zazo, "A fitting algorithm for random modeling the PLC channel," *IEEE Trans. Power Del.*, vol. 27, no. 3, pp. 1477–1484, 2012.

[119] M. Zimmermann and K. Dostert, "A multipath model for the powerline channel," *IEEE Trans. Commun.*, vol. 50, no. 4, pp. 553–559, 2002.

[120] H. Meng, S. Chen, Y. L. Guan, C. L. Law, P. L. So, E. Gunawan, and T. T. Lie, "Modeling of transfer characteristics for the broadband power line communication channel," *IEEE Trans. Power Del.*, vol. 19, no. 3, pp. 1057–1064, 2004.

[121] J. Anatory, M. M. Kissaka, and N. H. Mvungi, "Channel model for broadband power-line communication," *IEEE Trans. Power Del.*, vol. 22, no. 1, pp. 135–141, 2007.

[122] G. Moreno-Rodriguez and L. T. Berger, "An IIR-filter approach to time variant PLC-channel modelling," in *Proc. IEEE Int. Symp. Power Line Commun. Appl. (ISPLC)*, Jeju City, South Korea, 2008, pp. 87–92.

[123] A. M. Tonello and T. Zheng, "Bottom-up transfer function generator for broadband PLC statistical channel modeling," in *Proc. IEEE Int. Symp. Power Line Commun. Appl. (ISPLC)*, Dresden, Germany, 2009, pp. 7–12.

[124] A. Aloui, O. Ben Rhouma, and C. Rebai, "Comparison of different channel modeling techniques used in nb-plc systems," in *Proc. Int. Conf. Adv. Systems Electric Technol. (ICASET)*, Hammamet, Tunisia, 2018, pp. 125–131.

[125] B. Adebisi, A. Khalid, Y. Tsado, and B. Honary, "Narrowband PLC channel modelling for smart grid applications," in *Proc. Int. Symp. Commun. Syst. Netw. Digital Signal Process. (CSNDSP)*, Manchester, UK, 2014, pp. 67–72.

[126] S. Souissi, O. B. Rhouma, and C. Rebai, "Bottom-up approach for narrow-band powerline channel modeling," in *Proc. IEEE Global Commun. Conf. (GLOBECOM)*, Atlanta, GA, USA, 2013, pp. 2987–2992.

[127] D. Weston, *Electromagnetic compatibility: Principles and Application.* CRC Press, 2001, vol. 4.

[128] X. Wu and Y. Rong, "On the location of plug-in relay devices for indoor power line communication environment," in *Proc. Int. Conf. on Signal Process. and Commun. Systems (ICSPCS)*, Gold Coast, QLD, Australia, Dec 2014, pp. 1–6.

[129] M. Noori and L. Lampe, "Improving data rate in relay-aided power line communications using network coding," in *IEEE Global Commun. Conf. (GLOBECOM)*, Atlanta, GA, USA, Dec 2013, pp. 2975–2980.

[130] X. Wu and Y. Rong, "Joint terminals and relay optimization for two-way power line information exchange systems with QoS constraints," *EURASIP J. Adv. Signal Process.*, vol. 2015, no. 1, p. 84, Sep 2015.

[131] X. Wu, B. Zhu, Y. Wang, and Y. Rong, "Optimization for relay-assisted broadband power line communication systems with QoS requirements under time-varying channel conditions," *KSII Trans. Internet Inf. Syst.*, vol. 11, pp. 4865–4886, 10 2017.

[132] F. Jameel, Z. Hamid, F. Jabeen, S. Zeadally, and M. A. Javed, "A survey of device-to-device communications: Research issues and challenges," *IEEE Commun. Surveys Tuts.*, vol. 20, no. 3, pp. 2133–2168, thirdquarter 2018.

[133] J. Joung and J. Choi, "Space–time line codes with power allocation for regenerative two-way relay systems," *IEEE Trans. Veh. Technol*, vol. 68, no. 5, pp. 4884–4893, May 2019.

[134] K. X. Nguyen, Y. Rong, and S. Nordholm, "MMSE-based joint source and relay optimization for interference MIMO relay systems," *EURASIP J. Wireless Commun. Netw.*, vol. 73, pp. 1–9, 2015.

[135] W. Liu, J. Ding, J. Zheng, X. Chen, and C. L. I, "Relay-assisted technology in optical wireless communications: a survey," *IEEE Access*, vol. 8, pp. 194 384–194 409, 2020.

[136] G. Prasad, L. Lampe, and S. Shekhar, "In-band full duplex broadband power line communications," *IEEE Trans. Commun.*, vol. 64, no. 9, pp. 3915–3931, Sep. 2016.

[137] F. Passerini and A. M. Tonello, "Full duplex power line communication modems for network sensing," in *Proc. IEEE Int. Conf. Smart Grid Commun.(SmartGridComm)*, Dresden, Germany, Oct 2017, pp. 213–217.

[138] F. J. Cañete, G. Prasad, and L. Lampe, "PLC networks with in-band full-duplex relays," in *Proc. IEEE Int. Symp. on Power Line Commun. and Its Appl. (ISPLC)*, Málaga, Spain, May 2020, pp. 1–6.

[139] M. E. Hazen, "The technology behind HomePlug AV powerline communications," *Computer*, vol. 41, no. 6, pp. 90–92, Jun. 2008.

[140] H. A. Latchman, S. Katar, L. Yonge, and S. Gavette, *HomePlug AV and IEEE 1901: a handbook for PLC designers and users*. IEEE Press, 2013.

[141] L. Guerrieri, P. Bisaglia, G. Dell'Amico, and E. Guerrini, "Performance of the turbo coded HomePlug AV system over power-line channels," in *Proc. IEEE Int. Symp. on Power Line Commun. and Its Appl. (ISPLC)*, Pisa, Italy, Mar. 2007, pp. 138–143.

[142] N. Papandreou and T. Antonakopoulos, "Bit and power allocation in constrainted multicarrier systems: the single-user case," *EURASIP J. Adv. Signal Process.*, no. 6, Nov. 2008.